

Advances in Inhalation Gas Dosimetry for Derivation of a Reference Concentration (RfC) and Use in Risk Assessment

September 2012

U.S. Environmental Protection Agency
Washington, DC

DISCLAIMER

This report has been reviewed in accordance with U.S. Environmental Protection Agency Policy and approved for publication. Mention of trade names or commercial products does not constitute endorsement or recommendation for use.

TABLE OF CONTENTS

AUTHORS, CONTRIBUTORS, AND REVIEWERS	VI
GLOSSARY	IX
ABBREVIATIONS AND ACRONYMS	XII
EXECUTIVE SUMMARY	XIV
1 INTRODUCTION AND PURPOSE	1-1
2 REVIEW OF THE 1994 RfC METHODS FOR GAS DOSIMETRY	2-1
2.1 Gas Categorizations - General	2-1
2.1.1 The <i>RfC Methods</i> Gas Categorization Scheme	2-1
Figure 2-1 Gas categorization scheme based on water solubility and reactivity as major determinants of gas uptake.	2-2
Table 2-1 Gas categorization characteristics and examples according to RfC Methods classification scheme	2-3
2.2 Conceptual and Historical Basis for Comparative Dosimetry of Inspired Gases in <i>RfC Methods</i> – Minute Ventilation/Surface Area of the Respiratory Tract (V_E/SA_{RT})	2-3
2.2.1 Factors Controlling Comparative Inhaled Dose	2-3
2.2.1.1 Comparative Respiratory Anatomy and Physiology	2-4
2.2.1.2 Regions of the Respiratory Tract Common among Species	2-4
Table 2-2 Respiratory tract regions	2-5
Figure 2-2 Diagrammatic representation of the three respiratory tract regions designated in humans.	2-6
Table 2-3 Default surface areas for the extrathoracic (ET), tracheobronchial (TB), and pulmonary (PU) regions of the respiratory tract in various species	2-7
Table 2-4 Intercept (b_0) and coefficient (b_1) values used to calculate default ventilation rates based on body weight ^a	2-8
Table 2-5 Default ventilation rate and body weights for multiple species	2-9
2.2.2 Normalization of Inhaled Concentration to Surface Area of Respiratory Tract Regions	2-9
2.2.2.1 Dose-Response in Respiratory Tract Tissues is Based on External Exposure Concentration	2-9
2.2.2.2 Normalization of External Exposure Concentration to Surface Areas	2-10
2.4 Interspecies Gas Dosimetry in the RfC - Application of V_E/SA in Calculation of the Human Equivalent Concentration, HEC: The Default Approach for Inspired Gases	2-10
Table 2-6 Hierarchy of model structures for dosimetry and interspecies extrapolation	2-11
2.4.1 The Dosimetric Adjustment Factor (DAF)	2-11
2.4.2 The DAF for POE Effects; the Regional Gas Dose Ratio, RGDR _r	2-12
2.4.3 Assumptions in the Application of V_E/SA	2-13
2.5 Current Applications Using the Default DAFs – RGDR _{ET} , RGDR _{TB} , RGDR _{PU} , and $H_{b/g}$	2-14
2.5.1 The RGDR for the Extrathoracic Region – RGDR _{ET}	2-14
2.5.2 The RGDR for the Tracheobronchial (TB) Region - RGDR _{TB}	2-15
2.5.3 The RGDR for the Pulmonary (PU) Region - RGDR _{PU}	2-16
2.5.4 Limitations in the Assumptions and Application of V_E/SA	2-17
Figure 2-3 Representation of the assumptions of uniformity following from V_E/SA as applied to comparative gas dosimetry.	2-18
2.6 The DAF for Systemic (SYS) Sites - $H_{b/g}$	2-19
Table 2-7 Some example blood:air partition coefficients ($H_{b/g}$) in humans and rats expressed as a ratio, A/H	2-21
2.7 Children's Dosimetry	2-21
Table 2-8 Human lifestages and corresponding age ranges through adolescence	2-22
3 ADVANCES	3-1
3.1 A Modified Gas Scheme: Descriptors versus Categories	3-1
Figure 3-1 A schematic representation of the physicochemical properties of reactivity and water solubility overlaid with descriptors of their practical limits.	3-2
3.2 Major Scientific Advances Related to Inhalation Gas Dosimetry in the ET Region	3-3

3.2.1	Tracer Dye-Flow in Cast Models	3-3
3.2.2	Computational Fluid Dynamic Modeling	3-4
3.2.2.1	CFD Air Flow Models of the Rat ET Region	3-4
3.2.2.2	CFD Air Flow Models of the Human ET Region	3-4
	Figure 3-2 The coronal sections are divided into sub-sections which are indicated by the letters.	3-5
	Table 3-1 Summary of CFD simulated flow apportionment (as a % of total at 15 L/min) on the coronal cross-sectional area in the middle turbinate (as mm ²) of the ET region in selected human models as analyzed by Wen et al. (2008).	3-6
3.2.2.3	CFD Air Flow Models - Predictions of Reactive Gas Distribution in the ET Region	3-6
3.2.2.4	Interspecies CFD Air Flow Models Predictions of Gas Distribution in the ET Region	3-7
	Figure 3-3 Nasal wall flux spectra of inhaled formaldehyde simulated in rats, monkey and humans at normal inspiratory flow rates.	3-8
	Table 3-2 Estimates of formaldehyde flux to ET surface walls for various species	3-8
3.2.3	Range and Distribution of Flux in ET Regions for Various Species	3-9
3.2.4	Correlation of High Flux with Lesions in the ET Region	3-9
	Figure 3-4 Graphs showing (A) the incidence of formaldehyde-induced squamous metaplasias and (B) modeled formaldehyde flux values along regions assigned to the perimeter of a transected nasal airway of rats.	3-11
	Figure 3-5 Schematic diagram of the transverse nasal section through the ethmoid turbinates (top left, Section 2 of the nasal cavity) with plot of lesion incidence at 30 and 80 ppm (top right).	3-12
	Figure 3-6 Representation of application of the state of the science to the assumptions and outcome of the <i>RfC Methods</i> basic default procedures for comparative gas dosimetry in the ET region.	3-14
3.2.5	Evaluation and Use of Models in Interspecies Inhalation Dosimetry - ET Region	3-14
3.2.5.1	Overview of CFD-PBPK Hybrid Modeling – Combination of Gas Transport in the Air Phase into the Liquid/Tissue Phase	3-15
3.2.5.2	CFD-PBPK Hybrid Modeling and the Overall Mass Transport Coefficient - K_g	3-16
3.2.5.3	Results and Analysis of Interspecies Inhalation Dosimetry Modeling – ET Region	3-18
	Table 3-3 Primary toxicological endpoint(s), uptake, properties, and physicochemical descriptor for representative gases—ranked by percentage of uptake in rats	3-19
	Table 3-4 Comparison of approaches for calculating the DAF for representative gases in determining the HEC - portal of entry ET or nasal effects	3-22
3.3	Major Scientific Advances Related to Inhalation Gas Dosimetry in the TB and PU Regions	3-24
3.3.1	Air Flow and Deposition Modeling in the TB Region	3-25
	Figure 3-7 Distributions of deposition enhancement factor (DEF) for MTBE vapor with $Q_{in} = 30$ L/min in the bifurcation airway models.	3-28
	Figure 3-8 Distributions of deposition enhancement factor (DEF) for ethanol vapor with $Q_{in} = 30$ L/min in the bifurcation airway models.	3-28
	Figure 3-9. The simulated local deposition patterns of naphthalene vapor for concurrent nasal and oral breathing for (A) $K=7.3$ cm ⁻¹ and (B) perfect wall absorption. This figure shows nonuniform deposition patterns and deposition in the upper airways is more uniformly distributed with lower wall absorption. The locations of enhanced deposition may not change; however, the maximum DEF value increases with increasing absorption.	3-30
	Figure 3-10. Total deposition fraction is independent of breathing mode at the larynx and beyond.	3-31
3.3.2	Advances in TB Inhalation Dosimetry Modeling	3-32
	Table 3-5 Modeled predictions of amount of O ₃ and SO ₂ absorbed at various sites in the airways of three species	3-33
3.3.3	Air Flow and Deposition Modeling in the PU Region	3-35
	Figure 3-11 Dynamic ventilation ³ He MRI after inhalation of hyperpolarized ³ He gas.	3-36
	Figure 3-12 Simulated flow velocities from CFD solutions in an alveolar sac model.	3-37
3.3.4	Advances in PU Inhalation Dosimetry Modeling	3-38
3.4	Advances in the Measurement of V _E and Airway Geometry	3-39
3.4.1	Lung Geometry and Surface Area	3-39
	Table 3-6 Estimates of right, left, and total lung volumes in male wistar rats	3-40
	Table 3-7 Summary data on human lung alveolar number and volume	3-41
	Table 3-8 Summary table of measures from right lungs of human cadavers	3-42
	Table 3-9 Functional and morphological features of the developing male rat lung	3-43
3.5	Major Scientific Advances in Inhalation Gas Dosimetry Related to Systemic (SYS) Sites	3-43
3.5.1	Methods and Advances for Estimating Blood:Gas (Air) Partition Coefficients	3-43
3.5.2	Quantitation using Inhalation PBPK Models for Systemic Sites	3-44

Table 3-10	Compilation of blood:gas (air) partition coefficients used in Inhalation PBPK models for animal to human interspecies extrapolation	3-45
3.5.3	Results and Analysis of Systemic Interspecies Inhalation Dosimetry Modeling	3-46
Table 3-11	Estimations from inhalation PBPK models of human equivalent concentrations (HECs) from effect levels and internal dose measures in laboratory animals	3-47
Table 3-12	Comparison of approaches for calculating human equivalent concentrations (HECs) for several gases with systemic (SYS) effects	3-49
3.6	Current Science Related to Children's Inhalation Dosimetry	3-50
3.6.1	Introduction and Focus	3-50
3.6.2	Results and Analysis of Inhalation Dosimetry Modeling Considering Children	3-52
Table 3-13	Human kinetic adjustment factors (UF_{H-TK}) obtained for inhalation exposure in each population group using a dose surrogate of 24 hour AUC_{pc}	3-54
Table 3-14	Air concentration of chloroform at various ages and genders corresponding to threshold of damage in human liver and kidney	3-56
Table 3-15	Age-dependent and gender-specific dose metric comparison of inhaled isopropanol	3-57
Table 3-16	Tissue concentrations in various compartments expressed as adult/child (1 to 2 years old) ratios for 8 different gases	3-59
3.6.3	Respiratory Tract Air Flow Models Considering Children	3-61
Table 3-17	Summary listing of findings on morphometry and gas flow/uptake simulations for human nasal cavities	3-62
Table 3-18	Selected morphologic and simulated modeling results of hydrogen sulfide dosimetry in casts of human nasal cavities	3-63
3.6.4	Respiratory Tract Growth	3-63
Figure 3-13	Alveoli count per lung as a function of age	3-68
Table 3-19	Lung weights (right and left) of males and females from birth to adulthood	3-70
4	FINDINGS AND CONCLUSIONS	4-1
Figure 4-1	A revised schematic representation of the outcomes for interspecies inhalation dosimetry of gases for the ET region following from the advances presented.	4-3
Table 4-1	Overview of major findings related to the state of the science for inhalation dosimetry of gases	4-6
Table 4-2	Summary of major finding related to state of the science of children's inhalation dosimetry	4-7
5	REFERENCES	5-1
APPENDIX A.	SUMMARY AND DISPOSITION OF INDEPENDENT EXTERNAL PEER REVIEW COMMENTS	A-1

AUTHORS, CONTRIBUTORS, AND REVIEWERS

AUTHORS

John J. Stanek

National Center for Environmental Assessment
U.S. Environmental Protection Agency
Research Triangle Park, NC

Eva D. McLanahan

National Center for Environmental Assessment
U.S. Environmental Protection Agency
Research Triangle Park, NC

REVIEWERS

This document has been reviewed by EPA scientists and has undergone a peer review performed by independent scientists external to EPA. A summary of significant comments made by the external peer reviewers, and EPA responses, is included in Appendix A.

INTERNAL EPA SCIENTIFIC CONTRIBUTORS AND REVIEWERS

Robert Benson

Region 8
U.S. Environmental Protection Agency
Denver, CO

Lyle Burgoon

National Center for Environmental Assessment
U.S. Environmental Protection Agency
Research Triangle Park, NC

Jeff Dawson

Office of Pesticide Programs
U.S. Environmental Protection Agency
Washington, DC

Rebecca Dzubow

Office of Children's Health Protection
U.S. Environmental Protection Agency
Washington, DC

Lynn Flowers

National Center for Environmental Assessment
U.S. Environmental Protection Agency
Washington, DC

Brenda Foos

Office of Children's Health Protection
U.S. Environmental Protection Agency
Washington, DC

Suril Mehta

Office of Children's Health Protection
U.S. Environmental Protection Agency
Washington, DC

Elizabeth Mendez

Office of Pesticide Programs
U.S. Environmental Protection Agency
Washington, DC

Deirdre Murphy

Office of Air Quality Planning and Standards
U.S. Environmental Protection Agency
Research Triangle Park, NC

Paul Schlosser

National Center for Environmental Assessment
U.S. Environmental Protection Agency
Washington, DC

Ravi Subramanian

National Center for Environmental Assessment
U.S. Environmental Protection Agency
Washington, DC

John Vandenberg

National Center for Environmental Assessment
U.S. Environmental Protection Agency
Research Triangle Park, NC

John Whalan

National Center for Environmental Assessment
U.S. Environmental Protection Agency
Washington, DC

INTERNAL EPA TECHNICAL REVIEW AND SUPPORT

Ellen Lorang

National Center for Environmental Assessment
U.S. Environmental Protection Agency
Research Triangle Park, NC

J. Sawyer Lucy

Student Services Authority
National Center for Environmental Assessment
U.S. Environmental Protection Agency
Research Triangle Park, NC

Connie Meacham

National Center for Environmental Assessment
U.S. Environmental Protection Agency
Research Triangle Park, NC

EXTERNAL REVIEWERS

Bahman Asgharian, Ph.D.

Principal Scientist
Applied Research Associates
Raleigh, NC

Donald E. Gardner, Ph.D.

President
Inhalation Toxicology Associates, Inc.
Savannah, GA

Panos G. Georgopoulos, Ph.D.

Professor, Department of Environmental and Occupational Medicine
University of Medicine and Dentistry of New Jersey
Robert Wood Johnson Medical School
Piscataway, NJ

Rogene F. Henderson, Ph.D., DABT
Senior Scientist (Retired)
Lovelace Respiratory Research Institute
Albuquerque, NM 87108

Robert F. Phalen, Ph.D.
Professor, Department of Medicine
University of California-Irvine
Irvine, CA

GLOSSARY

Aerosol - A suspension of liquid or solid particles in air.

Chronic Exposure - Multiple exposures occurring over an extended period of time, or a significant fraction of the animal's or the individual's lifetime.

Computational fluid dynamics (CFD) – (Three-dimensional) – A branch of fluid mechanics that uses numerical methods and algorithms to solve and analyze problems of fluid flows. Flows may apply to liquid and gases, including inspired and expired air, and are thus applicable to solving flows within the respiratory tract. The fundamental bases of any CFD problem are the Navier-Stokes equations, which define any single-phase fluid flow. These equations can be simplified by removing terms describing viscosity to yield the Euler equations.

Critical Effect - The first adverse effect, or its known precursor, that occurs as the dose rate increases. Designation is based on evaluation of overall data base.

Diffusion (gas) or Diffusivity (gas) - The transport of matter from one point to another by random molecular motions to become equalized with respect to concentration. For gases, rates of diffusion increase with the temperature and are inversely proportional to the pressure. The interdiffusion coefficients of gas mixtures are almost independent of the composition. Kinetic theory shows that diffusion of a pure gas is inversely proportional to both the square root of the molecular weight and the square of the molecular diameter.

Dorsal - On or near the upper surface (of the nasal tract).

Dosimetric Adjustment Factor (DAF) - A multiplicative factor used to adjust observed experimental or epidemiological data to human equivalent concentration (HEC) for assumed ambient scenario. See also regional gas dose ratio (RGDR).

Extrathoracic or Upper Respiratory Tract (ET/URT) – see Systemic.

Extrathoracic or Upper Respiratory Tract (ET/URT) – The region of the respiratory tract that extends from just posterior to the external nares to just anterior to the trachea.

Flux - The rate of flow of energy, gas or particles across a given surface.

Gas - Term referring to a compressible fluid phase of a substance. Fixed gases are gases for which no liquid or solid can form at the temperature of the gas, such as air at ambient temperatures.

Identical Path Model – (One- or two-dimensional) – An anatomical mathematical model where all paths from the nose or mouth entrance to the alveolar sacs are treated as being identical.

Inhalation Reference Concentration (RfC) - An estimate (with uncertainty spanning perhaps an order of magnitude) of a continuous inhalation exposure to the human population (including sensitive subgroups) that is likely to be without an appreciable risk of deleterious noncancer health effects during a lifetime. The inhalation reference concentration is for continuous inhalation exposures and is appropriately expressed in units of mg/m³.

Henry's Law Constant - The law can be expressed in several equivalent forms, a convenient form being: $C_g = H \times C_l$ where C_g and C_l are the gas-(g) and liquid-(l) phase concentrations. The constant (H) is the ratio at equilibrium of the gas phase concentration to the liquid-phase concentration of the gas (i.e., moles per liter in air/moles per liter in solution).

K_g – The overall mass transfer coefficient describing movement of gas from the air phase into the liquid phase of the respiratory tract (see also MTC).

k_g – The gas phase mass transfer coefficient describing movement of gas from the gas phase to liquid/tissue boundary (see also MTC).

Lowest-Observed-Adverse-Effect Level (LOAEL) - The lowest exposure level at which there are statistically and/or biologically significant increases in frequency or severity of adverse effects between the exposed population and its appropriate control group.

Mass Transfer Coefficient (MTC) - A diffusion rate constant that relates the mass transfer rate, mass transfer area, and concentration gradient as driving force between and through phases. These coefficients may also be viewed in terms of resistance to flow and movement. For purposes of this report (with phases of gas and solid) MTC requires units of mass, time, distance, and concentration: $\text{mol}/(\text{s}\cdot\text{m}^2)$, mol/m^3 , or m/s . Examples of MTCs used in this report relate to movement of gases in the respiratory tract. They include the MTC designated for the gas phase only, k_g , and an overall MTC inclusive of both the gas and liquid phases, K_g .

No-Observed-Adverse-Effect Level (NOAEL) - An exposure level at which there are no statistically and/or biologically significant increases in the frequency or severity of adverse effects between the exposed population and its appropriate control. Some effects may be produced at this level, but they are neither considered adverse nor immediate precursors to specific adverse effects. In an experiment with several NOAELs, the assessment focus is primarily on the highest one for a given critical effect, leading to the common usage of the term NOAEL as the highest exposure without adverse effect.

Physiologically-Based Pharmacokinetic (PBPK) Modeling – (Zero-dimensional) – A mathematical modeling technique for predicting the absorption, distribution, metabolism and excretion of a compound in humans and other animal species. PBPK models strive to be mechanistic by mathematically transcribing anatomical, physiological, physical, and chemical descriptions of the phenomena involved in complex pharmacokinetic processes. These models have an extended domain of applicability compared to that of classical, empirical function based, compartmental pharmacokinetic models.

Portal-of-Entry (POE) Effect - A local effect produced at the tissue or organ of first contact between the biological system and the toxicant.

Pulmonary (PU) – The region of the respiratory tract which includes the terminal bronchioles and alveolar sacs.

Regional Gas Dose (RGD_r) - The gas dose per respiratory tract surface area per minute ($\text{mg}/\text{cm}^2\text{-min}$) calculated for the respiratory tract region of interest (r) as related to the observed toxicity (e.g., calculated for the tracheobronchial region for an adverse effect in the conducting airways). Regions of interest may be the extrathoracic (ET), tracheobronchial (TB), or pulmonary (PU).

Regional Gas Dose Ratio (RGDR_r) - The ratio of the deposited gas dose in a respiratory tract region (r) for the laboratory animal species of interest to that of humans. This ratio is used to adjust the observed gas exposure level for interspecies dosimetric differences.

Sherwood Number (Sh) – A dimensionless term for the ratio of convective to diffusive forces. The air-phase mass transfer coefficient can be defined in terms of the Sherwood number.

Systemic (SYS) – Regions and organs of the body remote to the respiratory tract. Also Extrarespiratory (ER).

Tracheobronchial (TB) – The region of the respiratory tract defined as the trachea to the terminal bronchioles where proximal mucociliary transport begins.

Uncertainty Factors (UF) - Generally 3- or 10-fold factors, used in deriving the inhalation reference concentration (RfC) from experimental data. UFs are intended to account for (1) the variation in sensitivity among the members of the human population, (2) the uncertainty in extrapolating laboratory animal data to humans, (3) the uncertainty in extrapolating from data obtained in a study that is of less-than-lifetime exposure, (4) the uncertainty in using LOAEL data rather than NOAEL data, and (5) an incomplete characterization of the chemical's toxicity that could result in a lower reference concentration if additional data were available.

Vapor - A term referring to a gas phase at a temperature below the critical temperature of the substance where the same substance can also exist in the liquid or solid state. If the gas is in contact with the liquid or solid phase, the two phases will be in a state of equilibrium. This report is intended to consider those agents present as gaseous vapors at ambient temperatures.

Ventral - On or near the lower surface (of the nasal tract).

ABBREVIATIONS AND ACRONYMS

1,1,1-TCE	1,1,1-trichloroethane	GSH	glutathione
1,2,4-TMB	1,2,4-trimethylbenzene	³He	hyperpolarized helium-3
2-BE	2-butoxyethanol	H_{b/g}	blood:air or blood:gas partition coefficient
2-ME	ethylene glycol monomethyl ether	(H_{b/g})_A	animal blood:gas (air) partition coefficient
2D	two dimensional	(H_{b/g})_H	human blood:gas (air) partition coefficient
3D	three dimensional	H_{t/g}	tissue:gas partition coefficient
A	overall or summation hydrogen bond acidity	HEC	human equivalent concentration
ADAM	aerosol-derived airway morphometry	HP	hyperpolarized
ADC	apparent diffusion coefficient	hr	hour
ADH	alcohol dehydrogenase	K	absorption parameter
AMET	amount metabolized per 24 hour period	kg	kilogram
ASPM	axisymmetric single path model	k_g	gas-phase mass-transport coefficient
AUC	area under the curve	K_g	overall mass transfer coefficient
AUC_{pc}	area under the parent compound's arterial blood concentration vs. time curve	k₁	liquid/tissue phase mass transport coefficient
AV	alveolar volumes	L	log of the gas-hexadecane partition coefficient (unitless) at 25 °C
B	overall or summation hydrogen bond basicity	LBGK	Lattice Boltzmann variant
bb	bronchioles	LBM	Lattice Boltzmann method
BB	tracheobronchial	LFER	linear free energy relationship
BW	body weight	LRT	lower respiratory tract
C × t	concentration times time	MeI	methyl iodide
CA	arterial blood concentration	mM	millimolar
CATE	carbon tetrachloride	MR	magnetic resonance
CFD	computational fluid dynamic	MRI	magnetic resonance imaging
CFDM	computational fluid dynamic modeling	MTBE	methyl tertiary butyl ether
C_{max}	maximum concentration	NAS	National Academy of Science
CO₂	carbon dioxide	O₂	oxygen
CT	computed tomography	O₃	ozone
CV	venous blood concentration	PBPK	physiologically-based pharmacokinetic
d	day	PC	partition coefficient
D	diffusivity	PCE	perchloroethylene
D₂O	deuterium oxide	PD	pharmacodynamic
DAF	dosimetric adjustment factor	PDIR	physiological daily inhalation rate
DEF	deposition enhancement factor	PGME	propylene glycol methyl ether
DF	deposition fraction	PGMEA	propylene glycol methyl ether acetate
DLCO	diffusion capacity of carbon monoxide	PK	pharmacokinetic
DLW	doubly labeled water	POD	point of departure
E	solute excess molar refractivity with units of (dm ³ mol ⁻¹)/10	POD_{adj}	point of departure duration adjusted
E_{HR}	hepatic extraction ratio	ppb	parts-per-billion
EAD	effective air space dimension	ppm	parts-per-million
EBZ	ethylbenzene	PU	pulmonary
ECG	energy cost of growth	Q_{alv}	alveolar ventilation rate
EPA	Environmental Protection Agency	Q_b	regional blood flow
ER	extrathoracic	R	radius of the airway
ET	extrathoracic	R_fC	reference concentration
F	flux fraction	RGDR	regional gas dose ratio
fp	fractional penetration	S	solute dipolarity/ polarizability
FQPA	Food Quality Protection Act	SA	surface area
FVC	forced vital capacity	Sh	Sherwood number
g	gram	SO₂	sulfur dioxide
GCMS	gas chromatography mass spectrometry	S_p	available surface area

STP	standard temperature and pressure	URT	upper respiratory tract
SYS	systemic	v	viscosity
t_{1/2}	half-life	Vd	volume of distribution
TAV	time-activity-ventilation	V_E	ventilation rate or minute volume (L/min)
TB	tracheobronchial	VLD_{trans}	volume of gas required to reach transitional bronchioles into the lung
TCE	trichloroethylene	VQ	ventilator equivalent ratio
TDEE	total daily energy expenditure	wk	week
TLC	total lung capacity	XYL	m-xylene
UBA	upper bronchial airway	yr	year
UF_H	uncertainty factor for interindividual human variability		

EXECUTIVE SUMMARY

1 The purpose of this report is to present the findings and conclusions of new scientific
2 developments and advancements in inhalation gas dosimetry for the extrathoracic (ET) or
3 upper respiratory tract (URT), tracheobronchial (TB), pulmonary (PU), and
4 extrapulmonary (systemic, SYS) regions related to the U.S. EPA's 1994 *Methods for*
5 *Derivation of Inhalation Reference Concentrations and Applications of Inhalation*
6 *Dosimetry* ([U.S. EPA, 1994](#)) (hereafter *RfC Methods*). With few exceptions, the studies
7 that contribute to the overall findings and conclusions presented herein were detailed
8 previously in either the 2009 *Status Report: Advances in Inhalation Dosimetry of Gases*
9 *and Vapors with Portal of Entry Effects in the Upper Respiratory Tract* ([U.S. EPA,](#)
10 [2009b](#)) (hereafter *Status I Report*) or the 2011 *Status Report: Advances in Inhalation*
11 *Dosimetry for Gases with Lower Respiratory Tract and Systemic Effects* ([U.S. EPA,](#)
12 [2011b](#)) (hereafter *Status II Report*) and serve as the basis for this final report. A few
13 additional studies were identified since these reports were completed and have been
14 included in this report where appropriate.

15 In this report, as in the prior *Status Reports*, particular emphasis is placed on the kinetic
16 component of the animal to human dosimetric extrapolation in derivation of a chronic
17 reference concentration (RfC) for gases. In addition, as related to the derivation of a
18 chronic RfC, this report summarizes information on inhalation dosimetry throughout the
19 respiratory tract of children (i.e. early lifestages). The primary results from this multi-
20 year review include empirical information related to the assumptions underlying the
21 default approaches described in *RfC Methods*, as well as how the advanced dosimetry
22 modeling techniques and state of the science inform these assumptions. This series of
23 reports, and the conclusions summarized here, provides the scientific foundation
24 necessary for ensuring that methods and guidance used and implemented by EPA in
25 chronic inhalation risk assessment of gases reflect the state of the science. For the most
26 recent information pertaining to the derivation of acute reference concentrations, refer to
27 the Organization for Economic and Co-operation and Development's (OECD) *Guidance*
28 *Document for the Derivation of an Acute Reference Concentration (ARfC)* ([OECD,](#)
29 [2011](#)). For information on the state of the science regarding particulate dosimetry, refer to
30 Chapter 6 of the 2004 particulate matter air quality criteria document ([U.S. EPA, 2004](#))
31 and Chapter 4 and Annex B of the 2009 Particulate Matter Integrated Science
32 Assessment ([U.S. EPA, 2009c, a](#)).

33 **One of the principal findings from these reviews is that internal dose equivalency in**
34 **the ET region for rats and humans is achieved through similar external exposure**
35 **concentrations.** This finding and the underlying evaluation of internal dose equivalency

1 relates to EPA’s methods for interspecies extrapolation and not to potential differences in
2 dosimetry across the human population. Overall, the scientific advances support and, in
3 some cases, build further upon the approaches of the current default methodology, as
4 described in *RfC Methods*, for gas dosimetry in the TB, PU, and SYS regions. **An**
5 **additional overarching finding of this review is the general compatibility of the**
6 **evidence specific to gas dosimetry during early lifestages with the default approach**
7 **for derivation of a chronic RfC as described in *RfC Methods*. An additional**
8 **observation from this review suggests that in some cases, chemical-specific**
9 **information may indicate alternative chemical-specific approaches for shorter-term**
10 **reference values for some specific lifestages.** It is anticipated that information will
11 continue to become available to further inform this issue.

12 Comparative (animal to human) dosimetry is critical to all inhalation assessment
13 activities that relate effects observed in animals to humans. The basic principle involved
14 in comparative dosimetry is the determination of the internal target-tissue dose. This
15 principle, in turn, is founded on the fundamentals of risk, as is stated by the NRC in its
16 1994 publication “Science and Judgment in Risk Assessment” and discussed further in its
17 2009 publication “Science and Decisions: Advancing Risk Assessment”:

18 “... *the target-site dose is the ultimate determinant of risk...*” .

19 The goal of comparative inhalation dosimetry is to characterize the steps leading from (1)
20 estimation of the internal target-tissue dose in an animal resulting from a given external
21 air concentration followed by (2) estimation of the external air concentration to which
22 humans would be exposed to attain that same internal target-tissue dose. The external
23 concentration of a human exposure scenario that produces the equivalent internal target-
24 tissue dose is termed a human equivalent concentration (HEC) in the *RfC Methods*.

25 For gases producing portal-of-entry (POE) effects, the default approximation of the
26 internal target-tissue dose from the external exposure concentration presented in the 1994
27 *RfC Methods* uses species-specific overall minute ventilation (V_E) and the overall surface
28 area (SA) for the respiratory tract region of interest. In the default procedures for gas
29 dosimetry, the *RfC Methods* uses ratios (animal:human) of these measures as a dosimetric
30 adjustment factor (DAF) that is then applied to the animal external exposure
31 concentration to estimate a HEC. The application of the default approach typically results
32 in DAFs of 0.2-0.3 for the ET region and 2-3 for the TB and PU regions. The main
33 assumptions underlying the procedures on gas dosimetry currently in use by the Agency
34 that follow from the application of overall V_E /SA relationships are that there is
35 uniformity of airflow and uniformity of deposition on surfaces.

1 For the ET region, the state of the science presented in the *Status I Report* indicates
2 extensive nonuniformity associated with these measures. This is supported by detailed
3 state of the science estimations of target-tissue dose based on the quantitatively linked
4 airflow and tissue kinetic models. Overall, these advances both provide more information
5 related to airflow and gas deposition as included in the *RfC Methods* and present
6 solutions to accommodate nonuniformity. **A primary finding for gas deposition in the**
7 **ET region is that the internal target-tissue dose equivalency between humans and**
8 **rats is achieved through equivalency at the level of the externally applied**
9 **concentration, i.e., for both rats and humans, the same external air concentration,**
10 **rather than one adjusted by V_E/SA , leads to the similar internal target-tissue dose to**
11 **the URT.**

12 **In contrast, the studies identified in the *Status II Report* addressing overall concepts**
13 **and approaches for POE gas dosimetry in the TB and PU regions of the airways**
14 **support the principles and default procedures in *RfC Methods*.** In some cases these
15 studies suggest and provide examples of further refinement within the existing dosimetry
16 modeling framework of the *RfC Methods* through development and application of mass
17 transfer coefficients as regional measures of gas uptake. Alternative gas dosimetry
18 procedures published using simplified airway models inclusive of the TB and PU regions
19 arrive at tissue metrics that support the default approach of the *RfC Methods*. In addition,
20 recent advances in understanding the airflow to the TB and PU regions have been made.
21 Models and measurements of airflow and deposition in the human PU region generally
22 support the assumption of uniformity as methodological advances and increased
23 resolution of several in vivo imaging techniques indicate highly uniform and
24 homogenous flows in the alveolar regions. On the other hand, examination of the TB
25 regions with human models and advanced dynamic fluid flow programs reveal a degree
26 of nonuniformity of flow for this region although apparently not to the extent that has
27 been documented for the upper airway. As recently demonstrated by Corley et al. [Corley](#)
28 [et al. \(\)](#), the methods for extension of state of the science flow models to the TB and PU
29 areas promise further refinement and resolution for inhalation gas dosimetry.

30 Recently, refined methods for measurement of inhalation rates in humans have been
31 developed. The advent of the doubly labeled water (DLW) technique in estimation of
32 physiological daily inhalation rates (PDIR) has provided resolutions to concerns
33 regarding inhalation patterns of free-living individuals across all age groups including
34 children. These results were summarized in detail in the *Status II Report* ([U.S. EPA,](#)
35 [2011b](#)). DLW-based PDIR values are currently included in the *Child-Specific Exposure*
36 *Factors Handbook* ([U.S. EPA, 2008](#)), and are being proposed for inclusion in other key
37 Agency documents, including the updated *Exposure Factors Handbook* ([2011a](#)), for all
38 ages including children.

1 Marked advances in our understanding of the morphometry of upper respiratory tract
2 regions in both animals and humans are being achieved with the development and
3 application of stereology. These techniques, described as the estimation of higher
4 dimensional information from lower dimensional samples, have and continue to provide
5 more accurate estimates of flow to regions of the respiratory tract. Most of these
6 advancements, however, apply to humans and comparable information in the laboratory
7 animal, the critical comparative component of interspecies extrapolation, lags. The
8 currently available information in this area supports improvements in dosimetry
9 modeling.

10 As recognized by *RfC Methods*, with regard to dosimetry beyond the respiratory tract, the
11 principal determinative component for dosimetry is the highly chemical-specific
12 blood:gas (air) partition coefficient ($H_{b/g}$). The $H_{b/g}$ is also a key parameter of
13 physiologically-based pharmacokinetic (PBPK) models, models that are of ever
14 increasing utility to the risk assessment community. Different techniques and approaches
15 have been proposed to derive these values for both human and laboratory animals. A set
16 of key reviews ([Abraham et al., 2005](#); [Payne and Kenny, 2002](#)), compiling and analyzing
17 results from several of these approaches, makes several conclusions relevant to dosimetry
18 and risk assessment, including that there appears to be no difference between human and
19 laboratory animal values for a prominent subgroup of toxic gases, the volatile organics.
20 Examination and compilation of $H_{b/g}$ s in published inhalation PBPK models configured
21 for interspecies comparisons was also undertaken. **These findings also provide evidence**
22 **that the current default dosimetry approach of *RfC Methods* that uses $H_{b/g}$ s as a**
23 **basis of dosimetry for systemic toxicity remains valid.**

24 As presented in the *Status II Report*, recent research relevant to inhalation gas dosimetry
25 in children was found to closely follow the recommendations and guidance of the
26 National Academy of Sciences (NAS) on children's risk ([NRC, 1993](#)). These
27 recommendations include use of PBPK models to explore and evaluate potential child
28 susceptibility as well as the related effort to generate accurate measurements and
29 parameters to be used in these models. A number of studies were reviewed that followed
30 from these activities including development of physiological-based daily inhalation rates,
31 morphometry of conducting airways and lung tissue using advanced state of the science
32 techniques, as well as respiratory tract function using new highly refined in vivo analyses
33 of airway function. Sophisticated flow models that use these refined measures and that
34 are capable of examining uptake differences of gases in the upper airways of both adults
35 and children are also presented and discussed. Several PBPK models have been
36 configured and parameterized with results from these newer techniques to consider child
37 versus adult dosimetry. Although few datasets and models pertaining to gas dosimetry in
38 children exist, the spectrum of methods and approaches is robust. **In several cases, the**

1 **available methods and modeling approaches are fairly uniform in their indications**
2 **of potential higher inhaled doses in young children (3 mo), which may be 2- to 3-fold**
3 **more than in adults.** Individual instances exceeding this range are also found but no
4 apparent pattern appears to be associated with these occurrences. This range is within that
5 built into *RfC Methods* using the human interindividual uncertainty factor (UF_H) to
6 accommodate pharmacokinetic and pharmacodynamic variability and for consideration of
7 potential sensitive population and lifestages including children. It should be noted that
8 this finding is very similar to that of the NAS ([NRC, 1993](#)).

9 This review also provides a gas characterization scheme that differs fundamentally from
10 the categories that guide selection of a default dosimetric adjustment approach in *RfC*
11 *Methods*. The *RfC Methods* gas scheme related physicochemical properties of gases to a
12 numerical category; this category was then related to the observed toxicity, including that
13 of the target tissue. In its implementation, however, complexities associated with
14 categorizing gases often placed greater emphasis on physicochemical properties (rather
15 than target tissue observations) when identifying the default dosimetric adjustment
16 approach. The scheme featured in this report may provide the basis for constructing an
17 improved and simplified descriptor approach for characterizing gases that relates the
18 properties of the gas directly to the site of the observed toxicity without the need for
19 categorization. An improved scheme would also need to properly account for and
20 incorporate the potential role of metabolism.

1 INTRODUCTION AND PURPOSE

1 The purpose of this report is to evaluate and summarize the pertinent scientific
2 developments and advancements in gas dosimetry focusing on extrathoracic (ET) or
3 upper respiratory tract (URT), tracheobronchial (TB), pulmonary (PU), and
4 extrapulmonary (systemic, SYS) inhalation dosimetry related to the current methodology
5 used by EPA. Particular emphasis is placed on animal to human dosimetric extrapolation
6 performed in derivation of a chronic reference concentration (RfC). An RfC is defined as
7 an estimate (with uncertainty spanning perhaps an order of magnitude) of a continuous
8 inhalation exposure for a chronic duration (up to a lifetime) to the human population
9 (including sensitive subgroups) that is likely to be without an appreciable risk of
10 deleterious effects during a lifetime. In addition, this report summarizes available data
11 pertaining to inhalation dosimetry throughout the respiratory tract of children as it relates
12 to derivation of an RfC. This report provides the scientific foundation necessary for
13 ensuring that methods and guidance used and implemented by EPA in inhalation risk
14 assessment of gases reflects the state of the science.

15 The current guidance, *Methods for Derivation of Inhalation Reference Concentrations*
16 *and Application of Inhalation Dosimetry* ([U.S. EPA, 1994](#)) [hereafter *RfC Methods*], was
17 made publicly available in 1994. *RfC Methods* is used by EPA in developing RfCs for the
18 Agency's IRIS (Integrated Risk Information System) public database. *RfC Methods*
19 addresses broad areas of risk assessment but focuses especially on inhalation dosimetry
20 and provides methods for converting inhalation exposures in laboratory animals to human
21 equivalent exposure concentrations (HECs). Sections devoted to inhalation dosimetry are
22 extensive including information on respiratory tract function and anatomy, physiology,
23 and pathology in humans and typical laboratory animals. Other sections explore the
24 properties of inhaled agents (e.g., particles and gases). In critical areas where important
25 observations and application processes were not yet available, reasoned approaches based
26 on scientific theory were given. These data, theories, and empirical observations were
27 then synthesized into methods applicable to RfC derivation. These methods are also
28 discussed in *A Review of the Reference Dose and Reference Concentration Processes*
29 ([U.S. EPA, 2002](#)).

30 Since 1994, significant advancements have occurred throughout risk assessment sciences;
31 in particular, interspecies comparative dosimetry of gases eliciting effects in the upper
32 respiratory tract (URT). Since many of these advancements impact core components of
33 the *RfC Methods* a need was recognized to assess the state of the science in this area.

34 In 2009, the document *Status Report: Advances in Inhalation Dosimetry of Gases and*
35 *Vapors with Portal of Entry Effects in the Upper Respiratory Tract* ([U.S. EPA, 2009b](#)),
36 hereafter *Status I Report*, was completed. The purpose of the *Status I Report* was to
37 evaluate scientific developments and advancements since 1994 in the area of gas

1 dosimetry, focusing on the ET region, and to determine how this information might
2 inform our approach to gas dosimetry. In 2011, a similar report titled *Advances in*
3 *Inhalation Dosimetry for Gases with Lower Respiratory Tract and Systemic Effects* ([U.S.](#)
4 [EPA, 2011b](#)), hereafter *Status II Report*, was completed. The *Status II Report* focused on
5 the remaining regions comprising the lower respiratory tract or thoracic (TH) region as
6 designated by *RfC Methods*, the TB and PU regions. The *Status II Report* also included
7 new information to inform inhalation dosimetry for systemic effects of gases. The focus
8 of the evaluations in the *Status I and II Reports* were based on the results from an expert
9 panel assembled in 2005 and tasked with reviewing the state of the science of inhalation
10 gas dosimetry in relationship to the *RfC Methods*.

11 The *Status II Report* also evaluated new data and approaches for inhalation dosimetry of
12 gases in children (birth through adolescence). This area was included in recognition of
13 the Agency's commitment to ensuring that EPA actions are protective of children, given
14 the potential for sensitivity of childhood lifestages to some environmental exposures. *RfC*
15 *Methods* currently considers children within the intraspecies uncertainty factor intended
16 to account for intrahuman variability in response among sensitive populations and
17 lifestages within the population but devotes no further analysis to the matter.
18 Furthermore, U.S. EPA ([2002](#)) additionally considers children within the database
19 uncertainty factor.

2 REVIEW OF THE 1994 *RfC METHODS* FOR GAS DOSIMETRY

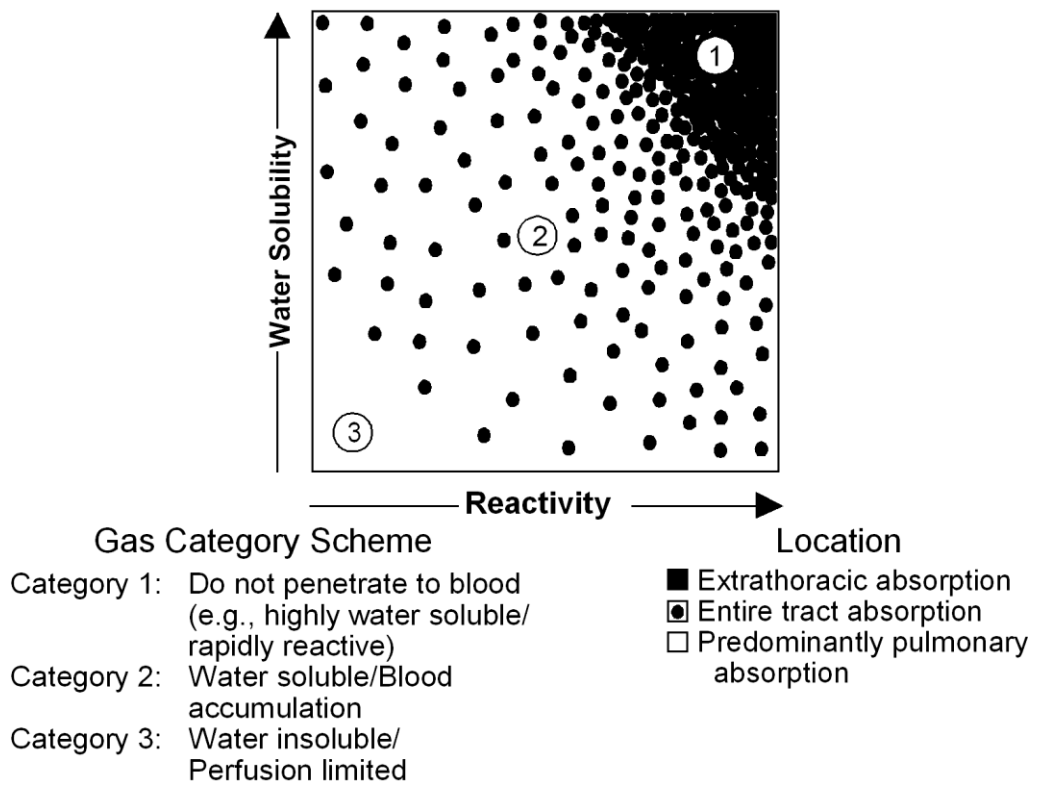
This section provides a brief overview of the important concepts governing the current default method for inhalation gas dosimetry and its application as outlined in the 1994 *RfC Methods*. In addition, an overview is provided regarding how the *RfC Methods* account for inhalation dosimetry in children. These concepts serve as the basis for comparison and examination with the state of the science provided in Section 3.

2.1 Gas Categorizations - General

Numerous model structures have been used for describing aspects of toxicant uptake, including gases and particles, in the respiratory tract. Common uptake modeling schemes are often founded on the physicochemical characteristics of the gases to which they are applied. These uptake schemes are frequently based on the chemical-specific physicochemical characteristics (e.g., solubility and reactivity) of the subject gases, and described in terms of a qualitative continuum (e.g., low, moderate, or high). Therefore, any model scheme comprised of discrete categories has limited application to the broad range of gases that exist and that the RfC methodology must evaluate.

2.1.1 The *RfC Methods* Gas Categorization Scheme

The three category gas scheme currently in *RfC Methods* was constructed based on physicochemical characteristics as determinants of gas uptake as shown in Figure 2-1. A similar scheme has been developed by the International Commission on Radiological Protection ([ICRP, 1993](#)). The numerical gas categories are placed on this scheme relative to their character of these determinants; Category 1 in the upper right hand corner corresponding to high reactivity and high water solubility; Category 3 in the lower left hand corner corresponding to low reactivity and low water solubility; and Category 2 occupying the area intermediate to the other two categories. Category 1 gases are indicated to be absorbed in the ET region which corresponds generally to the nasal cavity. Category 3 gases are indicated to be absorbed in the deeper pulmonary region, distal to the ET region, whereas Category 2 gases are indicated to be absorbed throughout the entire respiratory tract. Detail describing the regions of the respiratory tract is included in Section 2.2.1.2 of this report.



Note: Reactivity is defined to include both the propensity for dissociation as well as the ability to serve as a substrate for metabolism in the respiratory tract. Definitive characteristics of each category and anticipated location (region) for respiratory tract uptake are shown.

Source: U.S. EPA (1994).

Figure 2-1 Gas categorization scheme based on water solubility and reactivity as major determinants of gas uptake.

Table 2-1 summarizes the characteristics of these categories and provides examples in accordance with the *RfC Methods*. The definition of reactivity includes both the propensity for dissociation as well as the ability to serve as a substrate for metabolism in the respiratory tract.

Table 2-1 Gas categorization characteristics and examples according to RfC Methods classification scheme

Category	Characteristics				Examples
	Water solubility	Reactivity	Accumulation in blood	Site of Toxicity	
1	High	Rapidly irreversibly reactive	Not significant	Portal of entry	Hydrogen fluoride, chlorine, formaldehyde, volatile organic acids and esters
2	Moderate	Rapidly reversibly reactive, or moderately to slowly irreversibly metabolized in respiratory tract tissue	Potential	Portal of entry, maybe systemic	Ozone, sulfur dioxide, xylene, propanol, isoamyl alcohol
3	Low	Unreactive in surface liquid and tissue	Yes	Systemic toxicity	Styrene

2.2 Conceptual and Historical Basis for Comparative Dosimetry of Inspired Gases in *RfC Methods* – Minute Ventilation/Surface Area of the Respiratory Tract (V_E/SA_{RT})

The *RfC Methods* presents an in-depth consideration of what was known about dosimetry of inspired gases in different species *i* at the time of publication, with expansive commentary on the fundamental underlying determinants of dosimetry. These included species differences in anatomical and physiological characteristics of the respiratory tracts, the wide range of physicochemical properties associated with inhaled chemicals, the diversity of cell types that may be affected throughout the respiratory tract, as well as the many mechanistic and metabolic differences, all combining to make characterization of dosimetry particularly complex.

This section briefly reviews and summarizes knowledge of several of the most critical determinants of inhalation dosimetry that define and control the inhaled gas dose as well as presenting the underlying basis for the *RfC Methods* interspecies normalization of the gas dose. Scientific and technical advances informing these critical determinants are described in Section 3.

2.2.1 Factors Controlling Comparative Inhaled Dose

Factors that determine inhaled gas dose are related to (1) respiratory anatomy and physiology and (2) the physicochemical characteristics of the inhaled gas. The health

effect or response that results from an inhaled gas dose is directly related to the target-tissue dose. However, any description of the continuum defined by exposure, dose, and response requires integration of quantitative knowledge of determinants of chemical disposition, toxicant-target interactions, and tissue responses into an overall model of pathogenesis. Among other things, this process would involve determining the dose delivered to the target organ of various species as well as determining the sensitivity of the target organ to that dose. Once such aspects of dosimetry have been established and species sensitivity has been accounted for, the effective chemical concentration in laboratory animals can be quantitatively related to dose responses in humans. Models employed to perform this interspecies extrapolation would incorporate parameters such as species-specific anatomical and ventilatory differences, metabolic processes, as well as the physicochemical properties of the pollutant and should be based upon the physiological factors that govern transport and removal of the pollutant.

2.2.1.1 Comparative Respiratory Anatomy and Physiology

The respiratory systems of humans and various experimental animals, especially rodents which are the most frequently studied experimental species, differ markedly in numerous quantitative and qualitative aspects of anatomy and physiology. These differences affect critical aspects such as air flow patterns in the respiratory tract and thus deposition and retention of the agent. New information on measurements of anatomical and physiological parameters (i.e. V_E and SA) were discussed in the *Status II Report* according to respiratory regions and branching patterns as it related to derivation of an RfC. A summary of these findings are provided in Section 3.4 of this report.

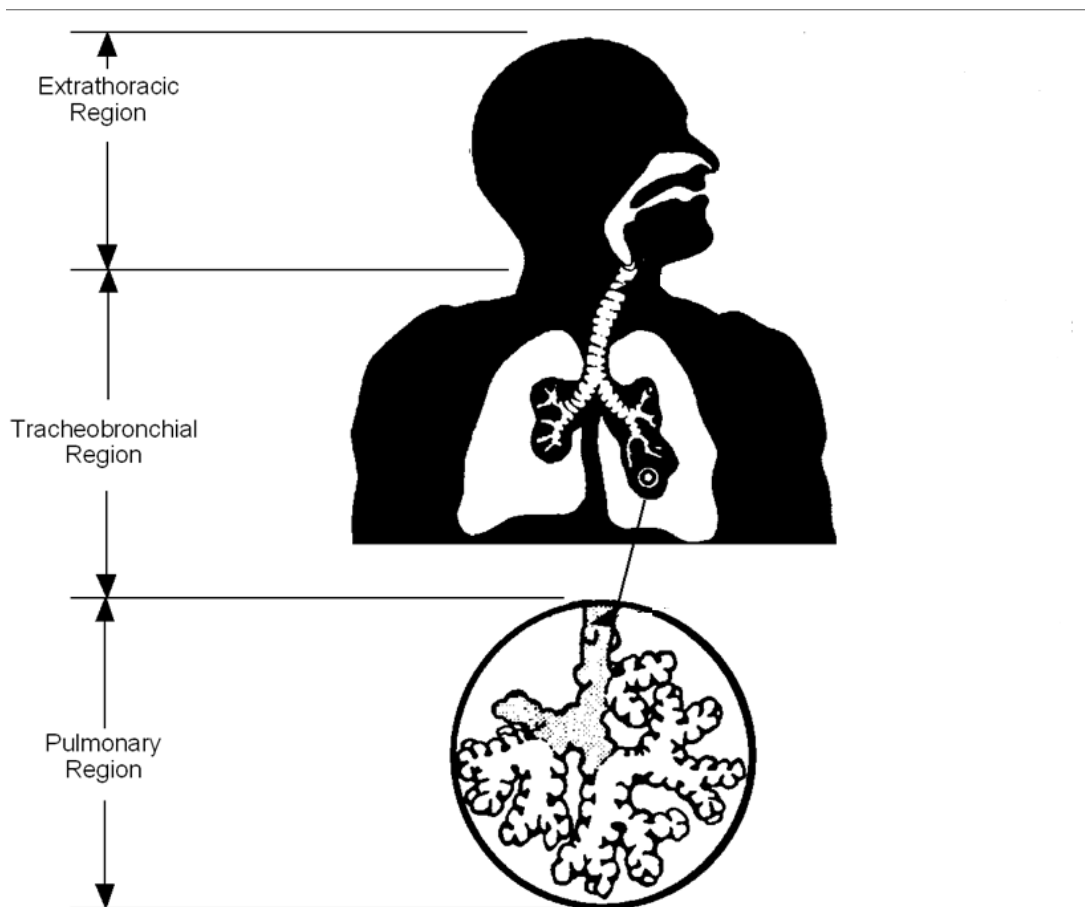
2.2.1.2 Regions of the Respiratory Tract Common among Species

The respiratory tract in both humans and experimental animals including the commonly used murine species (i.e., rats and mice) can be divided into three similar regions on the basis of structure and function: the extrathoracic region (ET) that extends from just posterior to the external nares to just anterior to the trachea, the tracheobronchial region (TB) defined as the trachea to the terminal bronchioles where proximal mucociliary transport begins, and the pulmonary region (PU) including the terminal bronchioles and alveolar sacs. The thoracic (TH) region or lower airways is defined as the TB and PU regions combined. The anatomic structures included in each of these respiratory tract regions are listed in Table 2-2 and Figure 2-2 provides a diagrammatic representation of these regions in humans.

Table 2-2 Respiratory tract regions

Region		Anatomic Structures	Other Terminology
Extrathoracic (ET)		Nose	Head airways region
		Mouth	Nasopharynx (NP)
		Nasopharynx	Upper respiratory tract (URT)
		Oropharynx	Upper airways
		Laryngopharynx	
		Larynx	
Thoracic (TH)	Tracheobronchial (TB)	Trachea Bronchi Bronchioles (to terminal bronchioles)	Conducting airways
	Pulmonary (PU)	Respiratory bronchioles (not found in rodents) Alveolar ducts and sacs Alveoli	Gas exchange region Alveolar region Parenchyma

Source: Adapted from Phalen et al. ([1988](#)).



Source: U.S. EPA (1994).

Figure 2-2 Diagrammatic representation of the three respiratory tract regions designated in humans.

These interspecies similarities occur only at this very general level of organization, as analysis at any more refined level begins to reveal marked differences. A more complete listing and analysis of comparative airway anatomy differences between humans and murine species is available in the *RfC Methods*.

2.2.1.2.1 Surface Areas (SA) of Common Respiratory Regions

The existence of these general functional regions, the ET, TB and the PU, within the respiratory tracts of humans and murine laboratory species has been thoroughly documented. It is through, within, around, and over these regions that inspiratory and expiratory air flows.

Considerable effort in the scientific community has been expended on estimating the surface areas (SA) for each of these respiratory tract regions for both humans and a

number of the common laboratory test species. Some accepted values for the SA of these various regions are given in the *RfC Methods* and reproduced below, complete with sources listed in the *RfC Methods* in Table 2-3.

Table 2-3 Default surface areas for the extrathoracic (ET),tracheobronchial (TB), and pulmonary (PU) regions of the respiratory tract in various species

Species	ET (cm ²)	Source	TB (cm ²)	Source	PU (cm ²)	Source
Human	200.0	Guilmette et al. (1989)	3,200	Mercer et al. (1994b)	540,000	Mercer et al. (1994a)
Mouse	3.0	Gross et al. (1982)	3.5	Mercer et al. (1994b)	500	Geelhaar and Weibel (1971); Mercer et al. (1994a)
Hamster	14.0 ^a		20.0	Yu and Xu (1987)	3,000	Lechner (1978)
Rat	15.0 ^b	Gross et al. (1982)	22.5	Mercer et al. (1994b)	3,400	Mercer et al. (1994a)
Guinea pig	30.0	Schreider and Hutchens (1980)	200.0	Schreider and Hutchens (1980)	9,000	Tenney and Remmers (1963)
Rabbit	30.0	Kliment (1973)	300.0	Kliment (1973)	59,000	Gehr et al. (1981)

^aNo measurements of hamster ET surface area were found in the literature. This value is estimated based on similarity of the other regional surface areas to the rat.

^bAdditional unpublished measurements of the surface area beyond the ethmoid turbinates are included.

Source: U.S. EPA (1994)

2.2.1.2.2 Comparative Respiratory Ventilation Rates (V_E)

The means by which exposures of any respiratory surface would occur from agents in the air is most likely and logically via the agent concentration present within the inspired and expired air -- the ventilation rate (i.e., minute volume), V_E.

The *RfC Methods* provides procedures and parameters for calculating typical ventilation rates, V_E, expressed as total volume of air inspired in a minute, both for laboratory test animals and for humans. The default values for ventilation rate [V_E = tidal volume (V_T) × breathing frequency (f)] are based on accepted body weight allometric scaling equations provided in the literature.

The basis of interspecies allometric scaling is to account for disproportionalities between species. It should be kept in mind that these disproportionalities manifest because smaller species have proportionally greater V_E per unit body weight than larger species. V_E also varies with age, activity, and disease.

RfC Methods provides species-specific values or algorithms to generate values for V_E required to derive the RGDR for the ET, TB, and PU regions. The listing of the coefficients used to generate V_E given in *RfC Methods* are presented below in Table 2-4. In addition, the typical default body weight and calculated V_E for several species and strains of laboratory animals used in chronic studies are shown in Table 2-5.

For purposes of interspecies scaling, the *RfC Methods* specifies a default body weight for the human of 70 kg, and a corresponding V_E of 13.8 L/min or 20 m³/day.

Table 2-4 Intercept (b_0) and coefficient (b_1) values used to calculate default ventilation rates based on body weight^a

Species	b_0	b_1
Rat	-0.578	0.821
Mouse	0.326	1.050
Hamster	-1.054	0.902
Guinea pig	-1.191	0.516
Rabbit	-0.783	0.830

^aCalculation of default ventilation rate based on body weight is conducted using the following algorithm:
 $((\ln V_E[\text{L/min}]) = b_0 + b_1 \times \ln (\text{BW}[\text{kg}]))$

Source: U.S. EPA ([1994](#))

Table 2-5 Default ventilation rate and body weights for multiple species

Species & Strain	V _E (L/min)		BW (kg)	
	Male	Female	Male	Female
Rats				
Fisher 344	0.254	0.167	0.380	0.229
Sprague-Dawley	0.445	0.381	0.523	0.338
Long-Evans	0.429	0.383	0.472	0.344
Osborne-Mendel	0.443	0.401	0.514	0.389
Wistar	0.426	0.364	0.462	0.297
Mice				
B6C3F1	0.043	0.041	0.037	0.035
BAF1	0.036	0.030	0.026	0.022
Hamsters				
Syrian	0.159	0.164	0.134	0.145
Chinese	0.100	0.097	0.041	0.038
Guinea pigs				
[Not specified]	0.296	0.294	0.890	0.860
Rabbits				
New Zealand	0.737	0.749	3.76	3.93

Source: U.S. EPA ([1994](#))

2.3 Normalization of Inhaled Concentration to Surface Area of Respiratory Tract Regions

2.3.1 Dose-Response in Respiratory Tract Tissues is Based on External Exposure Concentration

A central consistent observation from inhalation exposure has been the capacity of the external exposure concentration to establish and explain the response in the respiratory tract. Pathology in laboratory animals from inhalation exposure to a variety of agents has characterized responses in the ET, TB and PU regions of the respiratory tract. Response characterization based on external exposure concentration has been thorough, extending from the basis of structure and cell biology, from various mechanisms of toxic action, as well as response to injury. Some studies and responses to inhalation exposures have been characterized by inclusion of other variables, e.g. that some responses may follow a concentration \times duration ($C \times t$) relationship. Even with advanced dose-response modeling approaches for inhalation exposures, the inception of any analysis is the external exposure concentration.

Transformation of the external exposure concentration in air from typical units of ppm or mass chemical per unit volume air to other units, such as total mg/day, does not provide a metric with a direct relationship to response, especially when the response being characterized is a POE response involving one of the surfaces in the respiratory tract. For extremely reactive gases, deposition may only occur in the first few centimeters of the ET, thus invalidating even those metrics based on the overall surface area of the ET.

2.3.2 Normalization of External Exposure Concentration to Surface Areas

The basic dosimetry scheme put forth by the *RfC Methods* was based largely on conclusions of work by Chang and coworkers (1983) such that normalizing the dosimetry to nasal surface area could lead to better understanding of species differences in nasal toxicity. In the *RfC Methods*, inhaled dose to the respiratory tract is based on species – specific relationships of minute ventilation and surface areas associated with the target regions of the respiratory tract:

$$V_E / SA_{ET,TB} \text{ or } PU$$

2.4 Interspecies Gas Dosimetry in the RfC - Application of V_E/SA in Calculation of the Human Equivalent Concentration, HEC: The Default Approach for Inspired Gases

The overall goal of the RfC procedures is to estimate toxicokinetically equivalent doses to target tissues in laboratory animals to those of humans. *RfC Methods* gives application procedures for these various components to produce an estimate of a human equivalent concentration (HEC). *RfC Methods* elaborates upon and outlines practices and data requirements for other procedures that are arranged in a hierarchy of approaches for estimations of human equivalent concentrations for gases (see Table 2-6). The approach discussed and analyzed in this report relative to new information is that of the “default” approach only, the most generalized and data limited situation where information is limited to that discussed thus far in this report, principally species V_E and SA for the various regions of the respiratory tract. As indicated in the hierarchy scheme, the default approach would be bypassed when more sophisticated or chemical-specific models are available (e.g. PBPK, CFD, and CFD-PBPK hybrid).

Table 2-6 Hierarchy of model structures for dosimetry and interspecies extrapolation

Optimal model structure
Structure describes all significant mechanistic determinants of chemical disposition, toxicant-target interaction, and tissue response
Uses chemical-specific and species-specific parameters
Dose metric described at level of detail commensurate to toxicity data
Default model structure
Limited or default description of mechanistic determinants of chemical disposition, toxicant-target interaction, and tissue response
Uses categorical or default values for chemical and species parameters
Dose metric at generic level of detail

Source: U.S. EPA (1994)

2.4.1 The Dosimetric Adjustment Factor (DAF)

The purpose of dosimetry is to calculate an internal dose metric (e.g., target tissue dose, steady-state blood concentration) that results from an experimentally applied laboratory animal dose (or concentration) and estimate a human exposure dose (or concentration) that would result in an equivalent dose metric. Below, the steps currently used, according to the 1994 *RfC Methods*, for the dosimetric adjustment procedure for deposition in the TB and PU regions, as well as the SYS adjustment, are reviewed.

Equation 2-1 is a general equation that may be applied to estimate a human equivalent concentration (HEC) from an animal point of departure (POD). The POD corresponds to an exposure concentration at which a particular effect is observed (or not observed in the case of a NOAEL) in response to a particular exposure scenario of interest (duration and frequency). The subscript “ADJ” refers to a duration adjustment (i.e., $C \times t$) that converts the POD from the actual exposure concentration to an average daily exposure concentration for a continuous exposure scenario. This adjustment will not be considered further as it is not a focus of this report.

$$\text{POD}_{\text{HEC}} (\text{mg}/\text{m}^3) = \text{POD}_{\text{ADJ}} (\text{mg}/\text{m}^3) \times \text{DAF}_r$$

Equation 2-1

The DAF_r is the dosimetric adjustment factor for a respiratory tract region, where r in this report refers to ET, TB, PU, or SYS. As can be seen here, the DAF is a factor used to convert an average exposure concentration for a particular laboratory species to an

estimate of a constant exposure concentration for humans that would result in the same delivered dose, the HEC. When evaluating toxicity following inhalation exposure, in particular, dose refers to the mass of toxicant absorbed across an airway surface per unit surface area. Also, for such POE (e.g., ET, TB and PU) effects, the DAF is termed the regional gas dose ratio (RGDR) and depends on animal to human ratios of two important parameters: minute volume or ventilation rate (V_E), and surface area (SA) of the target region. When evaluating SYS effects, the DAF depends on the ratio of animal and human blood:gas partition coefficients ($H_{b/g}$).

2.4.2 The DAF for POE Effects; the Regional Gas Dose Ratio, RGDR_r

The equations to derive the regional gas dose ratio (RGDR_r) for different gas categories and for the various regions of the respiratory tract (versus remote sites) are provided and described further in *RfC Methods*. As outlined in more detail in the *Status I Report*, the basic default (or reduced) equation given in *RfC Methods* used to calculate the RGDR, i.e., the DAF, for gases incorporates basic determinants of inhaled dose — species-specific minute ventilation and surface areas:

$$\mathbf{RGDR_r = \frac{(V_E / SA_r)_A}{(V_E / SA_r)_H}}$$

Equation 2-2

where:

V_E = ventilation rate (L/min),

SA_r = surface area of the exposed respiratory tract region (cm²), and

A, H = subscripts denoting laboratory animal and human, respectively.

Basically, the RGDR_r is used as the DAF in Equation 2-1 to dosimetrically adjust the experimental POD (duration adjusted or not) to estimate an HEC POD (POD_{HEC}) as follows:

$$\mathbf{POD_{(HEC)} (mg/m^3) = POD_{(ADJ)} (mg/m^3) \times RGDR_r}$$

Equation 2-3

RGDR_r can be seen to be equal to the ratio of the RGD in laboratory animal species to that of humans (RGD_r)_A/(RGD_r)_H.

2.4.3 Assumptions in the Application of V_E/SA

Application of the species specific values of V_E/SA for dosimetric adjustment has resulted in considerable scientific debate. This debate has led to the identification and clarification of assumptions made, either explicitly or implicitly, underlying the default dosimetric procedures for interspecies extrapolation. It is these assumptions, the most critical and significant of which are listed below, that provide a basis for evaluation and refinement of the dosimetric procedures used by the Agency as they related to the state of the science.

Assumption 1 – Since V_E is the parameter used to describe the inspiratory flow, the flow of the gas through the respiratory tract region of interest is assumed to be uniform. At the time of the *RfC Methods* development, nonuniformity was suspected although there was no substantial basis to quantitatively evaluate its extent.

Assumption 2 – The SAs of the respiratory tract regions exposed to the inspired gas are uniform and equivalent, i.e., the cell types, relative amount, and distributions are equivalent in human and animal species. Although considered valid for the general regions of the respiratory tract, the available SAs incorporate no further refinement regarding tissue- or cell-types within any region. It represents an average for surface areas that usually contain nonuniform, sometimes widely divergent cell types. Under the *RfC Methods* the most refinement that can be achieved with V_E/SA is essentially limited to the SA term in the denominator. As discussed in the *Status I Report*, this report, and the *RfC Methods*, such an assumption may be most problematic for the ET, a region that may be considered the most anatomically complex, divergent, and varied in tissue type of all regions in the respiratory tract.

Assumption 3 - The inspired gas is uniformly distributed (deposited) over the entire surface of the respiratory tract region in question. A further assumption for gases with POE effects is that the deposition/uptake is complete or 100% in the region in question and is the same in animals and humans as deposition/uptake information for humans is frequently lacking. Together these assumptions allow for the application of V_E/SA . In addition, inspection of the V_E/SA relationship reveals that modulation of either V_E or SA would directly influence the “intensity” or flux of the gas deposited to the SA. For example, increasing V_E and decreasing the SA would increase the estimated flux at the SA; decreasing V_E and increasing the SA would decrease the flux at the SA. Perhaps the most obvious inconsistency of this assumption is the empirically demonstrable proximal to distal, high to low concentration response gradient is known to occur for gases that produce respiratory tract lesions. Also, for gases extensively scrubbed from the upper airways (the ET region) such as formaldehyde, the assumption of 100% uptake/absorption may be valid. However, this assumption cannot be valid for a great many other gases. These issues as well as many others critical to the practice of

inhalation interspecies dosimetry as outlined in *RfC Methods* are evaluated in the *Status I and II Reports* and briefly reviewed in Section 3.

2.5 Current Applications Using the Default DAFs – RGDR_{ET}, RGDR_{TB}, RGDR_{PU}, and H_{b/g}

2.5.1 The RGDR for the Extrathoracic Region – RGDR_{ET}

The DAF for the ET region is the “regional gas dose, extrathoracic” ratio (RGDR_{ET}). It is constructed with species-specific ventilation rates (or minute volumes) and surface areas for the ET region ([U.S. EPA, 1994](#)).

The equation for deriving a default RGDR_{ET} for reactive and water soluble (e.g., Category 1) gases as it appears in *RfC Methods* ([U.S. EPA, 1994](#)) (Equation 4-18 and Appendix I, Equation I-19) is shown in Equation 2-4, where V_E is the ventilation rate (L/min) and SA_{ET} the surface area (cm²) of the ET region for laboratory animals (A) or humans (H).

$$\text{RGDR}_{\text{ET}} = \frac{\left(\frac{V_E}{\text{SA}_{\text{ET}}}\right)_A}{\left(\frac{V_E}{\text{SA}_{\text{ET}}}\right)_H}$$

Equation 2-4

Shown below is an example calculation of the DAF for the ET region using Equation 2-4 for a rat to human extrapolation assuming a rat V_E of 0.250 L/min and SA of 15 cm² and a human V_E of 13.8 L/min and SA of 200 cm².

$$\text{RGDR}_{\text{ET}} = \frac{\left(\frac{0.25 \text{ L/min}}{15 \text{ cm}^2} \right)_{\text{A}}}{\left(\frac{13.8 \text{ L/min}}{200 \text{ cm}^2} \right)_{\text{H}}} = 0.24$$

Equation 2-4 (example)

The calculation using these default parameters ([U.S. EPA, 1994](#)) results in a RGDR_{ET} of 0.24 indicating an assumption that humans would receive approximately 4 times ($1/0.24 = 4.17$ -fold) more dose in the ET region on a per SA unit basis than rats.

2.5.2 The RGDR for the Tracheobronchial (TB) Region - RGDR_{TB}

The DAF for the TB region is the “regional gas dose, tracheobronchial” ratio (RGDR_{TB}). It is constructed with species-specific ventilation rates (or minute volumes) and surface areas for the TB region ([U.S. EPA, 1994](#)).

The equation for deriving a default RGDR_{TB} for reactive and water soluble (e.g., Category 1) gases as it appears in *RfC Methods* ([U.S. EPA, 1994](#)) (Equation 4-22 and Appendix I, Equation I-24) is shown in Equation 2-5, where V_{E} is the ventilation rate (L/min) and SA_{TB} the surface area (cm^2) of the TB region for laboratory animals (A) or humans (H). More detailed information on the derivation of the default equation is provided in the *Status II Report*.

$$\text{RGDR}_{\text{TB}} = \frac{\left(\frac{V_{\text{E}}}{\text{SA}_{\text{TB}}} \right)_{\text{A}}}{\left(\frac{V_{\text{E}}}{\text{SA}_{\text{TB}}} \right)_{\text{H}}}$$

Equation 2-5

Shown below is an example calculation of the DAF for the TB region using Equation 2-5 for a rat to human extrapolation assuming a rat V_{E} of 0.250 L/min and SA of 22.5 cm^2 and a human V_{E} of 13.8 L/min and SA of 3,200 cm^2 .

$$\text{RGDR}_{\text{ET}} = \frac{\left(\frac{0.25 \text{ L/min}}{22.5 \text{ cm}^2} \right)_{\text{A}}}{\left(\frac{13.8 \text{ L/min}}{3,200 \text{ cm}^2} \right)_{\text{H}}} = 2.6$$

Equation 2-5 (example)

The calculation using these default parameters ([U.S. EPA, 1994](#)) results in a RGDR_{TB} of 2.6 indicating the assumption that rats would receive nearly 3 times more dose in the TB region on a per SA unit basis than humans.

2.5.3 The RGDR for the Pulmonary (PU) Region - RGDR_{PU}

The DAF for the pulmonary region is the “regional gas dose ratio, pulmonary” ratio (RGDR_{PU}). It is constructed with species-specific ventilation values and surface areas for the PU region.

The equation for deriving a default RGDR_{PU} for reactive and water soluble (e.g., Category 1) gases as it appears in *RfC Methods* ([U.S. EPA, 1994](#)) (Equations 4-23, 4-25 and 4-28 and Appendix I Equations I-35, I-43 and I-46) is shown below as Equation 2-6 where Q_{alv} is the alveolar ventilation rate (L/min) and SA_{PU} the surface area of the pulmonary region for laboratory animals (A) or humans (H) (m^2). More detailed information on the derivation of the default equation is provided in the *Status II Report*.

$$\text{RGDR}_{\text{PU}} = \frac{\left(\frac{Q_{\text{alv}}}{\text{SA}_{\text{PU}}} \right)_{\text{A}}}{\left(\frac{Q_{\text{alv}}}{\text{SA}_{\text{PU}}} \right)_{\text{H}}}$$

Equation 2-6

Alveolar ventilation (Q_{alv}) in the RGDR_{PU} equations, refers to the gas that reaches the alveoli and takes part in gas exchange and excludes that which does not, often referred to as alveolar dead space or residual volume. However, Q_{alv} is often not measured or reported in laboratory animal inhalation studies, whereas V_{E} is readily measured and typically reported in epidemiological and laboratory animal studies. Thus, the equation to determine the RGDR_{PU} has been simplified through usage to the form presented in Equation 2-7:

$$\text{RGDR}_{\text{PU}} = \frac{\left(\frac{V_E}{\text{SA}_{\text{PU}}} \right)_A}{\left(\frac{V_E}{\text{SA}_{\text{PU}}} \right)_H}$$

Equation 2-7

Shown below is an example calculation of the DAF for the PU region using Equation 2-7 for a rat to human extrapolation assuming a rat V_E of 0.250 L/min and SA of 0.34 m² and a human V_E of 13.8 L/min and SA of 54 m².

$$\text{RGDR}_{\text{PU}} = \frac{\left(\frac{0.25 \text{ L/min}}{0.34 \text{ m}^2} \right)_A}{\left(\frac{13.8 \text{ L/min}}{54 \text{ m}^2} \right)_H} = 2.9$$

Equation 2-7 (example)

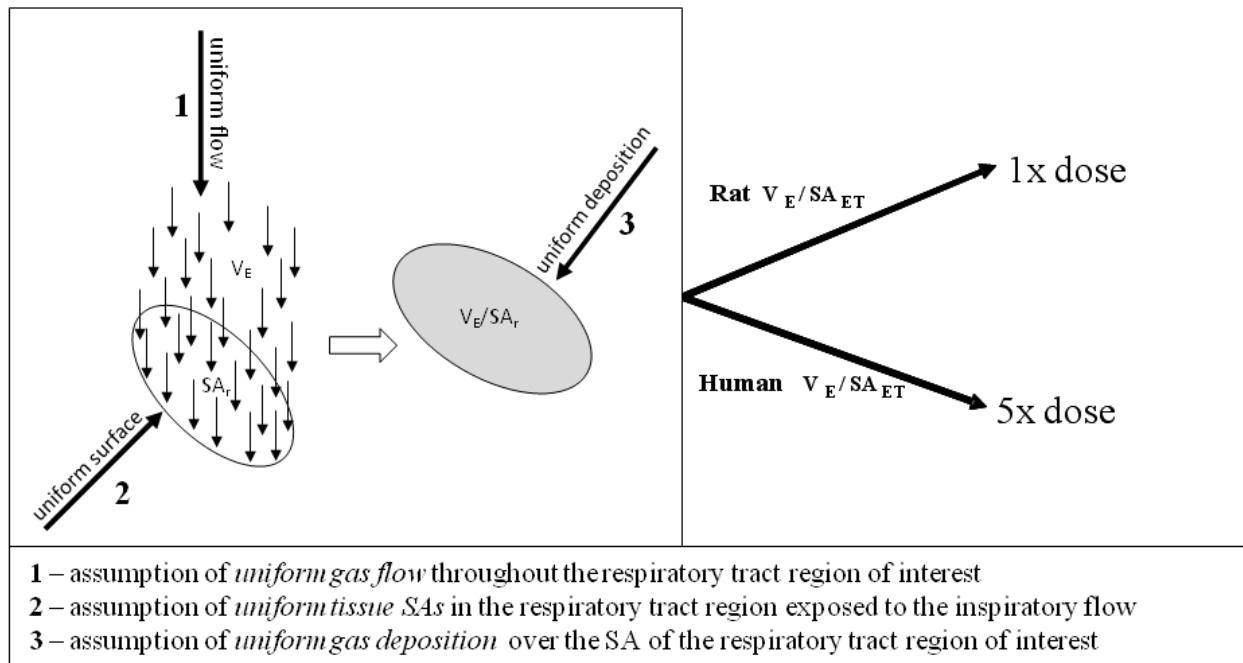
The calculation using these default parameters ([U.S. EPA, 1994](#)) results in a RGDR_{PU} of 2.9 indicating the assumption that rats would receive nearly 3 times more dose to the PU region on a per SA unit basis than humans.

2.5.4 Limitations in the Assumptions and Application of V_E / SA

Although inhalation dosimetry based on the measure of “dose” estimated through $V_E / \text{SA}_{\text{ET, TB, PU or Total}}$ has been demonstrated to be more explanatory of inhaled dose and responses in the respiratory tract and POE effects than alternatives discussed in the *Status I Report*, such an approach is put forth on assumptions, either explicit or implicit, whose existence, limitations and caveats need to be considered.

Perhaps the most debated aspect of this default dosimetric approach outlined in the *RfC Methods* with V_E / SA regarded as dose normalized to surface area concerns the outcome of the example above using the ET region. As demonstrated in Section 2.5.1, the default dosimetric adjustment for gas exposures in this region estimates that human ET tissues receive a three- to fivefold higher dose than do rat tissues. One primary reason the V_E / SA_r relationship is debated is its marked divergence from the closely related relationship of V_E / BW . Parallel construction of an RGDR based on body weight instead of SA_{ET} would yield a value of 3 $\left(\left[\frac{\text{rat } V_E / 0.3 \text{ kg}}{\text{human } V_E / 70 \text{ kg}} \right] = 0.6 / 0.2 = 3 \right)$ indicating that human tissues would receive threefold less dose than rat tissues. This outcome as

related to the underlying assumptions made in the application of the basic element of default dosimetry, i.e., V_E/SA is illustrated in Figure 2-3.



Note: The surface area (SA) of the various regions (r) of respiratory tract are exposed to inspired gas (V_E). The right side of this figure shows the comparative results of applying V_E/SA to the ET regions of rats and humans.

Figure 2-3 Representation of the assumptions of uniformity following from V_E/SA as applied to comparative gas dosimetry.

Figure 2-3 illustrates a major outcome following from the interspecies extrapolation for the ET region with these attendant V_E/SA_{ET} assumptions. With the accompanying assumption that all of the gas is absorbed in the region defined by SA, the approximate fivefold higher value for V_E/SA_{ET} in humans compared to rats indicates that the surface of the human ET would receive a fivefold higher dose than the rat ET. Another way to view the relationship is that surface area per unit of ventilation is five-fold lower in humans, because humans have less complex nasal passages, so there is more airflow delivery per unit surface area in humans.

This interspecies difference is reflected in the application of V_E/SA in actual calculation of an HEC where the DAF (the $RGDR_{ET}$) applied to the animal point of departure approximates the inverse of this ratio, i.e., 0.2-0.3 (i.e., $1/5 - 1/3$). Thus, human equivalent exposures based on responses in the ET from rat exposures are adjusted downward by this fraction. This adjustment lowers the overall estimate for a POD in

humans by a factor of 3 to 5 even before consideration of uncertainty factors. In contrast, application of the DAFs for the TB and PU region would raise the overall estimate for POD concentration in humans by a factor of 2 to 3 before consideration of uncertainty factors.

2.6 The DAF for Systemic (SYS) Sites - $H_{b/g}$

Gases with physicochemical properties that lessen their potential for effects in the respiratory tract (e.g., nonreactivity and higher lipid versus water solubility) may at the same time exhibit potential for significant uptake and accumulation in the blood where they can cause toxicity at systemic or remote sites. Based on these properties and other kinetic properties governing how such gases may be expected to distribute in the body, *RfC Methods* posits a fundamentally different DAF for gases that have little or no potential for reactivity in the respiratory tract.

This DAF is based on assumptions of dose-response that are consistent with basic principles of kinetics and toxicity applied to the scenario of systemic toxicity from an inhaled toxicant:

- toxicity is directly related to the concentration of the agent at the target site,
- the concentration of the agent at the target site is related to the concentration of the agent in the arterial blood at equilibrium and the duration of exposure¹;
- arterial blood concentration at equilibrium is related to its concentration in the inspired air.

The last link in this process, the partitioning of the agent from the inspired air into the blood at the alveolar endothelial interface, is determined by the blood:gas (air) partition coefficient, $H_{b/g}$. Further, it is reasonably anticipated that as properties of blood differ between species so will the partition coefficient itself. In application of this DAF, the *RfC Methods* outlines a number of additional assumptions. In making the assumption that differences will exist between species for the basic biological component of $H_{b/g}$, blood, assumptions also are made that similarities will exist between species. These assumptions include:

- chronic laboratory animal exposure scenarios are equivalent to human lifetime exposures,
- the human toxic effects observed will be the same as in the animal when the time-integrated arterial blood concentration (i.e., area under the curve or AUC) in humans is equal to that of the exposed laboratory animal

¹ The gas or its concentration multiplied by time ($C \times t$)

It is also emphasized in *RfC Methods* that the equilibrium referred to here is that which occurs during the portion of the exposure period that is under conditions of “periodicity”, i.e., when the periodic steady state concentration versus time profile is the same for every week. *RfC Methods* further states that conditions of periodicity should be met during “most” (elsewhere indicated as 90%) of the exposure duration.

Thus, the DAF for SYS sites is based upon the species-specific (animal / human) ratio of the blood:gas (air) partition coefficient ($H_{b/g}$) at equilibrium shown here in Equation 2-8:

$$DAF_{SYS} = \frac{(H_{b/g})_A}{(H_{b/g})_H}$$

Equation 2-8

Appendix J of the *RfC Methods* provides a mathematical derivation and application of this procedure as well as a case study employing a physiologically-based pharmacokinetic (PBPK) model parameterized for interspecies extrapolation.

In the *RfC Methods*, the DAF derivation for SYS effects is based more on science policy than on an empirical procedure. Further, this policy is bi-level; (1) where if $H_{b/g}$ values are unknown the default value for $(H_{b/g})_A / (H_{b/g})_H = 1$; (2) if $(H_{b/g})_A$ is greater than $(H_{b/g})_H$ then a default value of 1 is also used. These procedures are justified by *RfC Methods* on the animal human datasets that were available at the time ([Gargas et al., 1989](#)). Gargas et al. (1989), reported that for an appreciable number of volatile and nonvolatile agents the $(H_{b/g})_A$ was greater than the corresponding $(H_{b/g})_H$. These values as well as their A/H ratio are also shown below in Table 2-7.

Table 2-7 Some example blood:air partition coefficients ($H_{b/g}$) in humans and rats expressed as a ratio, A/H

Chemical	Human ($H_{b/g}$)	Animal (rat, $H_{b/g}$)	Animal/Human
Chloroform	6.85	20.8	3.0
Dichloromethane	8.94	19.4	2.2
Carbon tetrachloride	2.73	4.52	1.7
Chlorodibromomethane	52.7	116	2.2
Chloroethane	2.69	4.08	1.5
1,1-Dichloroethane	4.94	11.2	2.3
1,2-Dichloroethane	19.5	30.4	1.6
1,1,1-Trichloroethane	2.53	5.67	2.2
1,1,2-Trichloroethane	35.7	58	1.6
1,1,1,2-Tetrachloroethane	30.2	41.7	1.4
1,1,2,2-Tetrachloroethane	116	142	1.2
Hexachloroethane	52.4	62.7	1.2
Methylchloride	2.48	2.47	1.0

Source: Reprinted with permission of Elsevier; Gargas et al. (1989)

2.7 Children's Dosimetry

Consideration in *RfC Methods* of dosimetry for various human conditions or lifestages, including childhood is discussed as a component of the intraspecies uncertainty factor (UF_H) that accounts for unknown pharmacokinetic and pharmacodynamic differences. The default value of this UF is 10 and is applied where appropriate to the underlying evidence to account for uncertainty and potential variations in susceptibility within the human population (interhuman variability) and the possibility that the available database is not representative of the population groups that may be most sensitive to the health hazards. Early lifestages (including (1) embryo, fetus, and neonate and (2) young children – ages 1 to 4) are also listed in Table 2-4 of the *RfC Methods* as 2 of 5 sensitive populations and lifestages who, based on empirical observations or compromised physiological functions, are assumed susceptible to toxicity elicited by certain groups of chemicals. It is discussed further that certain populations and lifestages may be differentially susceptible, e.g., elderly individuals could be more susceptible to some chemicals and children to others. *RfC Methods* acknowledged that very little is known about this important area of population sensitivity and that guidance should be developed concerning the prevalence of sensitive populations and lifestages and the range of sensitivities in the general population exposed to inhaled toxicants.

Two subsequent reports ([U.S. EPA](#)) further defined and outlined the various lifestages - including children - that could be considered when assessing potential health risks from exposure. For this purpose, lifestages are defined as periods of life with distinct anatomical, physiological, and behavioral or functional characteristics that contribute to potential differences in susceptibility to environmental exposures. These lifestages and their corresponding age ranges are shown in Table 2-8.

Table 2-8 Human lifestages and corresponding age ranges through adolescence

U.S. EPA (2002)		U.S. EPA (2006a)	
Lifestage	Age	Lifestage	Age
Embryonic	GD 0–58	Prenatal	Conception to birth (includes embryonic and fetal stages)
Fetal	GD 58-267		
Neonate	PND 0-30	Infant Child	Birth–1 yr 1yr–11 yrs
Infant	PND 30–1 yr		
Toddler	2-3 yrs		
Preschool	3-6 yrs		
Elementary School Age	6-12 yrs		
Adolescent	12-21 yrs	Adolescent	11-21 yrs

The Food Quality Protection Act (FQPA) of 1996 contains several requirements (directed primarily toward the evaluation of pesticides) related to its standard described as “reasonable certainty of no harm.” One of the specific requirements identified was that the EPA considers the specific risk pesticides might have for infants and children. In general, the manner in which this was to be accomplished was through application of uncertainty factors based on an evaluation of information relevant to children. This requirement engendered considerable interest, including interest in inhalation dosimetry in children. On the whole, these evaluations, including conclusions by the NAS ([1993](#)), indicate that for most chemicals the very large majority of people, including children, respond sufficiently similarly so that the 10-fold intraspecies uncertainty factor is adequate to cover any variability that may exist in the human population. However, there are some chemicals for which some humans may display a greater range of variability and sometimes that variability appears age-related, with children exhibiting a greater degree of sensitivity than adults. U.S. EPA ([U.S. EPA, 2002](#)) also considers potential children’s sensitivity within the database uncertainty factor. Further considerations of these matters are included in the section on children’s dosimetry in the *Status II Report* and Section 3.6 of this report.

3 ADVANCES

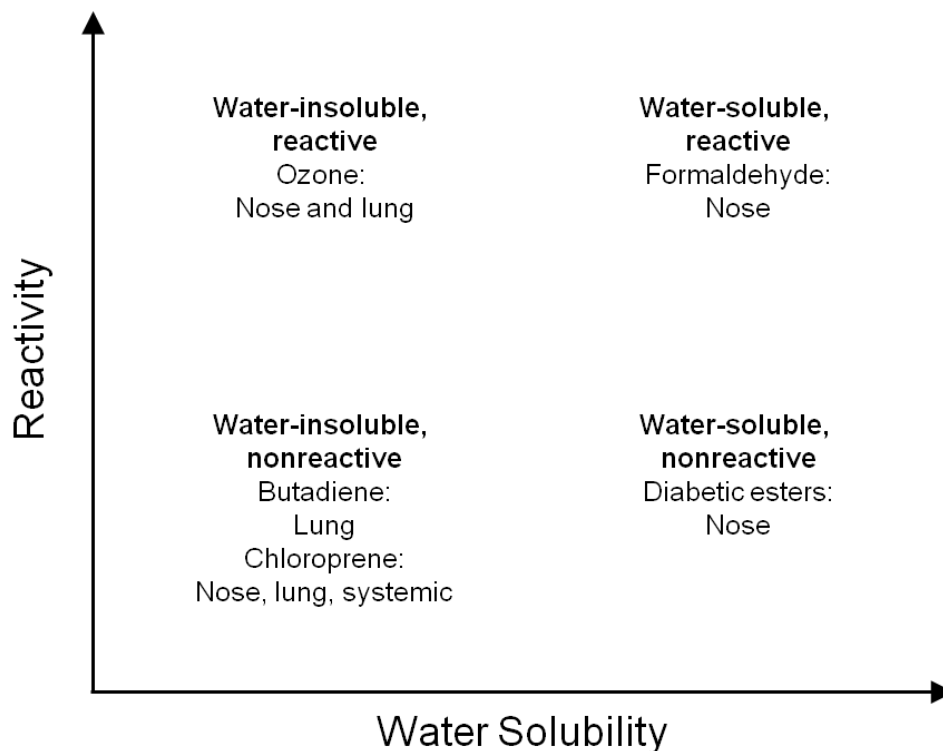
Section 2 briefly summarized the origins, underlying principles and concepts, and demonstrated the application of the default procedure in the *RfC Methods* for performing inhalation dosimetry of gases. *RfC Methods* was a state-of-the-art document for inhalation dosimetry of gases in 1994. This Section summarizes the major scientific advances in inhalation gas dosimetry, originally presented in detail in the *Status I and II Reports*, related to the default approaches presented in the *RfC Methods* with the primary focus on interspecies extrapolation. Information evaluated related to the gas categorization scheme and the assumptions underlying the current approach as discussed in Section 2 is also presented. New information for measures of critical parameters such as V_E and SA are included where appropriate. Furthermore, a section devoted to summarizing the current state of the science for inhalation dosimetry in children is provided. A few additional studies that have recently been identified and were not presented in the earlier reports are also included in the appropriate sections. These findings will provide the scientific foundation necessary for ensuring that methods and guidance used and implemented by EPA in inhalation risk assessment of gases reflects the state of the science.

3.1 A Modified Gas Scheme: Descriptors versus Categories

Two physicochemical properties, water solubility and reactivity, have repeatedly been used as predictors of the site of gas uptake in the respiratory tract and/or absorption into blood, as well as the potential toxic actions in both inhalation POE sites and in sites remote from the inhalation POE.

Medinsky and Bond ([2001](#)) proposed a descriptor scheme based on water solubility and reactivity that differs from the *RfC Methods*. In the Medinsky and Bond ([2001](#)) scheme, water soluble gases are defined as gases that readily dissolve in the mucus lining of the upper respiratory tract followed by diffusion into the underlying epithelial cells and, potentially, into the blood for systemic distribution. Generally, water-insoluble gases penetrate the mucus lining more slowly and are transported to the lower respiratory tract where they may be absorbed into the blood. The other principal determinant, reactivity, defined in this scheme as the tendency of a gas to undergo chemical reaction, is simple to understand. However, reactivity at the level of organization relating to tissue dosimetry is complex. In the distance from the airway to the blood, reactive gases may undergo interactions with components in the air, mucus, and tissue. These reactions lead to rapid and substantive decreases in the concentration of the reactive gas across this distance. Chemical reactivity of the gas controls its molecular interactions with respiratory tissues and influences its penetration to the blood.

Rather than assigning specific numerical categories to gases, these descriptors are placed on a chart that represents reactivity and water solubility as continuous variables. This scheme, along with the descriptors for the boundary conditions of the variables, is shown in Figure 3-1. It is important to note that this scheme provides examples of gases that fit these discrete descriptors, but that the majority of gases may not fit one particular descriptor. Also depicted is the primary site(s) of toxicity associated with these gases. Just as gases may not fit a specific descriptor, the expected site of effect may not fit as well. For example, chloroprene is water-insoluble and nonreactive but has been found to induce POE and systemic effects at the same exposure concentration (IRIS). In addition, the potential role of metabolism and its influence on uptake and toxicity is not directly accounted for in this scheme. Therefore, this scheme also has its limitations. However, examination of these examples at the extremes should help facilitate understanding of the behavior of other gases.



Note: Examples of specific chemicals with their primary site(s) of toxicity are also presented.

Source: Adapted from Medinsky and Bond (2001).

Figure 3-1 A schematic representation of the physicochemical properties of reactivity and water solubility overlaid with descriptors of their practical limits.

Utilization of such a scheme yields information about the nature and site of toxicity that is based on the determinative variables of water solubility and reactivity. Such a scheme

would have best applicability in situations where gas exposure levels are relatively low and the effects observed are identified in the most sensitive target tissues. Information on the nature and site of toxicity is crucial to formulating an approach to inhalation dosimetry. This approach and scheme contrasts with the current *RfC Methods* scheme where the gas was often first placed in a numerical category, often irrespective of the sites and conditions of the observed toxicity. The current *RfC Methods* scheme has resulted in some confusion in that an unintended emphasis was placed on the numerical category and its associated dosimetric approach and outcome as opposed to the site of the effect of the toxicant.

3.2 Major Scientific Advances Related to Inhalation Gas Dosimetry in the ET Region

The following sections summarize the major scientific findings related to the current default procedure for interspecies inhalation dosimetric extrapolation for gases in the ET region. The information evaluated includes results and observations from anatomically based airflow and fluid dynamics modeling as well as from chemical specific interspecies physiologically based pharmacokinetic (PBPK), computational fluid dynamics (CFD), and hybrid CFD-PBPK models.

3.2.1 Tracer Dye-Flow in Cast Models

Morgan and co-workers ([1991](#)) laid the foundation for studying airflow distribution patterns in the ET region, - the nasal tract, using solid acrylic casts through which water was pulled with tracer dye streaks introduced, allowing for direct observation of the flow field. Consequences of these (and other similar) observations are significant on several levels. First, the complex but generally consistent and orderly streamlines revealed by the cast method show a sensitive dependence of nasal airflow patterns on nostril geometry throughout the ET region. Second, all observations indicate overwhelmingly that flow into the nasal area, either liquid or air, is in no way uniform but has discernible patterns that could only result in highly nonuniform deposition onto surfaces (i.e., nasal epithelial surfaces).

Use of this approach for dosimetric comparisons is limited. These limitations include the accuracy, representativeness and resolution of the casting process itself and the inability to quantitatively evaluate any of the flows and flow rates observed. These limitations remained to be addressed with quantitative mathematical airflow models which are presented and discussed in the following sections.

3.2.2 Computational Fluid Dynamic Modeling

Computational fluid dynamics (CFD), allows for quantitative prediction of all variables of fluid flow (e.g., pressure and velocity) based on the mathematical laws governing fluid behavior and, with proper software, offers a three dimensional visualization of the predicted flow. CFD and its predictions are applied to quantitatively evaluate airflow and the distribution of dilute gases and vapors (toxicants) by that airflow in the airways of the respiratory tract.

The goal of inhalation dosimetry is to estimate dose or concentration in target tissues. Models of air flow, either dye-flow or CFD, visualize or estimate the movement of materials to surfaces. For the regions of the respiratory tract, flow models give estimates of the flux of materials present or entrained in the inhaled air to discrete areas. The rate of transfer across the boundary/surface (i.e. level of flux) may be regarded as an exposure to the agent or toxicant of concern in air having units of mass flow to a unit area. Thus, these model outputs may yield a quantitative estimate of materials flowing to the boundaries of their meshes (i.e., to the tissue surface) but to date do not afford an estimate of an actual dose to the tissue, whose units are typically mass to a volume or weight.

3.2.2.1 CFD Air Flow Models of the Rat ET Region

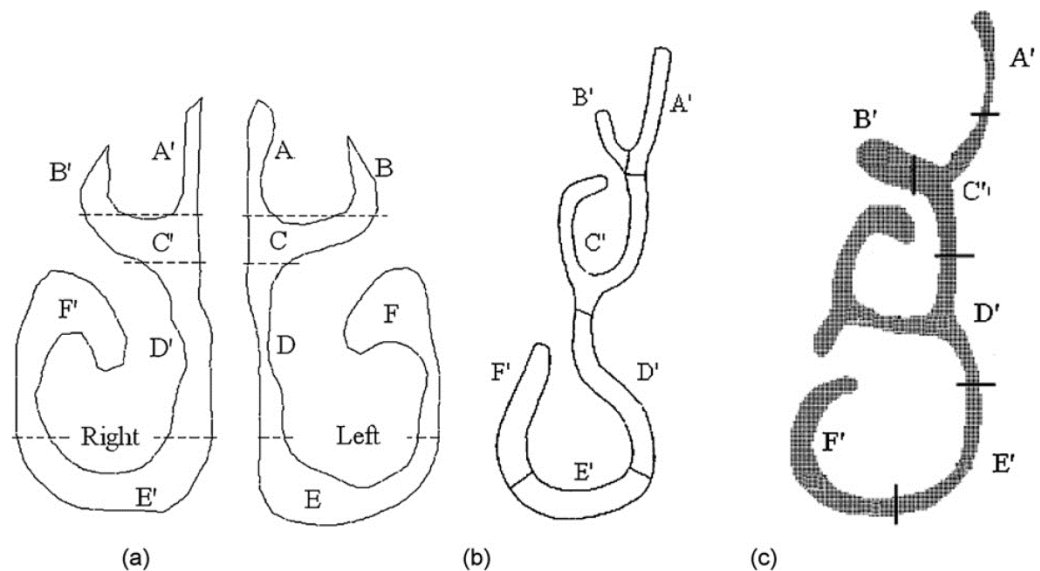
As summarized in detail in the *Status I Report*, the observations reported by Kimbell et al. ([1997a](#)) clearly illustrate the applicability of CFD modeling techniques for resolution of flow occurring in the ET region of the rat. Two independent approaches, dye-visualized and computer-simulated, consistently revealed a high degree of complexity and nonuniformity of airflow patterns in the ET region. Furthermore, simulations revealed marked differences in flow rates. Flow in the ethmoid substructure was more than an order of magnitude slower than flow in interior and ventral portions of the nasal airway.

3.2.2.2 CFD Air Flow Models of the Human ET Region

Wen et al. ([2008](#)) reviewed the work of several investigators ([Subramaniam et al., 1998](#); [Keyhani et al., 1995](#); [Schreck et al., 1993](#)) who developed intricate mesh models based on highly refined human MRI and CAT scans and to simulate and characterize flow in, through, and around the ET region. Results analogous to those observed in rat analyses are obvious with medial, ventral, lateral, and dorsal airflow streams being observed from the simulations. These simulations of flow in human ET regions also predict low flow apportionments to the dorsal regions with accompanying vortices. Increased airflow

resulted in increased complexity, especially in the dorsal regions where larger and multiple vortices were simulated.

Localized volumetric flows and their apportionments were also determined in a number of these studies. These results indicate a wide range of flow values to these subsections of the ET. Also, simplistic apportionment of percent flow per mm² surface area of these various sections can be seen to result in a range of values; e.g., from 0.12%/mm² (1.2%/9.7 mm²) in section B as reported by Wen (2008) to 1.03%/mm² (28.7%/27.9 mm²) in section E as reported by Keyhani et al. (1995) (Figure 3-2 and Table 3-1). These composite simulated results clearly indicate a high degree of nonuniformity of flow within the human ET region and variability between models.



Note: The section is located at (a) 6.1 cm from the anterior tip of the nose used in Wen (2008), (b) 6.2 cm from the anterior tip of the nose used by Keyhani et al. (1995) and (c) 6.0 cm from the anterior end of the nose used by Subramaniam et al. (1998).

Source: Wen (2008).

Figure 3-2 The coronal sections are divided into sub-sections which are indicated by the letters.

Table 3-1 Summary of CFD simulated flow apportionment (as a % of total at 15 L/min) on the coronal cross-sectional area in the middle turbinate (as mm²) of the ET region in selected human models as analyzed by Wen et al. (2008).

Sections: Dorsal (A) to Ventral (E,F)	Wen et al. (2008) (left)		Subramaniam et al. (1998)		Keyhani et al. (1995)	
	Cross-sectional area	% Flow	Cross- sectional area	% Flow	Cross- sectional area	% Flow
A	13.7	11.6	7.9	1.9	15.6	11.4
B	9.7	1.2	15.4	1.9	6.0	3.0
C	23.2	21.4	20.8	11.3	35.5	27.3
D	21.6	20.3	54.8	46.7	27.9	18.3
E	50.3	43.7	20.5	24.4	27.9	28.7
F	42.8	1.8	28.9	13.9	26.5	11.3
Total	161.3	100	148.3	100	139.4	100

Source: Wen et al. (2008)

These results indicate that inspired airflow to the various areas of the ET region is highly nonuniform. Some reasons for the nonuniformity of flow have their basis in the extensive departures from unimpeded flow that airway morphology in different species impose on the incoming airstream.

Finck et al. (2007) described an approach to describe nasal flows in an artificial model of the nose using a variant of the lattice Boltzmann method (LBGK), an alternative to Navier-Stokes solvers. This approach provided several advantages over the conventional Navier-Stokes approach, such that lattice-BGK enabled higher resolution, faster grid generation, and easy implementation of boundary conditions. Using this novel method, Finck et al. (2007) performed computations for steady flows at the inspiration and expiration phase of nose breathing. More recently, Mosges (2010) used the lattice Boltzmann method (LBM) and a computed tomography (CT) dataset to describe nasal cavity flow in a human. The CT allowed for visualization of the flow, while LBM provided higher resolution of this flow field (compared to Navier-Stokes solutions).

3.2.2.3 CFD Air Flow Models - Predictions of Reactive Gas Distribution in the ET Region

The *Status I Report* presented detailed information on the application of CFD to address the fate of inspired gases within the upper respiratory tract. Briefly, Kimbell and co-workers (Kimbell et al., 2001a; Kimbell et al., 2001b; Kimbell and Subramanian, 2001; Kimbell et al., 1997a; Kimbell et al., 1997b; Kimbell et al., 1993) used CFD modeling of airflow in the ET regions of laboratory animals and humans as a basis to describe

deposition of inhaled gases using formaldehyde, a highly water soluble and reactive gas, as an example.

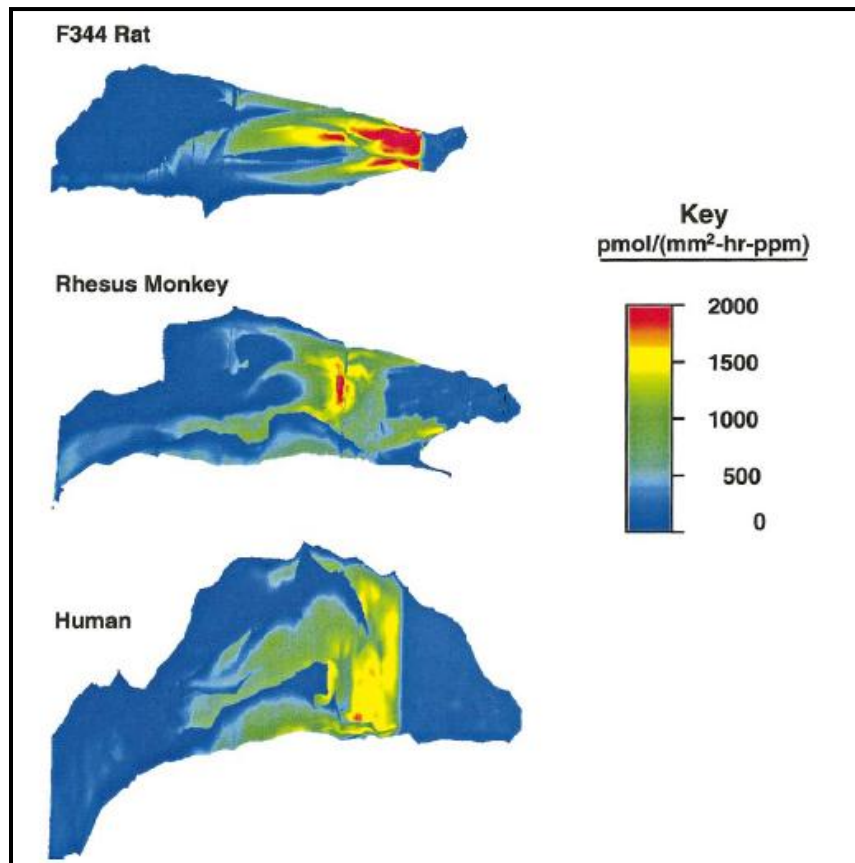
The results of the study by Kimbell et al. ([1993](#)) were among the first to demonstrate the application of CFD to regional dosimetry of inhaled gases in predicting quantitative mass flux patterns to surface (mesh) walls, which acted as a sink. Consistent with other advances related to predictive dosimetry for the ET region, these results also give indications that considerable levels of nonuniformity exists across the surfaces of the ET region, in this instance for mass flux.

3.2.2.4 Interspecies CFD Air Flow Models Predictions of Gas Distribution in the ET Region

Subsequent to the initial studies of Kimbell et al. ([1993](#)), a number of investigators developed and published similar sophisticated models for various species and gases of different solubilities and reactivities. A listing of these studies is provided in

Table 3-3 of the *Status I Report*.

Kimbell et al. (2001b) constructed anatomically accurate, 3-dimensional computational fluid dynamics models of nasal passages of F344 rat, Rhesus monkey, and humans for the purposes of modeling inhaled formaldehyde (see the *Status I Report* for details). Simulations configured for uptake of formaldehyde were run for all three of the ET models, the results of which are shown in Figure 3-3. Despite the difference in size, with the rat ET being 13-fold smaller than the human ET based on surface area, comparative aspects regarding flux are apparent. Visual inspection of Figure 3-3 shows clearly, for example, that relative proportions of area for the highest formaldehyde flux in the ET region (“red” in color) is highest in rat, with the rank order following rat > monkey > human. The authors estimated both maximum and average formaldehyde flux over the whole ET in each species. The difference between the maximum:average flux ranged from 3- to 10-fold among these three species (Table 3-2).



Note : Nostrils are to the right.

Source: Kimbell et al. (2001b).

Figure 3-3 Nasal wall flux spectra of inhaled formaldehyde simulated in rats, monkey and humans at normal inspiratory flow rates. Table 3-2 Estimates of formaldehyde flux to ET surface walls for various species

Formaldehyde flux estimate (pmol/[mm²-hr-ppm])^{a,b}			
Area	Rat	Monkey	Human
Whole nose: maximum	3210	4492	2082
Whole nose: average	336	508	568
Maximum/Average	10	9	4
Nonsquamous: maximum	2620	4492	2082
Nonsquamous: average	284	535	611
Maximum/Average	9	8	3

^aSimulations conducted at inhaled concentration of 1 ppm formaldehyde.

^bSimulations conducted at flow rates of twice the minute ventilation for rat (576 mL/min), monkey (4.8 L/min), and human (15.0 L/min).

Source: Adapted from Kimbell et al. (2001b).

3.2.3 Range and Distribution of Flux in ET Regions for Various Species

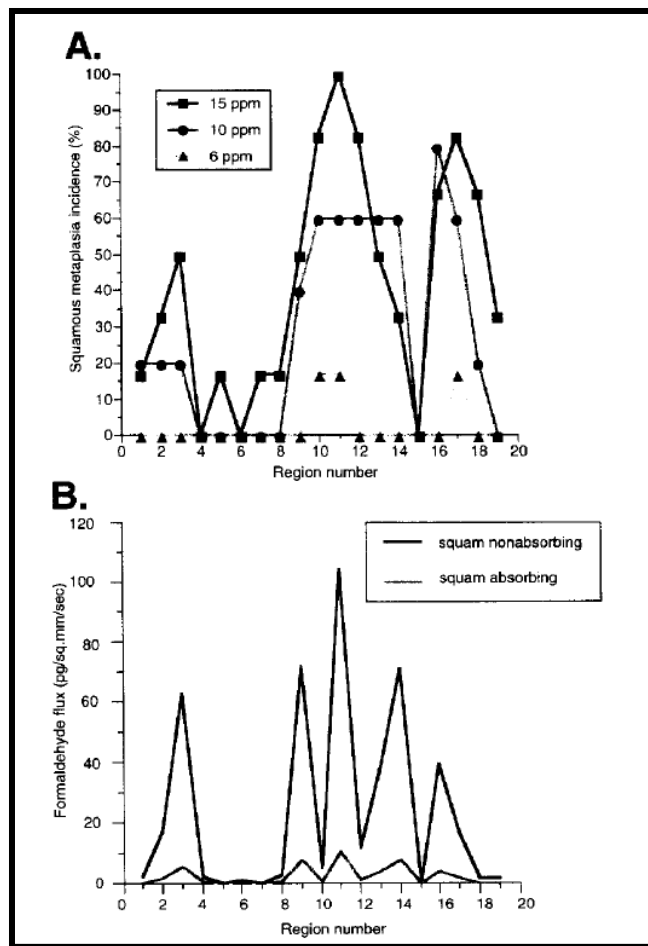
The general ranges of rat and human flux in the ET region estimated from visual inspection in Figure 3-2 and from the average and maximum ranges in Table 3-2 were further analyzed by Kimbell et al. (2001b). The ET regions for each species were first partitioned into 20 evenly spaced flux levels between zero and the maximum predicted flux value for each species; 2620 pmol/(mm²-hr-ppm) at a flow rate of 576 mL/min in the rat and 2082 pmol/(mm²-hr-ppm) at a flow rate of 15 L/min in the human. Surface areas of the ET found to be within these flux levels were then assigned or “binned” accordingly. This strategy allowed for estimating the distribution of flux levels over the surface area of the ET, each species being “normalized” to its respective range of flux. The binning revealed that flux values higher than half the maximum flux value (flux median) were predicted for nearly 20% of human ET surfaces whereas only 5% of rat ET surfaces were associated with fluxes higher than flux medians. This relationship was maintained for flux levels higher than 75% of the maximum flux value with approximately 1.8% of human but only approximately 0.6% of rat ET surfaces were exposed to this higher level of flux. Distribution within the ET region of what may be considered “high” flux will be examined in the next section in relation to actual occurrence of lesions in the ET region.

3.2.4 Correlation of High Flux with Lesions in the ET Region

Airflow and CFD modeling approaches have given very similar and internally consistent results concerning patterns and distributions of airflow and gases in the ET region of various species, including humans. Supporting empirical observations would, however,

provide a more robust basis for these modeling results. One logical strategy that could provide support and reinforcement for the modeling results would be to examine the extent of correlation between flux and lesions. There are currently several examples of such a correlation analysis in the current literature. Results from two of these studies, - formaldehyde ([Kimbell et al., 1997b](#)) and hydrogen sulfide ([Moulin et al., 2002](#)) - are summarized here.

Kimbell and colleagues ([1997b](#)) investigated the relationship between squamous metaplasia and areas of high formaldehyde flux in the nasal tissues of adult rats. They first performed a pathology analysis on the incidence of squamous metaplasia in specific areas of the nasal tracts of rats that had been exposed via inhalation to formaldehyde at 0, 0.7, 2, 6, 10 or 15 ppm for 6 hr/d, 5 d/wk for 6 months. These specific target tissue areas were then divided into 20 regions based on anatomical landmarks and the location of major airflow streams. Transport of formaldehyde through the air and into the nasal epithelium was assumed by the model to occur by convective forces and molecular diffusion. Incidence of squamous metaplasia was then calculated for each region and flux values modeled for each region, ranked high to low and statistically analyzed for correlation. The results, shown in Figure 3-4, provide clear evidence that, at high flux levels (and high exposures) of formaldehyde, the distribution of squamous metaplasia is closely related to the location of regions of high formaldehyde flux into airway walls.

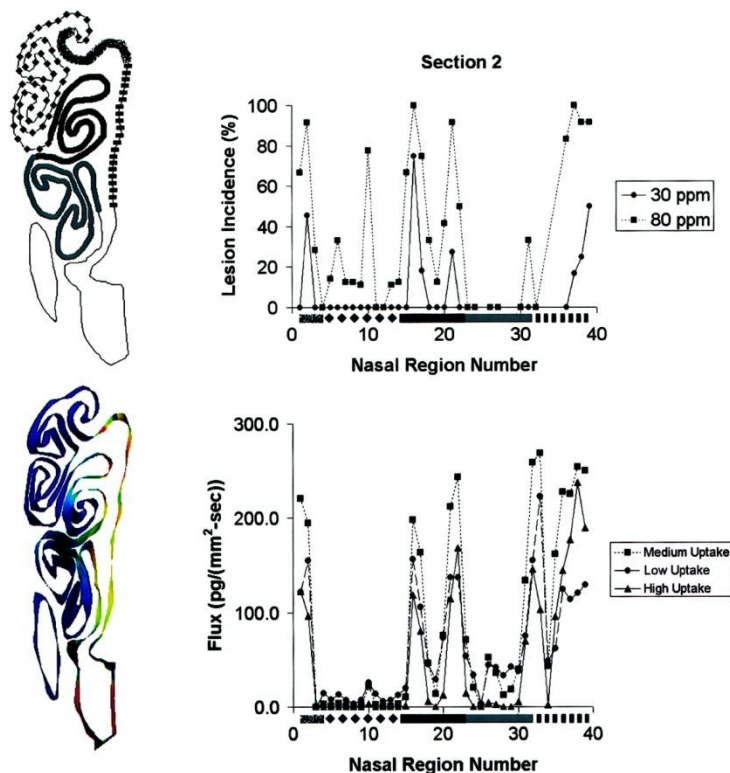


Source: Kimbell et al. (1997b).

Figure 3-4 Graphs showing (A) the incidence of formaldehyde-induced squamous metaplasias and (B) modeled formaldehyde flux values along regions assigned to the perimeter of a transected nasal airway of rats.

Moulin et al. (2002) used a similar approach to investigate the relationship between lesions in olfactory epithelia and areas of high hydrogen sulfide flux in the nasal cavity of adult rats. They also performed a pathology analysis on the incidence of lesions (olfactory neuronal loss and basal cell hyperplasia) in adult male rats ($n = 12/\text{concentration}$) that had been exposed to hydrogen sulfide at either 0, 10, 30 or 80 ppm for 6 hr/d for 70 days. The CFD modeled flux predictions at 80 ppm hydrogen sulfide were made at the same level of the transverse nasal section (through the ethmoid turbinates) that had been divided into 39 regions. Transport of hydrogen sulfide through the air and to the nasal epithelium was assumed by the model to occur by convective forces and molecular diffusion. Rank correlations between lesion incidence and flux were then carried out. Distinct hot spots of regional flux occurred in the ethmoid turbinate section at those regions corresponding to high airstream flow. These results are presented in Figure 3-5. These regions of high flux were closely associated with hydrogen sulfide-induced nasal lesions if that region was lined by olfactory epithelium. An additional

observation made regarding high hydrogen sulfide flux was that lesions were not observed in those regions lined with respiratory tissue other than olfactory epithelium. This lack of correlation between high flux and non-olfactory epithelium lesions is apparently due to resistance of this tissue to hydrogen-sulfide toxicity.



Note: coding of surface areas in schematic to the x-axis of plot. Plot of predicted hydrogen sulfide flux under different assumptions of uptake: low – 20%, medium – 40%, and high – 80% (bottom right). Diagram of same section (bottom left) under intermediate uptake conditions at 80 ppm where red corresponds to 320 pg/(mm²-s) and blue corresponds to 0 pg/(mm²-s). Plot of predicted flux at 80 ppm (bottom right) on designated regions of Section 2.

Source: Moulin et al. (2002).

Figure 3-5 Schematic diagram of the transverse nasal section through the ethmoid turbinates (top left, Section 2 of the nasal cavity) with plot of lesion incidence at 30 and 80 ppm (top right).

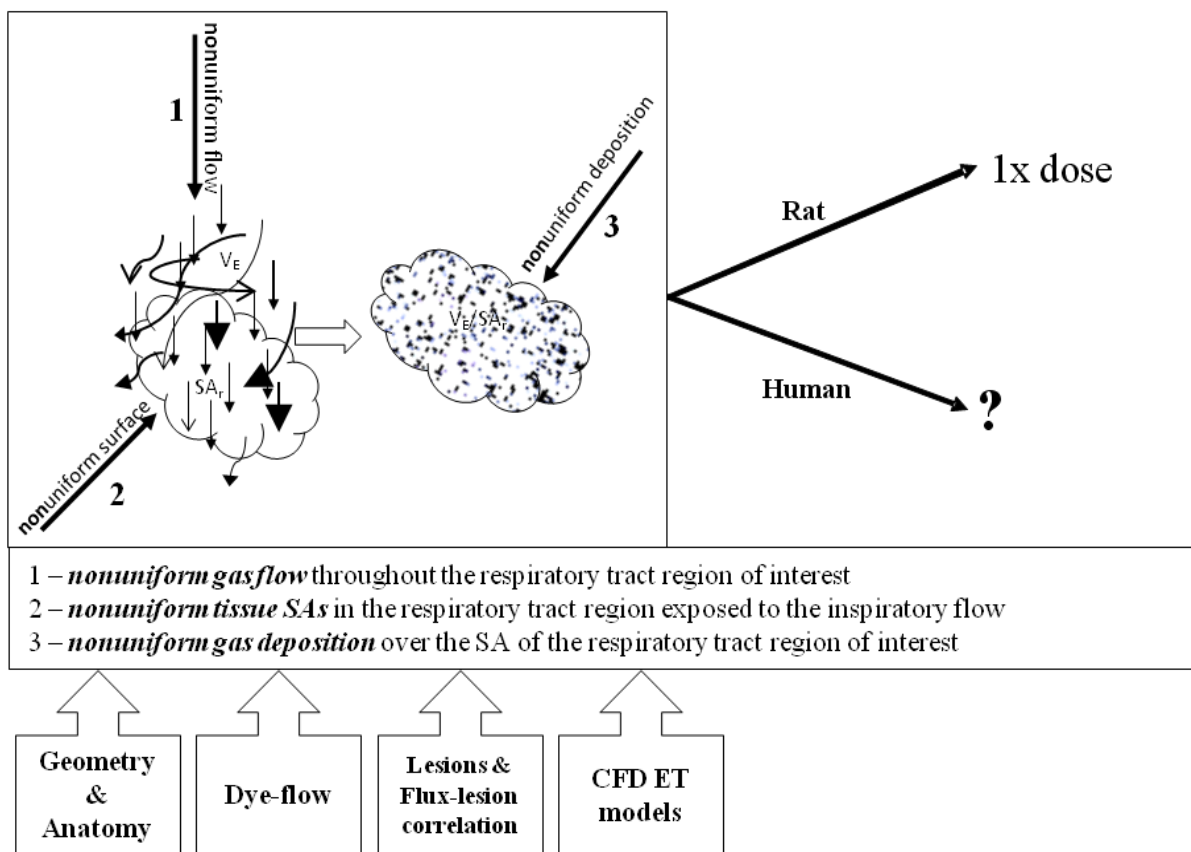
Similar correlations between lesion incidence and tissue dose were also observed for acrolein (Schroeter et al., 2008) and diacetyl (Morris and Hubbs, 2009). For acrolein, predicted air:tissue flux from the rat nasal CFD model compared well with the distribution of nasal lesions observed in a subchronic inhalation study. In the case of diacetyl, a strong correlation of injury location and pathology severity scores with CFD-PBPK hybrid model predicted tissue concentrations was observed in nasal tissues.

These examples provide strong support for a direct relationship between flux and responses in tissues in four independent cases. The hydrogen sulfide case offers resolution sufficient to demonstrate expected target tissue specificity as responses were

only seen in olfactory epithelium despite equivalent flux levels in more proximal respiratory epithelium. In the case of formaldehyde, the relationship between flux intensity and response appears to be one in which high flux is more predictive of lesions than are low flux levels (i.e., either appreciably above or below the median flux level). Similar relationships between flux intensity and response were observed with acrolein and diacetyl. These additional observations indicate the flux-response relationship to have a high degree of resolution as well as providing predictability of a dose-response relationship. Thus, results from these four examples may be regarded further as providing compelling support for a close correlation between flux and tissue-specific responses. However, the weaker correlation for low flux areas suggests that other factors also impact site specificity at low exposure levels.

In summary, the intent of this portion of the report is to identify and discuss the findings that inform the shortcomings of the basic assumptions following from the use of V_E/SA_r , and in particular V_E/SA_{ET} , as the basis for default interspecies dosimetry of inspired gases. Section 2 presented the reasoning behind the use of V_E as a surrogate for gas dose and use of SA_r for normalization of dose along with acknowledgment of the general advancement this concept made to inhalation dosimetry. Figure 3-6 provides an illustrative summary and perspective of what airflow and CFD models have presented regarding the default procedure. This figure illustrates the assumptions of uniformity underlying V_E/SA originally shown in Figure 2-3. The composite evidence and results from this information indicate nonuniform air flow, surface areas, and deposition for gases in the ET region. In addition, this information indicates that humans do not receive 5 times the “dose” to the ET region compared to rats.

Thus, more extensive quantitative models are needed to integrate newer information that may lead to more informed estimates of interspecies dosimetry. These models and the results from their application are the principal subject of Section 3.2.5 of this report.



Note: The text-containing arrows below the figure represent the information presented in this chapter that has addressed the assumptions of uniformity. The arrows and labels extending to the right demonstrate the outcome of applying this information to the overall process introduced in Figure 2-3.

Figure 3-6 Representation of application of the state of the science to the assumptions and outcome of the *RfC Methods* basic default procedures for comparative gas dosimetry in the ET region.

3.2.5 Evaluation and Use of Models in Interspecies Inhalation Dosimetry - ET Region

As discussed previously, the default RfC method for interspecies dose-extrapolation for the ET region is determined by the ratio V_E/SA_{ET} of animals to humans. When applied for an interspecies comparison with rats, for example, the calculation results in a RGDR of approximately 0.2 – 0.3, indicating a default assumption that the inhalation delivered dose to humans is up to fivefold greater than to the rat.

Current evidence indicates that flow and distribution of V_E in the respiratory tract is not uniform, and that CFD modeling offers refined and characterized disposition of airflow and of the gases present in V_E . However, CFD offers resolution only to the surface of the tissues in contact with the airflow. It does not and cannot offer resolution of interspecies tissue dosimetry, that is, the concentration of the gas in the target tissues of the respiratory tract.

The purpose of this section is to summarize new information that relates these basic issues of dosimetry in the airways, i.e., flux of gas to the tissue surfaces and the concentration of gas in the airway tissues. The focus of this section is on the results and insights gained from the combination of modeling approaches of CFD on airflow and gas disposition in the airways with the state of the science developments from physiologically-based pharmacokinetic or PBPK models describing pharmacokinetics in respiratory tract tissues.

Various models have been developed and utilized to examine and quantitatively estimate dose to target tissues via the inhalation route of exposure in both animals and humans. As discussed above, 3-D, anatomically accurate CFD models were developed to model inspiratory airflow and estimate regional uptake and amount of inhaled gas reaching sites in the nose, with formaldehyde serving as the vanguard example for this application ([Kimbell et al., 2001a](#); [Kimbell et al., 2001b](#); [Kimbell and Subramanian, 2001](#); [Kimbell et al., 1997a](#); [Kimbell et al., 1997b](#); [Kimbell et al., 1993](#)). One output of these simulations is an estimate of flux which is the rate of mass transport in the direction perpendicular to the nasal wall, typically with units of pmol/(mm²-h-ppm). In this regard, the CFD model estimates a “dose” of gas delivered to the tissue boundary but not into the tissue itself. CFD modeling simulations can also be utilized to estimate the surface area and volume of specific anatomical features, the allocation of inspired air to specific flow streams, and gas phase mass transfer coefficients ([Kimbell and Subramanian, 2001](#)). While representing a major step forward in describing and refining interspecies inhalation dosimetry compared to the current default RfC methods, the nature of CFD model output (in terms of flux) does not provide a definitive measure of target tissue dose. Developments in tissue physiology and kinetic models, however, have provided this information and allow for more refined and accurate dosimetry in and between species. Combination of these two modeling approaches led to the development of CFD-PBPK hybrid models allowing for the most highly refined and accurate estimates of target tissue dose currently available. More detail on these modeling approaches is provided in the *Status I Report*.

3.2.5.1 Overview of CFD-PBPK Hybrid Modeling – Combination of Gas Transport in the Air Phase into the Liquid/Tissue Phase

CFD-PBPK hybrid modeling represents the state-of-the-art science for examining inhalation dosimetry. As discussed in Bush et al. ([1998](#)), combined CFD and PBPK models were developed to help address how factors related to airway anatomy might be a reason that other models assuming uniformity, such as the ventilation-perfusion model, failed to fully explain the effects of gas flow on total vapor uptake in different animal species. Consequently, Bush and colleagues ([1998](#)) developed a hybrid model based on combining these two aspects, the CFD model for consideration of gas disposition in the

air phase and the PBPK models for consideration of gas disposition into the liquid and tissue phases within the rat nose. This was accomplished by coupling PBPK and CFD models at the gas-tissue phase interface with a permeability coefficient – termed K_{gm} – that incorporated the gas phase mass transfer coefficient (k_g) with a mucus phase diffusion parameter.

The model and its predictions were then validated by using overall uptake data from rat inhalation studies for three nonreactive vapors that were either completely inert (acetone), reversibly ionized in aqueous media (acrylic acid), or prevented from being metabolized by an enzyme inhibitor (isoamyl alcohol). This CFD-PBPK hybrid model was thus parameterized and validated with empirical observational data to model actual uptake into tissues such that actual tissue concentration of the test case vapors could be predicted. The results of this modeling work showed variation of surface area, cross-sectional area, and values of k_g along the differing flow paths among the regions, reflecting the convoluted nature and complexity of the rat nasal geometry.

3.2.5.2 CFD-PBPK Hybrid Modeling and the Overall Mass Transport Coefficient - K_g

In the hybrid modeling approach described by Bush et al. (1998), the PBPK and CFD models were coupled at the gas-tissue phase interface by K_{gm} . The aim of this approach was to determine the regional dose within the respiratory tract by characterizing the transport of gases between the air phase, the intervening surface liquid and tissue, and the blood. K_{gm} is also referred to as the overall mass transport coefficient or K_g .

As described in Appendix I of the *RfC Methods*, the concept of K_g (the overall mass transport coefficient, MTC) is used to describe transport through several different phases including air and liquid. The basic structure of this approach, which relies on K_g , was used in the CFD-PBPK hybrid models developed by Bush et al. (1998) and subsequently by Frederick et al. (1998), both of which incorporate the output from CFD simulations to describe anatomy, airflow, k_g , and flux of inhaled gas in the POE (air phase) linked to a PBPK model describing the systemic compartments (tissue phase).

Bush et al. (1998) and Frederick et al. (1998) provide an updated and modified version of the approach presented in Appendix I to describe gas phase mass transport in which the estimate of the overall transport or flux, N , across and air:liquid interface is expressed by

$$N = K_g (C_g - C_t/PC)$$

Equation 3-1

where K_g (cm/min) is the overall mass transfer coefficient, C_g ($\mu\text{mol}/\text{cm}^3$) is the air phase gas concentration, and C_t ($\mu\text{mol}/\text{cm}^3$) is the concentration in the liquid/tissue phase, and PC (unitless) is the surface liquid/tissue:air partition coefficient.

In general, the overall mass transport coefficient, K_g , from the air phase into the liquid phase may be determined from the transport coefficients of each individual phase, such that

$$1/ K_g = 1/ k_g + 1/(PC*k_t)$$

Equation 3-2

where k_g (cm/min) is the gas phase mass transfer coefficient as defined above, and k_t (cm/min) is the liquid phase mass transfer coefficient. Contextually, K_g may be considered analogous to a tissue clearance term used in compartmental pharmacokinetic studies as similar principles apply ([Frederick et al., 1998](#)). In the case where the surface liquid and tissue cannot be assumed to be a single compartment, a separate partition coefficient and transport coefficient would need to be incorporated to account for additional compartments. For example, in cases where gas diffuses through the tissue into the blood and contributes to overall absorption, additional mass transport resistances must be considered to describe this additional compartment. This is important because significant accumulation and recirculation of gas in the bloodstream may reduce the concentration driving force (and thereby reduce the absorption rate) and contribute to the development of a “back pressure”, which may result in desorption during exhalation due to the reversal in the concentration gradient between the air and tissue.

An initial difficulty identified in the *RfC Methods* in using such approaches, i.e., to determine or decompose an empirically founded K_g , was lack of k_g values in airways of laboratory animals (and humans), and the lack of a data base in which PC_t could be determined. However, much of this difficulty has been overcome and resolved by the advancement and validation of CFD models to obtain estimates of k_g as the gas phase term is dependent on flow rate, flow geometry, and the gas phase diffusivity. In cross-species comparisons, the flow geometry differences of the species are likely to predominately determine k_g . For both CFD and PBPK models, the increase in the amount of data available from various sources defining the gas and water diffusivities, and partition coefficients for many compounds, as well as parameters such as tissue surface area, thickness, volume, air flow, etc., used to describe the anatomical and physiological “compartments” in both animals and humans has aided in advancing these approaches. Several of the models represented below use k_g values determined specifically for that study or the compartmental (or regional) k_g values determined by the CFD simulations conducted by Frederick et al. ([1998](#)) for both animals and humans for the purpose of describing interspecies inhalation dosimetry.

3.2.5.3 Results and Analysis of Interspecies Inhalation Dosimetry Modeling – ET Region

The purpose of this section is to provide an example-based overview of concepts related to the various aspects of inhalation gas dosimetry discussed in the preceding sections and as presented in more detail in the *Status I Report*.

Table 3-3 provides information for various gases including primary toxicological endpoint(s), measured nasal uptake in the rat (if available), as well as water solubilities and partition coefficients. This information was used to provide a physicochemical descriptor for each gas based on the scheme outlined by Medinsky and Bond (2001). Table 3-4 compares the various methods for interspecies dose-extrapolation (i.e., determination of the HEC) between animals and humans for the ET region based on CFD, CFD-PBPK hybrid, or PBPK modeling for these gases to the default RfC method based on \dot{V}_E/SA .

In comparing these physicochemical properties, reactivity, and measured uptake for the representative gases shown in

Table 3-3, a general pattern emerges. Those gases with high uptake (>90% - formaldehyde, acrylic acid) in the ET region are reactive, have higher liquid/tissue:gas (air) partition coefficients (PC), and water solubility. Reactive gases with moderate uptake (acrolein, acetaldehyde, and diacetyl) in the ET region have moderate to low liquid/tissue:gas (air) PC values and water solubility. Gases with low uptake (<25% - hydrogen sulfide, ethyl acrylate and propylene oxide) have among the lowest liquid/tissue:gas (air) PC values in this group of gases. However, these gases also exhibit a range of water solubilities and reactivities. In general, high ET uptake gases tend to be more reactive and scrubbed more efficiently in nasal tissues with little penetration to the lower respiratory tract and less potential for systemic distribution. Likewise, low ET uptake gases have the potential to reach the lower respiratory tract and produce an effect and/or be more readily distributed systemically via the gas exchange area of the lung. An important consideration in examining the relationship among these properties and uptake is that they are substantiated by experimental observations of uptake in the rat.

Table 3-3 Primary toxicological endpoint(s), uptake, properties, and physicochemical descriptor for representative gases—ranked by percentage of uptake in rats

	Endpoint/ Effect	Uptake in Rat ^a	Liquid/tissue :gas (air) PC values	Water Solubility	Physico- chemical Descriptor ^b	References
Formaldehyde	RE Tumors and squamous metaplasia ^c	> 90%	72,000 (calculated)	400 g/L	soluble-reactive	Kimbell et al. (2001b)
Acrylic Acid	OE degeneration	> 90%	6,100	1,000 g/L	soluble-reactive	Frederick et al. (1998); Andersen et al. (2000)
Acrolein	OE degeneration and atrophy	80 – 60%	88 (or 200)	212 g/L	soluble-reactive	Schroeter et al. (2008); Morris (1998); Corley et al.
Acetaldehyde	RE and OE degeneration	80 – 40%	140	1,000 g/L	soluble-reactive	Teegaurden et al. (2008); Dorman et al. (2008); Morris et al. (1997)
Diacetyl	Nasal, tracheal, bronchial toxicity	76 – 36%	550	200 g/L	soluble-reactive	Morris and Hubbs (2009)
Vinyl Acetate	OE degeneration	93 – 40%	29	20 g/L	nonsoluble-nonreactive	Bogdanffy et al. (1999)
Hydrogen Sulfide	OE degeneration and necrosis	26 – 18%	2.8	4-5 g/L	nonsoluble-nonreactive	Schroeter et al. (2006)
Ethyl Acrylate	OE toxicity	25 – 18%	86	15 g/L	nonsoluble-nonreactive	Sweeney et al. (2004); Frederick et al. (2002)
Dimethyl Sulfate	Nasal tissue tumors	NA ^d	100	28 g/L	moderately soluble-reactive	Sarangapani et al. (2004)
Propylene Oxide	RE hyperplasia and OE degeneration	23 – 11%	68	590 g/L	moderately soluble-reactive	Csanády et al. (2007); Morris et al. (2004)

^aUptake – measured percent of inspired vapor that is retained or deposited in the URT of the rat

^bPhysicochemical Descriptor from Medinsky and Bond (2001) (see text for details)

^cRE = respiratory epithelium; OE = olfactory epithelium

^dNA = not available

However, these generalizations do not always hold. For example, propylene oxide has less nasal uptake than might be predicted based solely on its water solubility and/or reactivity and comparable liquid/tissue:gas (air) PC to that of acrolein, thus highlighting its hazard categorization. Conversely, the nasal uptake of vinyl acetate is greater than might be predicted based on those same two properties as well as its relatively low

liquid/tissue:gas (air) PC. In the case of vinyl acetate, nasal metabolism via carboxylesterase greatly enhances its uptake into nasal tissues and also plays a role in its toxicity. Yet, the primary toxicity induced by both of these gases is damage to the nasal epithelium. In addition, it is critical to note the potential that systemic circulation can contribute to effects in regions remote to the site of deposition. For example, some gases can be distributed to remote sites after absorption in nasal tissues, while other gases may be absorbed primarily in the lungs and result in POE effects. These observations highlight the complexity of interspecies dose extrapolation for inhalation as well as the limitations in the application of a strict categorization or descriptor scheme. Therefore, it is important that dosimetry extrapolations/calculations should be based on the effect and the target tissue, and not based solely on physicochemical properties.

Using the physicochemical descriptors scheme proposed by Medinsky and Bond ([2001](#)), an attempt was made to characterize or classify the selected gases based on their criteria as discussed in Section 3.1. For the majority of the chemicals shown in

Table 3-3, application of these descriptors appears straightforward. For example, formaldehyde and acrylic acid are highly soluble and/or reactive with tissue components with little potential for systemic distribution, have high liquid/tissue:gas (air) PC values, and high uptake in the nasal cavity. Acrolein, acetaldehyde, and diacetyl are also best described as soluble and/or reactive with some potential for systemic distribution because of their water solubility, moderate to high liquid/tissue:gas (air) PC values, and moderate to high uptake in the nasal cavity. On the other hand, hydrogen sulfide is best described as non-soluble based on its low water solubility, low liquid/tissue:gas (air) PC and low uptake, and nonreactive based on its hypothesized mode of action – inhibition of cytochrome oxidase due to competitive binding. Also, ethyl acrylate is best described as non-soluble based on its low water solubility, moderate liquid/tissue:gas (air) PC, and low uptake, and nonreactive as its toxicity is mediated via metabolism to acrylic acid. However, similar to the 1994 *RfC Methods*, a set of qualitative descriptors cannot capture the impact of multiple, interacting quantitative properties; once again highlighting the limitations in applying a strict categorization or descriptor scheme. As discussed above, vinyl acetate exemplifies these limitations for a number of reasons. It is relatively non-soluble as a result of its low solubility and partition coefficient and is non-reactive. Both its toxicity mediated by being a reactive aldehyde and its acid metabolites and higher than expected uptake is due to the presence of carboxylesterase in nasal tissues. Further adding to the complexity and limitations of applying such a scheme in a strict manner is the consideration of metabolism. Metabolism may also be considered a component of reactivity in characterizing gas transport in the tissue and predicting site of gas uptake and effect, but based on the examples provided by Medinsky and Bond (2001), metabolism appears to be excluded in designating the parent gas as “reactive”.

As discussed in the previous section, two parameters integral to these models shown are K_g and one of its components k_g . K_g , the overall mass transfer coefficient, describes the movement of gas from the air phase into the liquid or tissue phase by combining k_g , the gas phase mass transfer coefficient, with a liquid or mucus phase transfer coefficient, k_l or k_{mc} . The CFD-PBPK model developed by Bush et al. (1998) and expanded upon by Frederick et al. (1998) describes and highlights the importance of these parameters in the basic model structure for estimating target tissue dose for a wide range of inhaled gases in regions of the nasal cavity for different exposure scenarios. The model was initially used to evaluate the rodent nasal deposition of several poorly metabolized gases, but was further validated using the physicochemical and toxicity properties information for acrylic acid. As a result, several of the examples presented in Table 3-4 also used this same approach, employing the CFD derived k_g values from Frederick et al. (1998).

The modeling results for acrylic acid demonstrated several important findings regarding interspecies differences in inhalation target tissue dosimetry (Frederick et al., 1998). First, the CFD simulations provided estimates of the volume of the airflow through the various regions of the rat and human nasal cavities at various flow rates. These data

confirmed the results observed in other studies showing that a relatively small fraction of inspired air ventilates the human olfactory region compared to the rat. Second, the CFD simulations also showed that where the data can be compared, the regional k_g values for the rat are higher (up to one to two orders of magnitude in the respiratory epithelium) than those for the human. This difference in k_g values indicates that rat nasal cavity is much more efficient in scrubbing gas from inspired air than the human. On a regional basis in the nasal cavity, this interspecies difference in the delivery of inspired gases in the overall nasal cavity is significant due to differences in air flow patterns and distribution of target epithelium.

Table 3-4 shows the DAFs (and HECs) calculated from various state of the science inhalation dosimetry models compared to the default RfC Method. The most critical observation is that the default DAF for the ET region is approximately 0.2 – 0.3 for each of the gases whereas DAF values based on modeling are different for nearly every gas, over a range of sevenfold in this group. These differences are indications of the models' capacity to employ and integrate numerous critical gas- and species-specific parameters and variables in characterizing gas transport through the air and tissue phases for the ET region. For example, the models for ethyl acrylate and dimethyl sulfate indicate that a DAF of 3 or 7, respectively, be applied to the rat POD to determine the HEC. The model predicted DAF for each gas is based on more detailed dose metrics: for ethyl acrylate, internal metabolite concentration; and for dimethyl sulfate, specific DNA adduct concentration. The fact that quantitative differences exist in the DAF values estimated for the ET region is an indication that the comparative dosimetry is sensitive to some combination of these parameters and variables. On the other hand, the default method is *de facto* restricted in its use of the relationship between just two general parameters, V_E and SA_{ET} , to characterize gas transport through the air and tissues phases. Another observation from Table 3-4 is that the DAF values from modeling are all one or greater despite the wide range of gas descriptions and characteristics shown in

Table 3-3, including uptake (11 - >90%), water solubility (5 – 1,000 g/L), and tissue:air partition coefficient values (<3 to >6000). Additionally, these modeled outputs of DAF \geq 1 were achieved through a similarly wide range of dose metrics including those based on maximum target tissue flux and/or maximum target tissue flux at the rat NOAEL, target tissue concentration, target tissue metabolite concentration, adduct concentration, and even changes in intracellular pH. Despite these wide ranges of sensitive parameters and variables, and gas descriptors ranging from “soluble-reactive”, to “nonsoluble-reactive” to “nonsoluble-nonreactive”, the gases in Table 3-4 all achieved the same internal target tissue dose in both rats and humans at either similar (DAF \approx 1) or greater (DAF > 1) external concentration. It is important to note that molecular markers are emerging as useful dosimeters ([Osterman-Golkar et al., 2003](#); [Ríos-Blanco et al., 2003](#)) and as noted for dimethyl sulfate ([Sarangapani et al., 2004](#)).

Table 3-4 Comparison of approaches for calculating the DAF for representative gases in determining the HEC - portal of entry ET or nasal effects

	V/SA _{ET} ^a	CFD ^b	CFD-PBPK hybrid ^c	PBPK ^c	References
Formaldehyde	HEC = 0.2 × AEL	DAF = 1.26 (based on the target tissue max flux of 2620 in Rat and 2082 in Human at 1 ppm)			Kimbell et al. (2001b)
Acrylic Acid	HEC = 0.2 * AEL		DAF = 1.36 (based on target tissue dose at the Rat NOAEL of 25 ppm)		Frederick et al. (1998); Andersen et al. (2000)
Acrolein	HEC = 0.2 * AEL	DAF = 1.4 (based on Rat OE ^D NOAEL = 0.6 ppm: highest flux of 682 in Rat and 476 in Human)			Schroeter et al. (2008); Morris et al. (1998)
	HEC = 0.2 * AEL	DAF = 2.1 (based on 0.6 ppm model results of max flux rates in the anterior nasal airways of 1,400 in Rat and 660 in Human)			Corley et al.
Acetaldehyde	HEC = 0.2 * AEL		DAF = 1.4 (based on steady-state tissue concentrations at the Rat NOAEL = 50 ppm)		Teegaarden et al. (2008); Dorman et al. (2008); Morris et al. (1997)

	V/SA _{ET} ^a	CFD ^b	CFD-PBPK hybrid ^c	PBPK ^c	References
Diacetyl	HEC = 0.2 * AEL		DAF = 1 (based on nasal and tracheal target tissue concentration)		Morris and Hubss (2009)
Vinyl Acetate	HEC = 0.2 * AEL		DAF = 1.14 (based on equivalent change in OE intracellular pH at the Rat NOAEL)		Bogdanffy et al. (1999)
Hydrogen Sulfide	HEC = 0.2 * AEL	DAF = 2.6 (based on Rat OE NOAEL = 10 ppm: highest flux of 34 in Rat and 13 In Human)			Schroeter et al. (2006)
EthylAcrylate	HEC = 0.2 * AEL		DAF = 3 (based on target internal metabolite concentration)		Sweeney et al. (2004); Frederick et al. (2002)
Propylene Oxide	HEC = 0.2 * AEL			DAF = 1 (based on equivalent concentrations in RE and venous blood at < 50ppm)	Csanády et al. (2007); Morris (2004)
Dimethyl Sulfate	HEC = 0.2 * AEL		RE: DAF = 7; OE: DAF = 2 (based on tissue N7mG adduct concentration)		Sarangapani et al. (2004)

^aCalculated based on procedures in U.S. EPA (1994) RfC Methodology where:

- HEC = DAF (RGDR) x Adjusted Exposure Level (AEL - based on NOAEL, LOAEL, or BMCLx)
- DAF or RGDR = $V_E / SA_{ET-animal} / V_E / SA_{ET-human}$
- $DAF_{ET} = (0.18 \text{ L/min}/15 \text{ cm}^2) / (13.8 \text{ L/min}/200 \text{ cm}^2) = 0.18 \text{ or } 0.2$
($SA_{ET-animal} = 15 \text{ cm}^2$; $V_E = 0.18 \text{ L/min}$ for a 250 g rat; $SA_{ET-human} = 200 \text{ cm}^2$; $V_E = 13.8 \text{ L/min}$ for a 70 kg human)

^bResults from CFD simulation modeling – DAF based on comparative animal (rat): human flux values as indicated

^cResults from CFD-PBPK hybrid or PBPK modeling – DAF based on modeled target tissue dose or dose metric as indicated

^dRE = respiratory epithelium; OE = olfactory epithelium

As is the case with all “state of the science” techniques and approaches, limitations and restrictions need be considered, including those of the CFD-PBPK hybrid models presented and described here. These hybrid models may be considered somewhat limited in their refinement of typical PBPK models relative to the linked CFD model. The surface area characterized by the PBPK tissue “stack” is much less refined and defined than the flux values to that same area characterized by the linked CFD model. The gas

flux portion of the hybrid model for this area is represented by a localized k_g into which some of the flux has been collapsed and incorporated. Therefore, small localized areas of very high flux may be diluted or not sufficiently characterized especially for gases exhibiting high flux, i.e., gases that are highly reactive and that have high uptake. Conversely, this refinement limitation would be less applicable to gases that are not highly reactive and that have lower uptake. In addition, due to the common practice of having and utilizing a single constant value for partition coefficients, these models are most appropriately used under exposure conditions that do not approach the limits of solubility and the concomitant establishment of biphasic conditions. In general, these conditions would be those within the linear range of solubility that also allow for maximization of all clearance processes, i.e. low level, long term exposures. Thus, although the currently available CFD-PBPK models are considered to provide better estimates of target tissue dose compared to conventional default methods, they may also be characterized as providing more certainty for relatively nonreactive gases versus highly reactive gases and for lower rather than higher concentrations of reactive gases.

3.3 Major Scientific Advances Related to Inhalation Gas Dosimetry in the TB and PU Regions

Complexity of airway structure, large variations in the geometry of lung airways, multi-scale dimensions of airway parameters (length, diameter, etc.), lack of measurements of all airways including the alveoli, uncertainty regarding airflow distribution among pathways of the lung, and inter-subject variability (also true for the upper airways) combine to make modeling in these regions a challenge. In order of preference, the approaches for lung uptake modeling are (1) CFD modeling, (2) hybrid whole lung-CFD modeling, and (3) whole-lung modeling. The use of CFD for a region and entire lung should be attempted when pertinent information is available. In the hybrid model, MRI- or CT-based images of the upper airway (including nasal and first few generations) are reconstructed computationally and are attached by whole-lung models at the distal ends to create a computational domain for the entire lung. The advantage of hybrid model is that it uses state-of-the-art in computational resources and fills in the missing information with mechanistically-based whole-lung models. For the whole-lung modeling, representative geometry of the entire respiratory tract is used in the area-averaged mass balance (convective-diffusion) equation for gases to find regional gas uptake.

The following sections summarize the major scientific findings related to the current default procedure for interspecies inhalation dosimetric extrapolation for gases in the TB and PU regions. The information evaluated includes results and observations from anatomically based airflow, deposition, and fluid dynamics modeling as well as from chemical specific interspecies physiologically based pharmacokinetic (PBPK),

computational fluid dynamics (CFD), CFD-PBPK hybrid models, and whole-lung modeling.

3.3.1 Air Flow and Deposition Modeling in the TB Region

A number of conceptual and simulation modeling approaches for both the TB and PU region are under investigation. However, many of these approaches are being examined using only human model structures thus limiting their utility in directly informing interspecies dosimetric extrapolation for risk assessment purposes. Nonetheless, several studies provide useful qualitative information relative to the current default approach of V_E/SA .

Taylor et al. (2007) examined the pattern of lung injury resulting from exposure to ozone. The distribution of ozone uptake was studied in a single, symmetrically branched airway bifurcation using CFD. Separate simulations for inspiratory and expiratory flows were conducted at laminar flow conditions to examine the effect of flow rate on uptake. The simulations demonstrated the total rate of ozone uptake increased with increasing flow rate during both inspiration and expiration and that flux progressively decreased along the parent branch. In addition, hotspots of ozone flux were observed at the carina of the bifurcation for all simulated flow rates. Compared to a straight tube with a similar surface area, the presence of branching resulted in an enhancement of overall uptake.

Padaki et al. (2009) used CFD modeling to simulate the transport and uptake of ozone for comparison between an idealized model of the larynx, trachea, and first bifurcation and a “control” model in which the larynx was replaced by an equivalent, cylindrical tube segment. This comparison was performed in order to examine the effect of laryngeal geometry on flow behavior. The results revealed a strong laryngeal jet with a reattachment point in the proximal trachea indicated by an increase in flow velocity and abrupt geometry change in flow. Jet turbulence occurred only at the high Reynolds numbers and was attenuated by the first bifurcation. Hotspots previously reported at the first carina were confirmed by the local fractional uptake data; additional hotspots at the glottis and proximal trachea were also observed. Maximal laryngeal effects (~15% enhancement of uptake efficiency) occurred at the highest flow rate. Although the increase in regional uptake subsided by the end of the model (i.e. the first bifurcation), the effect of the larynx on cumulative uptake persisted further downstream. Together, these results suggested that with prolonged exposure to a reactive gas entire regions of the larynx and proximal trachea could show effects of tissue exposure.

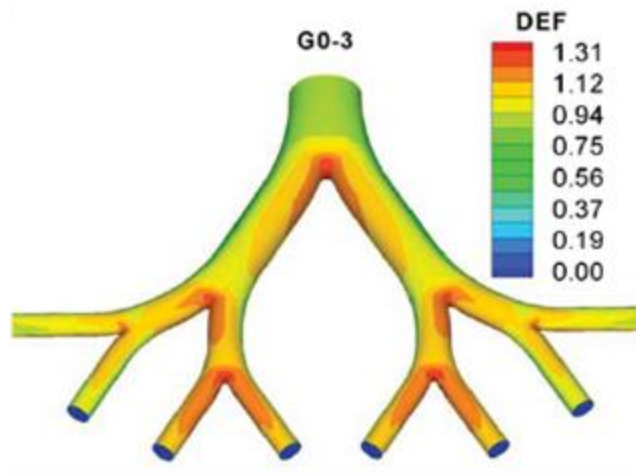
Zhang et al. (2006) employed a representative human upper airway model to describe uptake and deposition of MTBE and ethanol vapors. This description was accomplished using CFD approach. Model simulations were done under varying conditions, including 3 inspiratory flow rates ($Q_{in} = 15, 30, \text{ and } 60 \text{ L/min}$). The airway model utilized was

created from a human cast consisting of two parts: the oral airway, including oral cavity, pharynx, larynx and trachea; and a symmetric triple bifurcation representing generations G0 (trachea) to G3 (referred to in their report as the “upper bronchial airway” or UBA). To attain representative modeling of airflow in such a model, a low-Reynolds-number model was selected (to assure laminar flow and constant fluid motion) and adapted to the laminar-to-turbulent flow regimes that are likely to occur in the human airway during inhalation at the flow rates employed in the simulations. The deposition of vapors in each airway segment was described by the deposition fraction (DF), which was calculated with the regional mass balance and the sum of local wall mass flux. An uptake parameter (K) was also calculated for both ethanol and MTBE using available values of diffusivity of vapor in air and liquid mucus phase and equilibrium partition coefficients in gas and liquid interfaces. The respiratory mass transfer coefficient (called h_m by the authors) was also estimated.

The simulations showed that flow rate had a strong effect on vapor deposition; the lower the flow rate, the higher the deposition fraction due to the extended vapor residence times. Results showed that as the flow rate decreased from 60 L/min to 15 L/min, DF for MTBE increased from 2.5% to 7.7% in the UBA. The simulation showed further that the DFs increased in a nearly linear fashion with the distance into the airway, indicating consistent deposition efficiency along the airway passage. Compared with MTBE, DF values of ethanol were approximately three to six times greater in the oral airways and two to five times greater in the UBA in the range of flow rates used. The higher deposition of ethanol vapor may be attributed not only to its higher diffusivity but, more importantly, to its higher solubility in the mucus layer as indicated by the value of K for ethanol (413) compared to MTBE (11). Vapors that pass through the upper airway may further penetrate into and deposit partly in the lower airway and alveolar regions. Compared to ethanol, this suggests MTBE may penetrate further and thus deposit in the lower airways.

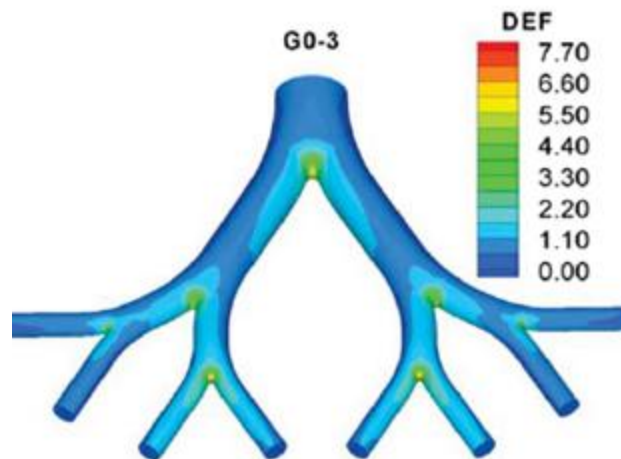
Simulations based on the mesh were analyzed by the authors on a more refined scale. Local vapor deposition patterns were quantified in terms of a deposition enhancement factor (DEF), which is defined as the ratio of local to average deposition densities, DEF therefore being an indication and representation of vapor deposition “hotspots” in a given region. Figure 3-7 and Figure 3-8 show the distributions of these DEFs in the airway components of the model. These deposition patterns were clearly not homogeneous and were nonuniform for ethanol, which is relatively highly absorbed in the UBA, and for MTBE, which is not highly absorbed. The maximum DEF was ~ 1.5 for MTBE in the UBA with the value reaching 7.8 in the UBA model for ethanol. The low maximum DEF values for MTBE indicated that deposition of MTBE vapor was relatively uniformly distributed in the upper airways with relatively little absorbed by the airway walls whereas the opposite appears to be the case for ethanol with the greater overall absorption allowing for more contrasting differences and higher DEF “hotspots.”

In the bifurcation airway model, enhanced deposition occurred mainly at the carina ridges and the inside walls around the carina ridges, due to the complicated airflows and large concentration gradients in these regions. When the absorption parameter (K) increases above the typical value, however, deposition of MTBE increases but with deposition patterns being about the same. With increasing absorption, however, the locations of enhanced deposition receive even greater deposition and the maximum DEF values increase.



Source: Reprinted with permission of Informa Healthcare; Zhang et al. (2006)

Figure 3-7 Distributions of deposition enhancement factor (DEF) for MTBE vapor with $Q_{in} = 30$ L/min in the bifurcation airway models.



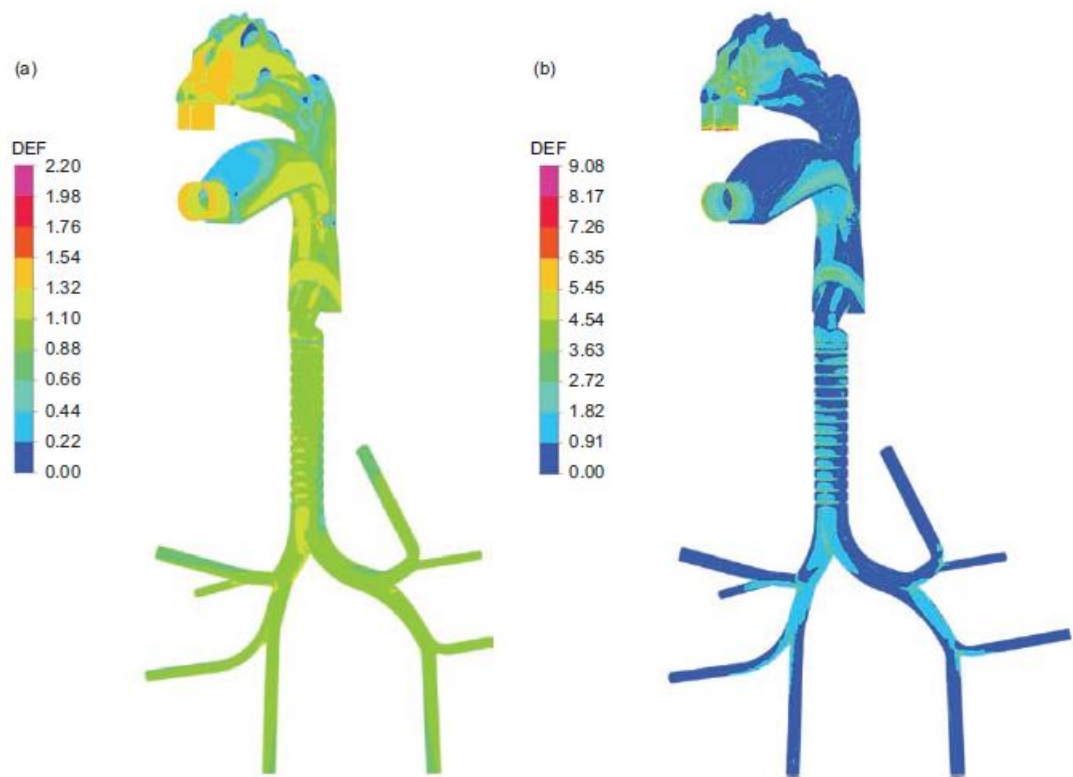
Source: Reprinted with permission of Informa Healthcare; Zhang et al. (2006)

Figure 3-8 Distributions of deposition enhancement factor (DEF) for ethanol vapor with $Q_{in} = 30$ L/min in the bifurcation airway models.

These simulations utilized a three dimensional computational fluid dynamic simulation method and provided detailed local deposition patterns for both MTBE and ethanol, agents widely disparate in uptake, transport and deposition. These deposition patterns showed clearly that tissue burdens at local sites may exceed by many times the average dose of the airways, i.e. they are highly nonuniform. Whereas flow rates greatly affected deposition fractions, deposition patterns were not much altered. The localized deposition pattern suggested that the uptake pathway may have a preferential route along which local tissues are subjected to heavy exposure of vapors much the same as has been

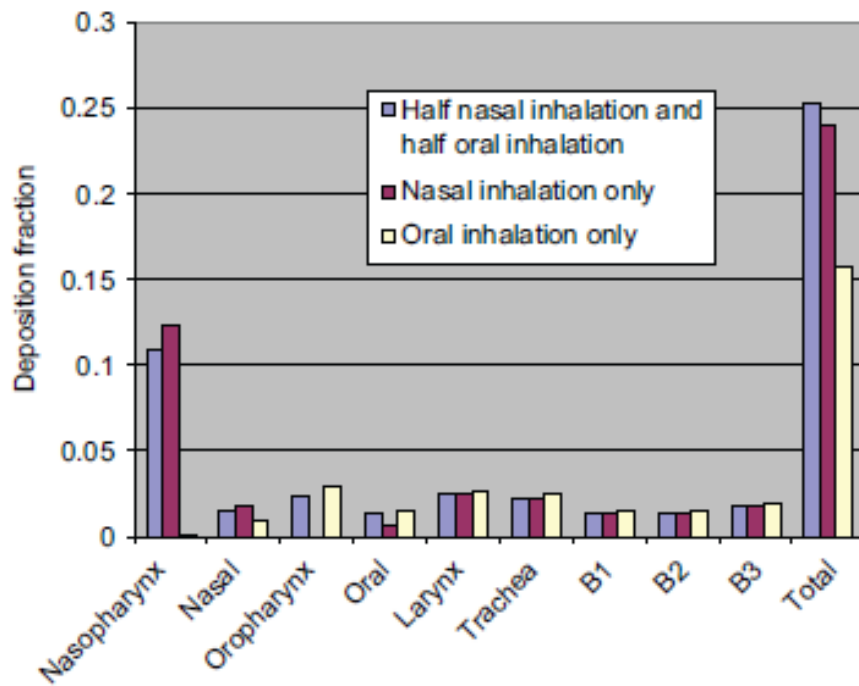
demonstrated for formaldehyde in the ET region of rats (e.g., [Kimbell et al., 1997b](#)). Thus, this enhanced deposition at local sites in this lower region of the respiratory tract may also result in tissue damage or other adverse biological responses at local sites in the first four generations of the human tracheobronchial tree.

In more recent work, Zhang et al. ([2011](#)) used a human CFD model to estimate local and regional uptake of naphthalene and tetradecane, considering three different breathing scenarios (nose-only, oral-only, and a combination). This upper airway CFD model consisting of the oral airways, nasal airways, and trachea (asymmetric bifurcations, G0-G3) was developed based on previously published geometries. The authors found the airway wall absorption is a key determinant of deposition in the respiratory system, while other parameters (e.g., diffusivity, airway geometry, breathing patterns, inspiratory flow rates) are also key factors. The representative absorption parameter, K , was 4 orders of magnitude greater for naphthalene (7.3 cm^{-1}) compared to tetradecane ($7.4 \times 10^{-4} \text{ cm}^{-1}$) because of physical properties of the chemicals and variations in the thickness of the mucus layer. Thus, tetradecane was found to have a DF <1% in the ET and TB regions, due to its low solubility in the mucus layer, while DFs in the alveolar region ranged from 7-24% depending on inhalation rate and mucus thickness. However, the opposite was true for naphthalene which deposits mostly in the ET (DF of 12-34%) and TB (DF of 66-87%) regions. Zhang et al. ([2011](#)) also investigated the local deposition patterns assuming perfect wall absorption ($K \rightarrow \infty$) (Figure 3-9. The simulated local deposition patterns of naphthalene vapor for concurrent nasal and oral breathing for (A) $K=7.3 \text{ cm}^{-1}$ and (B) perfect wall absorption. This figure shows nonuniform deposition patterns and deposition in the upper airways is more uniformly distributed with lower wall absorption. The locations of enhanced deposition may not change; however, the maximum DEF value increases with increasing absorption.). This showed nonuniform deposition patterns and that the vapor deposition in the upper airways is more uniformly distributed with lower wall absorption. Their results also showed that the variation in breathing route (nasal vs. oral) for both chemicals does not substantially impact vapor deposition beyond the larynx (Figure 3-10. Total deposition fraction is independent of breathing mode at the larynx and beyond.).



Source: Reprinted with permission of Informa Healthcare; Zhang et al. (2011).

Figure 3-9. The simulated local deposition patterns of naphthalene vapor for concurrent nasal and oral breathing for (A) $K=7.3 \text{ cm}^{-1}$ and (B) perfect wall absorption. This figure shows nonuniform deposition patterns and deposition in the upper airways is more uniformly distributed with lower wall absorption. The locations of enhanced deposition may not change; however, the maximum DEF value increases with increasing absorption.



Source: Reprinted with permission of Informa Healthcare; Zhang et al. (2011).

Figure 3-10. Total deposition fraction is independent of breathing mode at the larynx and beyond.

Madasu (2007) compared approaches to modeling inhaled dose in the pulmonary airways that can characterize the axial nature of dose and injury known to occur with various reactive agents. These authors' comparison was based on contrasting models representing the lower airways of the lung. The basis for comparative measurement of flow and absorption characteristics in these contrasting models is a representative 3-generational bifurcating unit of pulmonary airway. The first model reported was composed of Weibel geometry of repeated symmetric bifurcating tube geometry to which a 3D computational fluid dynamic model (CFDM) was applied (under conditions of steady expiratory flow). The second model was a two-dimensional model with geometry consisting of a series of rigid cylindrical tubes of decreasing diameter representing the branches in a generation. This model was termed by the authors as an axisymmetric single path model (ASPM). The basis of the comparison of these two models was their mass transfer coefficients for formaldehyde obtained from the designated gas characteristics and the gas flow conditions applied. The mass transfer coefficient (K_g) was defined to represent an overall coefficient of uptake or absorption. Numerical results were compared for two different inlet flow rates, wall mass transfer coefficients, and bifurcation angles. The results of these model simulations indicated that the mass transfer coefficients from the ASPM representation compared well with CFDM qualitatively and quantitatively. In general, the mass transfer coefficients from both models were noted to increase with bifurcation angle, inlet flow, and wall mass transfer coefficient. Further, the change in mass transfer

coefficients at each bifurcation unit was also closely predicted, and the average concentration variation axially was qualitatively the same in both the predictions from the CFDM and ASPM models with quantitative differences observed likely due to the differences in flow characteristics in the branches. The authors concluded that these results indicated that the “simplified” ASPM was very useful in predicting mass transfer coefficients, flux at the walls, and hence injury sites as accurately as the “complex” CFDM in symmetric lung systems where it was not possible to measure them. Similar observations were made by Madasu et al. (2008).

3.3.2 Advances in TB Inhalation Dosimetry Modeling

Recently, Morris and Hubbs (2009) characterized the inhalation dosimetry of diacetyl, a component of butter flavoring vapors, through development of a CFD-PBPK hybrid model. Upper respiratory tract (URT) uptake of diacetyl was measured experimentally and used to validate the model. Model simulations were then performed to estimate tissue (anterior and posterior) and airborne concentrations of diacetyl for the URT (i.e. nasal) and trachea in rats and humans. At an exposure concentration of 100 ppm, tissue concentrations in the nose were estimated to be 1.6 and 1.4 mM in rats and 1.4 and 1.2 mM in humans, and in the trachea were estimated to be 1.2 and 1.1 mM in rats and 1.2 mM in humans. The air exiting the URT was estimated to be 67 ppm in rats and 82 ppm in humans, and air exiting the trachea was estimated to be 61 ppm in rats and 79 ppm in humans. When the human model was run for mouth breathing only, the tissue concentrations in the trachea were predicted to be 1.5 mM and the air exiting this region to be 96 ppm. These results demonstrated that target tissue concentrations of diacetyl in the trachea were highly similar in rats and humans and that diacetyl may penetrate to the lower airways of humans to a greater degree than in rats. The authors concluded that based on these dosimetric relationships and differences in regional uptake efficiencies, upper airway injury in the rat may be predictive of lower airway injury in humans.

Tsujino et al. (2005) developed a simplified mathematical airway model to simulate the transport of gases (ozone [O₃] and sulfur dioxide [SO₂]) in airways of laboratory animals (rats and dogs) and humans. The aim of the study was to examine through model simulations how interspecies anatomical and physiological differences influence the transport of the inhaled gases throughout the airways and alveoli. This comparison could potentially provide an interspecies comparison of gas dosimetry in airways. The authors acknowledge and document that nearly all input parameters used were assumed or scaled, albeit with reasonable assumptions and allometry. Gas absorption at the surface of the airways was determined by mathematical formulations incorporating the basic elements of diffusivity and absorption constants (which included the absorption rate at the airway surface) that were scaled to each gas. The basis for this scaling was actual absorption data and concentration differences for these gases obtained by direct measurements in dog

airways. Real-time changes in gas concentrations were simulated at three airway sites in each species: (1) the upper airway, (2) the lower airways consisting of the 5th or 10th bronchial generation and (3) the alveolar region. The amount of O₃ and SO₂ absorbed (modeled assuming a 10% concentration) at the airway surface was then calculated. Interspecies comparison was also performed for the amount of gas absorbed per body weight (g/BW), and for the corrected amount of gas absorbed per unit of airway surface area (g/cm²). The results obtained for O₃ and SO₂ are shown in Table 3-5 below.

Table 3-5 Modeled predictions of amount of O₃ and SO₂ absorbed at various sites in the airways of three species

Parameter	Rats	Dogs	Humans
Ozone			
Total absorbed amount (g/kg BW)	1.1 × 10 ⁻⁷	1.46 × 10 ⁻⁷	0.847 × 10 ⁻⁷
Upper airways (% of total)	73.9	80.7	34.4
Lower airways (% of total)	23.4	16.3	60.7
Alveolar region (% of total)	2.7	3.0	4.9
Absorbed amount per SA/unit time			
Upper airways (g/cm ² / min)	1.76 × 10 ⁻⁷	0.89 × 10 ⁻⁷	1.31 × 10 ⁻⁷
Lower airways (g/cm ² / min)	3.52 × 10 ⁻⁸	1.29 × 10 ⁻⁸	7.58 × 10 ⁻⁸
Alveolar region (g/cm ² / min)	1.56 × 10 ⁻¹³	1.23 × 10 ⁻¹³	1.40 × 10 ⁻¹³
Sulfur dioxide			
Total absorbed amount (g/kg BW)	1.77 × 10 ⁻⁷	3.24 × 10 ⁻⁷	1.61 × 10 ⁻⁷
Upper airways (% of total)	98.6	99.4	96.5
Lower airways (% of total)	1.4	0.6	3.5
Alveolar region (% of total)	0.0	0.0	0.0

Source: Reprinted with permission of Informa Healthcare; Tsujino et al. (2005)

These simulations indicate that the amount of O₃ absorbed per body weight throughout the airways was lowest in humans (Table 3-5). However, the amount of absorbed O₃ per surface area in each airway were fairly equivalent in the upper airways and alveolar regions, and were higher in humans in the lower airways - over 2 times that of rats. This trend was noted also for SO₂. Concentrations of SO₂ in the lower airways and alveoli were low in all species, which reflects the predicted rapid absorption of the gas in the upper airway. Also, these simulations were for short periods of inhalation and relatively high concentrations of these agents. It should be noted that many simplifications and assumptions were necessary in order to accomplish the simulations. Some of these were application of a simple three-compartment model of the airways and alveoli, without specific consideration of the effects of different branching patterns on the airway surface areas. Coaxial diffusion of gas molecules was not taken into account in the simulations,

as it is well known that gas molecules in airways are transported by both bulk flow and diffusion. Thus the modeled gas concentrations might not accurately reflect actual concentrations, particularly in the peripheral airways and in the alveoli. Nonetheless this study is of considerable value for further hypothesis testing regarding the variations in the kinetics of inhaled gases among experimental animals and humans. It numerically demonstrated that interspecies variations in anatomy and respiratory patterns cause significant differences in gas transport in the airways and alveoli of rats, dogs, and humans.

The results of Morris and Hubbs (2009) and Tsujino et al. (2005) estimate similar target tissue doses in the TB and PU regions between rats and humans albeit by different modeling approaches (i.e. CFD-PBPK hybrid vs. simplified mathematical model). These indicate and support an approximate DAF of 1 when extrapolating from rats to humans. This is in contrast to the results obtained when applying the default RfC Method using V_E/SA which gives rat to human DAFs of approximately 2.6 for the TB region and 3 for the PU region.

Flux-based dosimetry estimates for formaldehyde gas to the TB and PU regions were developed by Overton and coworkers (2001). These estimates were inclusive of calculations for overall mass transport coefficients for the lower respiratory tract. Formaldehyde transport and uptake for the generations comprising the TB and PU regions were all approximated by a one-dimensional (1D) convection-dispersion equation that accounted principally for molecular diffusion and absorption at the air-liquid surface. The mass transfer coefficients in the nasal cavity were estimated by matching (within 0.2%) the percent uptake predicted by an existing CFD model of transport during inspiratory flow through an anatomically accurate reconstruction of the nasal passages of an adult human male. The resulting overall identical-path nasal airway mass transfer coefficients multiplied by the nasal surface area, corresponding to minute volumes of 7.5, 9.0, 25, and 50 L/min (nasal steady-state inspired flows rates of 15, 18, 50, and 46 L/min) were 1.68, 1.78, 2.98, and 2.83 cm/s, respectively. The K_g for the lower airways was calculated with extensive consideration given to the k_g component. The 1D equation of mass transport was then applied to each generation airway and airway passage of a symmetric, bifurcating respiratory tract anatomical model to provide predictions of local formaldehyde surface fluxes (dose). The results obtained included the following:

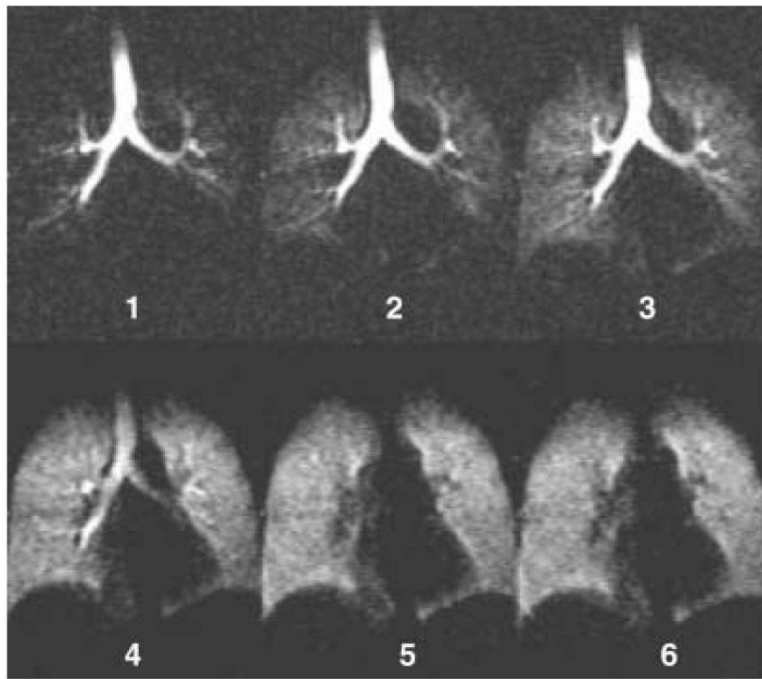
- More than 95% of inhaled formaldehyde is predicted to be retained by the respiratory tract for all activity states simulated (for a total of 4 different minute volumes).
- In the lower respiratory tract, surface flux (dose) is predicted to increase for several generations and then decrease rapidly.

- Compared to first pulmonary generation fluxes, the first few tracheobronchial generation fluxes are over 1,000 times larger.
- There is essentially no flux in the alveolar sacs.

The authors stated the predicted fluxes based on the 1D model for those lower regions of the respiratory tract can be used in dose-response modeling. This work provided information on mass transfer coefficients for the PU and TB regions including their derivation, and demonstrated their use in a dosimetry model for these regions.

3.3.3 Air Flow and Deposition Modeling in the PU Region

^3He MRI has been especially used to visualize dynamic ventilation during both inspiration and expiration of ventilation in normal individuals ([Kauczor et al., 2002](#)). Application of this technique indicates that normal ventilation in healthy lungs is represented by a completely homogeneous distribution at the level of resolution of ^3He signal. Figure 3- illustrates the in-life rapid and homogenous filling of the airspaces bilaterally (the numbers correspond to the sequence imaging times). In volunteers the inflow of ^3He was shown to be very rapid with the discernible signal appearing almost simultaneously in the upper, middle and lower portions of the lung with a uniform wash-in and wash-out of the gas also observed. Further advances, involving echo-planar imaging of axial slices having rapid temporal resolution times of 122 ms, are able to demonstrate preferential ventilation of the posterior lung zones in supine individuals, again through visualization of areas of nonhomogenous flow in the lung. Further demonstrations of the resolution of the ^3He - imaging is the capacity to observe even small (2 cm) transient ventilation defects in the lungs of smokers that appear as nonhomogeneous flow and distribution. In clinically healthy smokers even markedly smaller ventilation defects leading to nonhomogenous flow, such as those thought to correspond to chronic inflammation and obstruction of small airways caused by smoking, can be detected with ^3He MRI. Thus, these techniques provide an approach to acquire regional information on lung morphology and pulmonary function.

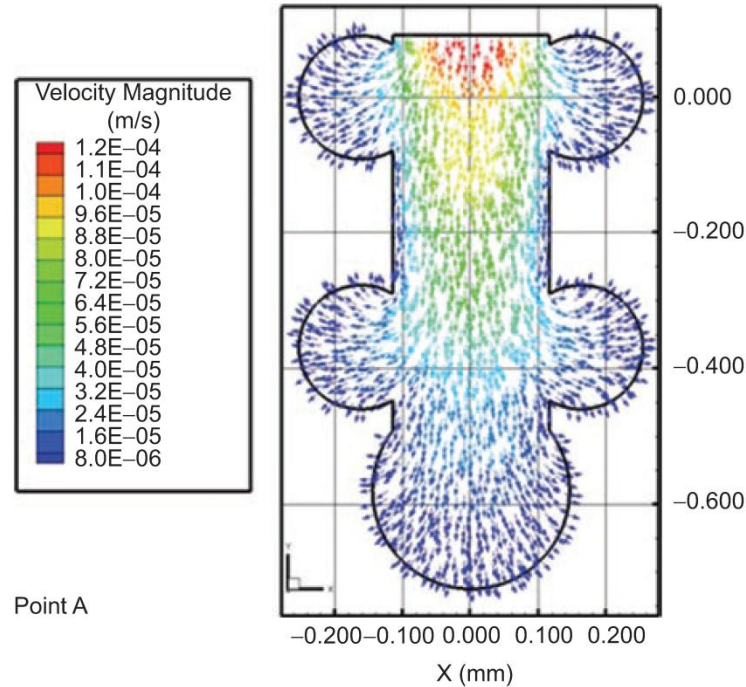


Source: Reprinted with permission of Springer Berlin/Heidelberg; Kauczor et al. (2002)

Figure 3-11 Dynamic ventilation ^3He MRI after inhalation of hyperpolarized ^3He gas.

Whole-lung dosimetry models do not account for the flow field to the level of inside the alveoli and therefore may not accurately describe alveolar flow or deposition. To better understand the fluid characteristics at this level of the lung, Harding and Robinson (2010) employed CFD to a model of a terminal air sac much in the manner that it has been applied to other respiratory tract regions, notably the extrathoracic (ET) region. An expanding terminal alveolar sac using truncated spheres to represent individual alveoli was modeled numerically, based on dimensions from human lung casts. The flow field is quantified for a breathing cycle derived from pulmonary function test measurements. The alveolar sac model was considered representative of a terminal air unit in humans that could be present in Weibel generations 19 and below based upon dimensions from literature. The wall motion of the alveolar sac model (full expansion of 15.6% over the initial volume or functional residual capacity - FRC) was obtained in vivo using a spirometer for a 21-year-old female breathing normally in the sitting position. Model output was obtained for detailed regional flow rates, alveolar mouth to depth flow rate ratio, and penetration depth of residual air. Figure 3- demonstrates the directionality and range of regional flow velocities as well as their extent of incursion into the sac, all obtained from the model (Harding and Robinson, 2010). Examination of the flow field in the alveoli revealed no recirculation during any point in the breathing cycle. Other parameters addressed with the model included the flow rate ratios of alveolar mouth to duct flow that were noted in the range of 0.18–0.36. Penetration depths were less than 33% into the air sac during inhalation, decreasing in length for air inside the sac to zero

near the wall. These results indicated dominance of diffusive motion over convective motion and flow at the level of the alveoli. However, more studies are needed before quantification of flow fields in the alveolar region can be clearly understood as the ratios that are present in vivo are also unknown.



Source: Reprinted with permission of Informa Healthcare; Harding and Robinson ([Harding and Robinson, 2010](#)).

Figure 3-9 Simulated flow velocities from CFD solutions in an alveolar sac model.

In an earlier study, Tsuda et al. ([2002](#)) observed flow patterns of different colored polymerizable fluids, representing tidal and residual air, injected into rat lungs in a manner to simulate inhalation of tidal air. These authors concluded that the swirls seen in the solidified cast in the large, medium, and alveolar airways were characteristic of chaotic flow. They observed swirl patterns in alveoli that became more intense with increasing number of cycles, which were not seen by Harding and Robinson ([2010](#)), who utilized a model of terminal air sacs. Although these authors did not indicate whether their observations were from a terminal sac or a respiratory bronchiole, it is possible that the patterns observed by Tsuda et al. ([2002](#)) occurred higher up in respiratory bronchioles where the flow rate ratio was large enough to cause irreversibility.

It is clear that more studies are needed on pulmonary fluid flow to better understand the nature of tidal and residual air mixing and the conditions under which mixing occur. It is apparent from these disparate results that more corroborating evidence is needed before actual flow fields in the terminal air sacs are understood. In addition, the occurrence of significant localized deposition cannot be excluded without additional studies.

3.3.4 Advances in PU Inhalation Dosimetry Modeling

Following from the work of Morris and Hubbs (2009), Gloede et al. (2011) developed a CFD-PBPK model for inhalation dosimetry of diacetyl in rats and humans to compare respiratory tract vapor absorption focused on the lower respiratory tract. The CFD-PBPK modeling approach that had been utilized for URT dosimetry was expanded to include the lower respiratory tract (LRT) based on anatomical models reported elsewhere in the literature. Using this detailed model, they estimated human and rat bronchiolar tissue concentrations of diacetyl. The difference between the human and the rat were more marked under light exercise and mouth breathing. The largest difference was in diacetyl bronchiolar concentrations for the mouth breathing-lightly exercising human that exceeded the nose breathing rat by 20- to 40-fold. Diacetyl bronchiolar concentrations in other human scenarios (human nose breathing at rest and human mouth breathing at rest) were only 3-7 times greater than the nose breathing rat for a 10 minute simulation at 1ppm (Gloede et al., 2011). These differences may in large part be due to the greater distal penetration of inspired diacetyl in the human than in the rat as also shown in Morris and Hubbs (2009). This CFD-PBPK model provided a method to predict diacetyl concentrations in tissues under multiple scenarios that are not easily obtainable via controlled laboratory experiments.

More recently, Asgharian et al. (2012) published a mechanistic model of vapor uptake for inhaled soluble, reactive vapors (formaldehyde, acrolein, and acetaldehyde) in the human lung for a single breath. Since formaldehyde is highly reactive and soluble, it was mostly absorbed in the trachea with 97% of the inhaled dose estimated to be absorbed. On the other hand, acrolein and acetaldehyde are moderately soluble, thus they were absorbed deeper in the lung, with acetaldehyde being absorbed more distally than acrolein. However, overall uptake for acrolein was slightly greater (84%) than for acetaldehyde (80%). Tissue concentrations, following inhalation of 1 mg/m^3 , of each chemical were calculated during the inhalation, pause, and exhalation phase of one breathing cycle. This mechanistic lung dosimetry model is the first to provide a prediction of the transient tissue concentrations over the entire breathing cycle and how the tissue concentrations impact the absorption from the airway. The model showed that flux patterns do not always correspond to tissue dose and concentration and confirmed that tissue thickness is a critical determinant for absorption into systemic circulation.

The Asgharian et al. (2012) model lacks description of the URT which does impact the dose delivered to the lung; however, Corley et al. (2012) report a more complete CFD-PBPK model for acrolein that extended from the nasal cavity to on average 9, 17, or 19 generations in the pulmonary region for the human, rat, and monkey, respectively. This model found flux values in ET region to be greatest in the rat compared to the monkey followed by the human; comparisons were not made for the TB or PU regions. In the LRT flux rates were low in comparison with those observed in the URT. Hot spots were identified in areas with changing airflow directions and velocities and potential sites of

metabolism. When the model was run at twice the V_E , peak concentrations were 258% higher. These results are similar to what was found in acrolein nasal extraction studies by Morris and Hubbs (2009) and the light-exercising human diacetyl nasal extraction estimations of Gloede et al. (2011) in which an increase in flow rate increased distal penetration.

3.4 Advances in the Measurement of V_E and Airway Geometry

Within the past decade, advancements have been made in the methods used to measure ventilation rate (V_E) and determination of airway geometry. The advancements in determination of V_E were presented in detail in the *Status II Report* (U.S. EPA, 2011b).

Briefly, two prominent approaches for inhalation rate measurement in a nonclinical setting include (1) activity pattern questionnaires where oxygen consumption is calculated from daily activity patterns/energy intake and (2) differential dilution of isotopes in water administered orally as a bolus, usually over a two-week period. This latter method, the doubly labeled water (DLW) method, measures oxygen lost through carbon dioxide production. The DLW method was used to calculate the physiological daily inhalation rates (PDIR) for 2,210 individuals aged 3 weeks to 96 years (Brochu et al., 2006b). These were considered state of the science and included in EPA's recently updated *Exposure Factors Handbook* (U.S. EPA, 2011a) and evaluated in the *Status II Report* (U.S. EPA, 2011b). More recently, Brochu et al. (2011) improved upon their initial calculations of PDIRs by including both daytime and nighttime respiratory parameters (oxygen uptake factors and ventilatory equivalents) in the calculation, thereby providing more precise PDIRs for use in risk assessment. In general, these values were within 10% of the values reported earlier by Brochu (2006b, a; 2006c). Kawahara et al. (In Press, 2011) also calculated PDIR values for 5-6 year old Japanese children for an average of weekday and weekend activities. Overall, these results were slightly less than the values determined by Brochu et al. for both genders.

In addition, methods to determine airway geometry and surface area have evolved, providing more reliable values for use in inhalation gas dosimetry. These are summarized below and more detail is also provided in the *Status II Report* (U.S. EPA, 2011b).

3.4.1 Lung Geometry and Surface Area

The estimation of alveolar number in the lung has traditionally been done by assuming a specific geometric shape. These geometries are then applied to small sampled volumes of pulmonary tissue. However, the realizations that there exists a diversity of alveolar shapes and that statistical error from small sample size and bias may be considerable, have led to alternative approaches. Hyde et al. (2004) synthesized recent approaches and

technologies that were designed to be less prone to error and bias and therefore produce more reliable counts. These authors employed the following for the counting of alveoli in the lungs of monkeys and rats: a fractionator which allows for systematic random sampling from blocks of variable slab thickness (thereby minimizing the inaccuracy inherent in using section sampling fractions based on the average thickness of sections of variable thicknesses); use of the Euler characteristic of the net of alveolar openings to estimate alveolar number; the disector principle (usually a counting probe for isolated objects) as a sampling probe of the Euler characteristic. The Euler characteristic of structure (an integer)² applies to any level of topological complexity and is not biased toward any specific geometry (as have other attempts to count alveoli).

Lung tissues from four male and one female rhesus macaques (*Macaca mulatta*) ranging in age from 28 to 157 months and in body weight from 3.4 to 11.6 kg, as well as tissue from five male Wistar rats with age not given and varying in body weight from 503 to 625g were used for this study. Using this approach on these tissues indicated the number of alveoli in the two left lung lobes in the monkey ranged from 48.8×10^6 to 67.1×10^6 with a mean of 57.7×10^6 . The average number of alveoli in the rat lung ranged from 17.3×10^6 to 24.6×10^6 , with a mean of 20.1×10^6 . With age (2-13 years) the alveolar volume increased 3-fold (as did parenchymal volume) in monkeys, but the alveolar number was unchanged. The lung volumes as estimated in rats are presented in Table 3-6.

Table 3-6 Estimates of right, left, and total lung volumes in male wistar rats

Animal #	Body Weight (g)	Lung Volumes (cm ³)		
		Right Lung	Left Lung	Total Lung
R5	503	10.6	8.8	19.4
R3	528	8.0	4.2	12.2
R4	573	11.4	5.5	16.9
R1	595	10.2	5.3	15.5
R2	625	12.3	6.1	18.4
Mean	565; (CV 0.09)	10.5; (CV 0.15)	6.0; (CV 0.29)	16.5; (CV 0.17)

CV = coefficient of variation

Source: Reprinted with permission of John Wiley and Sons; Hyde et al. (2004)

Ochs et al. (2004) performed advanced stereologic analysis of human lungs for the purpose of evaluating the number of alveoli present in the total lung (Table 3-7). The

² The Euler characteristic is a number that describes a shape or structure regardless of its orientation or the manner in which it may be bent. For simple structures it may be determined from the formula $\chi = V - E + F$, where χ is the Euler characteristic, V the vertices, E the edges, and F the faces of a polyhedron shape. For a tetrahedron, for example, the Euler characteristic from this formula is $4 - 6 + 4 = 2$.

stereologic method for the estimation of alveoli utilized the Euler number as the basis for quantification, eliminating assumptions and the resultant bias about the shape, the size, or the spatial orientation or distribution of alveoli. Alveolar number was estimated using light microscopic sections and concentrating on alveolar lumens, using their appearance or disappearance in a physical disector as counting events. Lungs for analysis were obtained from six cases of single lung transplantation, four females and two males. In six adult human lungs, the mean alveolar number determined by these procedures was 480 million (240 million \times 2 to account for both right and left lungs), with a range of 274-790 million and the coefficient of variation 37% (Table 3-7). Alveolar number was observed to be closely related to total lung volume, with larger lungs having considerably more alveoli. The mean size of a single alveolus was rather constant with $4.2 \times 10^6 \mu\text{m}^3$ (range: 3.3×10^6 to $4.8 \times 10^6 \mu\text{m}^3$; coefficient of variation 10%), irrespective of the lung size. The authors calculated that one cubic millimeter of lung parenchyma contains around 170 alveoli. No further attempts were made by the authors to obtain estimates for other parameters including surface areas, although such calculations were feasible.

Table 3-7 Summary data on human lung alveolar number and volume

Parameter	Lung 1	Lung 2	Lung 3	Lung 4	Lung 5	Lung 6	Mean Value
Gender (age)	Female (31)	Female (41)	Female (18)	Female (37)	Male (24)	Male (20)	
Lung analyzed	Left	Right	Right	Left	Right	Left	
N (alv), 10^6	137	226	220	185	275	395	240 ± 89
V (lung), cm^3	1,031	1,273	1,509	1,103	1,917	2,317	$1,534 \pm 521$
N/V (mm^3)	132	178	146	168	143	170	156

Source: Reprinted with permission of American Thoracic Society; Ochs et al. (2004).

Wiebe and Laursen (1995) compared a stereological morphometric method with a standard fluid displacement method for determination of volume of right human lungs obtained from 4 cadavers. Comparison showed that the two methods were in very close agreement (Table 3-8). These authors then completed a stereological estimation of alveolar surface area of these same lungs. Specifically sampled sections of lung tissue (vertical and isotropic uniform random, IUR) were evaluated by specific counting techniques related to a test line in a reference space whereas the volume of the section was evaluated with the Cavalieri principle³. The authors also estimated that of the total variation encountered in the processes only approximately 2% was due to the

³ For a 3-dimensional case, the Cavalieri principle is: suppose two regions in three-space (solids) are included between two parallel planes. If every plane parallel to these two planes intersects both regions in cross-sections of equal area, then the two regions have equal volumes. This provides an unbiased and efficient estimate of the volume of a solid object of arbitrary shape using systematic stereologic sectioning.

stereological variation. In evaluating their estimates of lung surface areas by these techniques, the authors compared their results with other known determinations of lung surface area (Table 3-8).

Table 3-8 Summary table of measures from right lungs of human cadavers

Lung Measure		Case #				Mean ± SD	Reference
		1	2	3	4		
Volume (L)	Fluid	1.9	1.7	1.9	2.0	1.9 ± 0.13	Wiebe and Laursen (1995)
	Cavalieri	2.2	1.7	2.2	2.2	2.1 ± 0.25	Wiebe and Laursen (1995)
Capillary length (m × 10 ⁵)	Vertical slices	12.3	5.6	7.5	6.3	7.9 ± 3.0	Wiebe and Laursen (1995)
	IUR	11.6	6.1	9.6	6.6	8.5 ± 2.6	Wiebe and Laursen (1995)
SA (m ²)	Vertical section	50.3	35.0	49.4	38.5	43.3 ± 7.7	Wiebe and Laursen (1995)
	IUR section	49.9	32.0	49.1	35.3	41.6 ± 9.3	Wiebe and Laursen (1995)
Total SA (m ²)						40–97 ^a	Thurlbeck (1967)
						78.4–81.6 ^b	Wiebe and Laursen (1995)

^aInternal surface area range for 25 pairs of lungs, free from acute or chronic disease, from patients ranging from 25 to 70 years of age.

^bCalculated by authors using right lung SA mean measurements of Vertical section $43.3/0.53 = 81.6 \text{ m}^2$ and of IUR section $41.6/0.53 = 78.4 \text{ m}^2$.

Source: Reprinted with permission of John Wiley and Sons; Wiebe and Laursen (1995)

Knust et al. (2009) employed advanced stereological morphometric techniques in measuring lung parameters in adult female CL57B6 mice (20.6 g average weight; no N given). Capillary length was measured using the harmonic mean of the surface weighted diameter. The Euler characteristic was applied in the physical fractionator with varying but known sampling fractions and enabled the estimation of alveolar number. The estimation of volume fractions of different lung compartments was carried out by point counting. All values were corrected for tissue shrinkage. The following measures were obtained for adult mice lungs (mean, CV):

- total values for alveolar number of 2.31×10^6 (0.23)
- alveolar surface area of 82.2 cm^2 (0.17)
- alveolar air spaces of 138 mm^3 (0.29)
- capillary surface area of 124 cm^2 (0.13)

- capillary length of 1.13 km (0.13)

Bolle et al. (2008) examined functional and morphological characteristics in the developing rat lung. Groups of specific pathogen-free Wistar-Kyoto (WKY) rats were used for the examinations. Measures recorded included lung volume, respiratory mechanics (intrapulmonary gas mixing, and gas exchange) and structural (alveolar surface area, mean linear intercept length, and alveolar septal thickness) at 7-90 days. Four males were sacrificed at each age for analysis. A selected set of measurements are presented from this report in Table 3-9.

Table 3-9 Functional and morphological features of the developing male rat lung

Parameter (n = 4)	7 Days	14 Days	21 Days	35 Days	90 Days
Body weight (g)	22 ± 1.4	34 ± 6.5	76 ± 8.5	165 ± 13.3	417 ± 22.6
Surface area (cm ²)	744 ± 20	1,175 ± 114	1,648 ± 188	3,571 ± 490	6,536 ± 488
Total lung capacity (mL)	1.54 ± 0.07	1.9 ± 0.46	4.6 ± 2.6	7.8 ± 0.83	16.7 ± 2.46
Alveolar wall thickness (µm)	13.4 ± 1.8	8.1 ± 0.6	5.4 ± 0.4	5.5 ± 0.8	6.4 ± 1.0

Source: Reprinted with permission of The American Physiology Society; Bolle et al. (2008)

3.5 Major Scientific Advances in Inhalation Gas Dosimetry Related to Systemic (SYS) Sites

3.5.1 Methods and Advances for Estimating Blood:Gas (Air) Partition Coefficients

The importance of blood:gas (air) partition coefficients ($H_{b/g}$) for PBPK models, and lack thereof, prompted several approaches and strategies to enhance their development and availability. Payne and Kenny (2002) reviewed, evaluated, and conducted a comparative analysis of several predictive methods and models utilized to calculate $H_{b/g}$. As a first step in their analysis, these authors gathered principal resources and approaches to derive $H_{b/g}$ (Meulenberg and Vijverberg, 2000; DeJongh et al., 1997; Poulin and Krishnan, 1995; Abraham and Weathersby, 1994; Gargas et al., 1989; Abraham et al., 1985). The results and comparisons of these various approaches are summarized and discussed in the *Status II Report*.

3.5.2 Quantitation using Inhalation PBPK Models for Systemic Sites

Physiologically-based pharmacokinetic (PBPK) models are biological, integrated functioning systems of flow, volumes, and partitioning processes, with the purpose to predict the time course distribution of a chemical in the body. The robustness of such models is demonstrated by their ability to predict empirical observations.

When model simulations successfully predict empirical results, typically obtained independent of the model, it is an indication that both the model and the sensitive critical parameters within the model have predictive utility. For example, when models that are parameterized and configured to predict interspecies dose extrapolation (e.g., between rats and humans) are successful in their predictions, the model and its parameters are both considered adequate. As referred to above, partition coefficients and in particular blood:gas (air) partition coefficients ($H_{b/g}$), are among these critical determinative parameters. It then follows that inhalation PBPK models that (1) are parameterized and configured for interspecies extrapolation and (2) are successful in predicting empirical results in animals and humans would be a source of representative $H_{b/g}$ for both humans and animals. It is the ratio of $H_{b/g}$ between animals and humans that is the basis for *RfC Methods* inhalation gas dosimetry for SYS effects (see Section 2.5.4). Consequently, validated inhalation PBPK models were obtained and examined for these critical parameters which were extracted and constructed as a ratio in accordance with the *RfC Methods*. The results of this investigation are presented in

Table 3-10. This table includes the PBPK model reference, chemical modeled, animal gender, species, and strain when available, the method used to determine the $H_{b/g}$ employed in the model, and the A/H $H_{b/g}$ ratio. Based on this analysis, the A/H ratios in three instances were less than 1 (e.g., 0.7, 0.6, and 0.6). For 2-BE and 2-ME, the rat values were assumed to be equal to human $H_{b/g}$ values; and for naphthalene and n-butanol, the human values were assumed to be equal to the rat $H_{b/g}$ values.

Table 3-10 Compilation of blood:gas (air) partition coefficients used in Inhalation PBPK models for animal to human interspecies extrapolation

Chemical ^a (Reference)	Animal			Human		A/H Ratio
	H _{b/g}	Species/ Strain	Method	H _{b/g}	Method	
PCE (Dallas et al., 1995)	18.9	♂SD rat	In vivo tissue conc – time course	10.3	Sealed vial	1.8
TCE (Cronin et al., 1995)	14.3	♀ Mouse	Not stated ⁱ	9.2	Not stated ⁱ	1.6
	13.2	♂ Mouse	Not stated ⁱ			1.4
Toluene (Tardif et al., 1997)	18	Rat	Sealed vial	15.6	Sealed vial	1.1
Toluene (Benignus et al., 1998)	18	Rat	In vivo	15.0	-	1.2
Xylene (Tardif et al., 1997)	46	Rat	Sealed vial	26.4	Sealed vial	1.7
EBZ (Tardif et al., 1997)	42.7	Rat	Sealed vial	28.0	Sealed vial	1.5
Ethanol (Pastino et al., 1997)	2,140	Rat	Sealed vial ^f	1,265	Sealed vial ^g	1.7
	1,244	Mouse	Sealed vial ^e			1.0
2-BE (Lee et al., 1998)	7,965	Rat	Not stated ^b	7,965	Sealed vial skin: air	1 ^b
	7,965	Mouse	Not stated ^b			1 ^b
2-ME (Gargas et al., 2000)	32,800	Pregnant SD rat	Sealed vial ^b	32,800	Sealed vial	1 ^b
Naphthalene (Willems et al., 2001)	571	Rat	Calculated	571 ^c	Calculated	1 ^c
Ethylene glycol (Corley et al., 2005)	17,901	♀ SD & Wistar rat	Sealed vial	17,542	Sealed vial	1.0
<i>n</i> -Butanol (Teeguarden et al., 2005)	1,160	Rat	Sealed vial	1,160 ^c	-	1 ^c
PGME (Corley et al., 2005)	4,866	Rat	Sealed vial	7,107	Sealed vial	(0.7)
PGMEA (Corley et al., 2005)	1,251	Rat	Sealed vial	609	Sealed vial	2.0
<i>n</i> -Decane (Hissink et al., 2007)	21	Rat	Sealed vial	37	Sealed vial	(0.6)
1,2,4-TMB (Hissink et al., 2007)	148	Rat	Sealed vial	85	Sealed vial	1.7
Chloroform (Liao et al., 2007)	20.8	Rat	Sealed vial ^h	7.43	Not Stated ^j	2.8
	21.3	Mouse	Sealed vial ^h			2.9
1,1,1-TCE (Lu et al., 2008)	5.76	Rat	Sealed vial ^d	2.53	Sealed vial ^d	2.3

Chemical ^a (Reference)	Animal			Human		A/H Ratio
	H _{b/g}	Species/ Strain	Method	H _{b/g}	Method	
Mel (Sweeney et al., 2009)	39.3	Rat	In vivo, sealed vial	18 (male)	Sealed vial	2.2
	16	Rabbit (adult)	In vivo, sealed vial	17.1 (female)	Sealed vial	1.0
	12	Rabbit (fetal)	In vivo, sealed vial	17.6 (fetal)	Sealed vial	(0.6)

^aChemical abbreviations: ethylene glycol monomethyl ether (2-ME); 2-butoxyethanol (2-BE); propylene glycol methyl ether (PGME); propylene glycol methyl ether acetate (PGMEA); trichloroethylene (TCE); perchloroethylene (PCE); 1,2,4-trimethylbenzene (1,2,4-TMB); ethylbenzene (EBZ); methyl iodide (MeI), 1,1,1-trichloroethane (1,1,1-TCE).

^bRat values were assumed to be equal to human H_{b/g} values in this model.

^cHuman values were assumed to be equal to the rat H_{b/g} values in this model.

^dExperiments and values first reported by Reitz et al. ([1988](#)).

^eExperiments and values first reported by Pastino et al. ([1996](#)).

^fExperiments and values first reported by Kaneko et al. ([1994](#)).

^gExperiments and values first reported for whole blood by Fiserova-Bergerova and Diaz ([1986](#)).

^hExperiments and values first reported by Gargas et al. ([1989](#)).

ⁱValues first reported by Fisher and Allen ([1993](#)).

^jValues first reported by Steward et al. ([1973](#)).

3.5.3 Results and Analysis of Systemic Interspecies Inhalation Dosimetry Modeling

Inhalation PBPK models use air and blood flows, predicted or measured absorption rates, various biological rate processes (e.g., metabolism) and partitioning over time, and a range of external exposure air concentrations to a given toxicant to predict dose metrics. As explained above, the H_{b/g} is a key, and often determinative, parameter.

A dose metric is the internal tissue concentration of a toxicant, or a form of that toxicant such as a metabolite, associated with the external exposure to a toxicant. For a tissue that is a focus of toxicity (i.e., a target tissue), the concentration of a toxicant in the tissue is considered to be an essential determinant of risk. The dose metric may be a concentration over time (e.g., area under the curve, AUC), a maximum concentration achieved (C_{max}), or a steady-state concentration. Examples of dose metrics are C_{max} of parent compound in the liver, AUC of a metabolite in the brain, or circulating blood concentration of parent compound at steady state. The concentration in the blood is often used instead of the concentration in a target tissue because blood concentrations are more readily measured, allowing for model calibration and validation, and average or steady-state tissue concentrations are expected to vary in proportion to blood levels.

PBPK models may be developed for a variety of purposes, one of which is interspecies extrapolation, the general subject of this report. The manner in which this is performed is to first use the animal model to estimate a dose metric (internal dose) associated with a

given level of toxicity or response and then use the human model to estimate the external concentration for humans that yields the same internal tissue dose metric. As stated previously, the human estimate of the external concentration that produces that same internal dose metric is the human equivalent concentration or HEC.

Several of the studies listed in

Table 3-10 developed inhalation models for purposes of interspecies extrapolation. Table 3-11 below presents specific descriptions of the dose metric and the modeling estimates of the human equivalent concentration that corresponds to the same internal dose metric calculated for the laboratory animal based on the animal exposure scenario.

Table 3-11 Estimations from inhalation PBPK models of human equivalent concentrations (HECs) from effect levels and internal dose measures in laboratory animals

Chemical ^a (Reference)	Level and Effect	Dose Metric	Comments	PBPK Derived HEC
Isopropanol (Gentry et al., 2002)	NOAEL 2,500 ppm renal tissue of female rats	Arterial blood concentrations, AUC	HEC derived from Table 4 (in (Gentry et al., 2002) by applying uncertainty factor of 30: (159.8 × 30 = 4,767 ppm); 189.8 ppm × 30 = 5,700 ppm. Animals exposed for 6 hr/day, 5 days/week. Contiguous exposure modeled in humans.	4,767 ppm
	LOAEL 3,500 ppm developmental			5,700 ppm
n-Butanol (Teeguarden et al., 2005)	NOAEL 500 ppm weight gain	Arterial blood concentrations, AUC	Weekly average blood conc. estimated for rats at 6 hr/d, 5 d/wk and continuous for humans. Model estimates compared against human blood levels from 30 min inhalation exposure. Tables and equations are provided for HEC calculation over wide range of butanol concentrations.	169 ppm
	NOAEL 3,000 ppm neurotoxicity	Arterial blood concentrations, AUC		1,066 ppm
PGME (Kirman et al., 2005b)	NOAEL 3,000 ppm presence of sedation	Cmax, richly perfused tissues	Model simulations estimated NOAEL internal dose metric values in rodents ranging from 2,300-5,000 mg/L for exposures from 3,000 ppm for 1-78 wks of exposure (6 hr/d, 5 d/wk). The arithmetic mean of the NOAEL was 4,036 mg/L. This value was used to estimate an HEC for a continuous 24 hr exposure.	560 ppm
White spirits (Hissink et al., 2007)	NOEL 600 mg/m ³ neurotoxicity	Brain concentration of 1,2,4-TMB or decane determined in rats exposed for 6 hr/day	Model and 4-hr HEC based on main components of WS, 1,2,4-TMB and decane. Estimates are for acute exposure CNS effects. Human model validated with blood and alveolar air kinetics.	344–721 ^c mg/m ³
	LOEL 2,400 mg/m ³ neurotoxicity			1,669 – 4,431 ^c mg/m ³
2-ME (Gargas et al., 2000)	NOEL 10 ppm developmental	Blood Cmax or average daily AUC for 2-MAA (acetic acid; metabolite of 2-ME)	The model was used to calculate an HEC for pregnant women exposed for 8 hr/day, 5 days/week for 270 days at various 2-ME. Human validation information from urinary excretion rates of 2-MAA from volunteers exposed to 5 ppm 2-ME	12 ppm
	LOEL 50 ppm developmental	in rats exposed for 6 hr/d, 5 d/wk		60 ppm

Chemical ^a (Reference)	Level and Effect	Dose Metric	Comments	PBPK Derived HEC
Ethylene glycol (Corley et al., 2005)	11 ppm (28 mg/m ³) ^b developmental	C _{max} for glycolic acid (GA) in blood	Model was used to generate a dose-response comparison of internal dose surrogates (C _{max} for GA in blood) in female Sprague-Dawley rats and in humans (Figure 10B in (Corley et al., 2005)). Several controlled rat and human metabolism studies were used to validate the PBPK model.	~79 ppm (~200 mg/m ³)
1,1,1-TCE (Lu et al., 2008)	NOAEL 1,500 ppm liver effects	Average daily venous blood, AUC. Calculated in rats exposed for 6 hr/d, 5 d/wk	Table 5 (in (Lu et al., 2008)) shows HEC calculations over a wide range of exposures concentrations for continuous human exposure. Four human data sets were used in evaluating model selection.	640 ppm

^aChemical abbreviations: ethylene glycol monomethyl ether (2-ME); propylene glycol methyl ether (PGME); 1,1,1-trichloroethane (1,1,1-TCE), 1,2,4-trimethylbenzene (1,2,4-TMB), 2-methoxyacetic acid (2-MAA), glycolic acid (GA), white spirit (WS).

^bThe threshold blood concentration for developmental effects of 2 mM is not attainable in humans based on the modeling and maximum tolerated inhalation exposures reported in this paper ([Corley et al., 2005](#)). The maximum vapor concentration for EG is only 79 ppm (~200 mg/m³) due to low volatility (0.06 mm Hg at 20°C) ([Corley et al., 2005](#)). Therefore, for this comparison, the human C_{max} at the maximum vapor concentration (200 mg/m³) was estimated by the model to be ~6.5 μM. The exposure concentration predicted by the model that would yield the same C_{max} in the rat is ~28 mg/m³.

^cRange of values is presented because exposure concentrations were estimated that yielded brain concentrations equivalent to observed values for 1,2,4-TMB or decane. Values at the lower end of the range correspond to WS estimates based on 1,2,4-TMB brain concentrations, while the higher values are based on decane brain concentrations.

Table 3-12 combines data from

Table 3-10 and Table 3-11 to present examples comparing approaches in estimating HEC from laboratory animal data for systemic effects. With n-butanol, for example, an systemic effect level of 500 ppm in the laboratory animal study is duration and dosimetrically adjusted to an HEC using the *RfC Methods* default approach (a DAF of 1; see Section 2) to yield 90 ppm. The neighboring column to the right shows the HEC derived using the PBPK model at 169 ppm. The ratio of these HECs are then compared to indicate the extent and direction of difference, such that the n-butanol default HEC is two-times less than estimated by the PBPK model. For further comparison, the actual A/H $H_{b/g}$ ratio is also given, here shown for n-butanol which in this case is the same as the *RfC Methods* default.

As can be seen, the extent of difference encountered between the default and PBPK HEC values is quite wide, spanning over 10-fold (e.g., isopropanol default method gives an HEC of 446 ppm and the PBPK method gives 4,767 ppm) even for this small set of example chemicals. In all cases, the default RfC Method provides a lower HEC than those derived using PBPK modeling, except for PGME which is nearly equal. Additional modeling results for propylene oxide and VOCs have shown DAFs to be approximately 1. The propylene oxide PBPK model of Csanády et al. (2007) predicted similar blood concentrations of propylene oxide in humans and rats up to 50 ppm exposure. The simplified, steady-state PBPK model solution for inhaled VOCs shows that on the basis of internal dose (blood concentration), humans develop similar liver venous blood concentrations and lower rates of metabolism per volume of liver and tend to develop target tissue doses that are similar to or lower than those in the experimental animals for the same external air concentration (Aylward et al., 2011). No general trend can be discerned to explain this range of differences, either between the default and PBPK HEC or between the actual $H_{b/g}$ and the PBPK HEC. It may be that other covariates, such as concentration-dependent metabolism may need to be further explored and evaluated. In application of PBPK models, it may also be necessary to thoroughly evaluate the origination of model parameters, including the $H_{b/g}$. Taken together, these results support the use of a default DAF of 1 for gases producing systemic effects.

Table 3-12 Comparison of approaches for calculating human equivalent concentrations (HECs) for several gases with systemic (SYS) effects

Chemical (Reference)	Rat POD (Table 3-7)	RfC Method				HEC - PBPK Method (Table 3-7)	PBPK/RfC HEC Ratio
		POD _{adj}	$(H_{b/g})_A / (H_{b/g})_H$ (Table 3-6)	DAF	HEC ^a		
n- Butanol (Teeguarden et al. (2005))	500 ppm	90 ppm	1.0	1	90 ppm	169 ppm	1.88
1,1,1-TCE (Lu et al. (2008))	1,500 ppm	270 ppm	2.3	1	270 ppm	640 ppm	2.4

PGME (Kirman et al. (2005a))	3,000 ppm	540 ppm	0.7	1	540 ppm	560 ppm	1.04
2-ME (Gargas et al. (2000))	10 ppm	1.8 ppm	1	1	1.8 ppm	2.9 ppm ^b	1.61
Isopropanol (Gentry et al. (2002))	2,500 ppm ^c	446 ppm	1.5	1	446 ppm	4,767 ppm	10.7
	3,500 ppm ^d	907 ppm			907 ppm	5,700 ppm	6.28
Ethylene glycol (Corley et al. (2005))	11 ppm	--	1	1	11 ppm	79 ppm	7.18

^aHEC derived by default *RfC Methods*: $POD_{adj} \times DAF = HEC$ where the POD_{adj} is the POD adjusted for duration of exposure in the animal study and a default DAF of 1 is applied for $(H_{b/g})_A / (H_{b/g})_H$. (e.g., for n-butanol, the $POD_{adj} = 500 \text{ ppm} \times 6 \text{ hr}/24 \text{ hr} \times 5 \text{ days}/7 \text{ days} = 90 \text{ ppm}$.)

^bIn the PBPK model for 2-ME, the HEC was calculated for a discontinuous exposure and was therefore adjusted for duration (8hr/24 hr \times 5 days/7 days).

^cBased on renal effects.

^dBased on developmental effects.

3.6 Current Science Related to Children's Inhalation Dosimetry

3.6.1 Introduction and Focus

This section is focused on identification and preliminary evaluation of data, evidence, and information relating directly to gas dosimetry in children.

The 1996 Food Quality Protection Act (FQPA), refocused interest in matters of child risk. Title III of this act specifically tasked the Agency in their assessments under the FQPA to "...ensure that there is a reasonable certainty that no harm will result to infants and children ...".

Although this Act was directed at oral ingestion of pesticides, specifically those used on foodstuffs, the Agency considered its implications both with regard to pesticide risk assessments and more broadly to EPA methodology. For example, EPA developed approaches for interpretation and implementation of the requirements specifically to FQPA-required pesticide assessments (e.g., see <http://www.epa.gov/oppfead1/trac/science/>), and additionally implemented a full review of the Agency's RfC/RfD processes to insure they appropriately considered the potential for increased childhood susceptibility (U.S. EPA, 2002).

This Act eventually affected many organizations and resulted in a spectrum of implementation actions and strategies. One of the most prominent is that undertaken by the state of California in implementing their Children's Environmental Health Protection Act (Senate Bill 25) of 1999. The state's Technical Support Document for the Derivation of Noncancer Reference Exposure Levels (OEHHA, 2008) provides extensive

information on children as a population of concern and on pharmacodynamic and pharmacokinetic differences between children and adults. Appendix E of that same document includes an extensive analysis of children related data and models, including PBPK models, that provide insight into the range of inter-individual variability in general, but focus extensively on the differences among infants, children and adults. This report does not intend to provide a comprehensive review of these reports, but notes them as examples of the risk assessment community's movement toward additional consideration of children in dosimetry and dose-response toxicity assessments.

In 1993, the NAS published its findings regarding chemical toxicity in children compared to adults ([NRC, 1993](#)). The report addressed both specific findings and recommendations. Conclusions of the committee included that infants and children may be more, or less, susceptible than adults depending upon the chemical and the age of the subject. It was acknowledged that substantial changes occur in organ size, structure, and function from infancy through puberty; such changes could substantially affect the pharmacokinetics and pharmacodynamics of chemicals. Accordingly, there may be periods, or lifestages of increased susceptibility, when developing tissues are much more sensitive to toxicants than later in life. The NAS report ([1993](#)) also stresses the importance of recognizing that the younger the individual, the more pronounced his/her structural and functional anomalies and thus the greatest differences from adults in susceptibility to chemical toxicity can be anticipated, with continuous diminishment of those differences thereafter. The report also stated the need for scientifically defensible means to deal with toxic agents that cannot be directly studied in children. A specific recommendation in the report following from this realized the need to use PBPK models. PBPK models can be used both to simulate the time course of parent compounds and bioactive metabolites in blood and tissues of adult animals and humans and to predict target organ doses of toxic chemicals/metabolites for different exposure scenarios in children of different ages.

A recommendation following from the potential use of PBPK models was that they be reliably developed by obtaining accurate measurements of respiratory parameters, circulation, metabolism, tissue and fat volumes, and partition coefficients. These parameters can be measured in primates or in children of different ages by noninvasive procedures. The parameters would be used in PBPK models, which could then be utilized to better estimate the concentration time course of chemicals/metabolites in potential target organs. It is the recommendations and statements from the NAS report ([NRC, 1993](#)) that guides the structure and content of this section of this report. This report focuses on those reports and studies that directly inform the state of the science related to gas dosimetry in children. How this information informs the default RfC Methods is also considered.

The 1994 *RfC Methods* considers all lifestages, including children, in the intraspecies uncertainty factor that is designed to incorporate the range of response variability in human populations. This uncertainty factor is typically considered to have two

components, pharmacodynamics and pharmacokinetics, with the latter component being the basis of dosimetry. It is within the kinetic portion of this uncertainty factor that potential dosimetry differences of susceptible lifestages, including children, are considered.

Recognizing that young children have a greater ventilation rate per body weight or per surface area in the respiratory tract compared with adults, Ginsberg et al. (2005) analyzed the outcomes of gas dosimetry approaches of *RfC Methods* utilizing infant child (3 mo) and adult male values available from various sources for the principal determinants of V_E , $SA_{ET,PU}$, and BW. The TB region was characterized differently from *RfC Methods* as comprising two separate regions termed tracheobronchial (BB) and bronchioles (bb) by the authors. Dosimetry was estimated for 3-month-old infants and adults for reactive and nonreactive gases. Estimations of comparative dosimetry were made using a reasonable range of assumed K_g values. The authors used the same K_g values for both children and adults indicating that no basis exists for assuming a difference. The modeling results suggested similar dosimetry of gases for infants and adults for the ET and BB regions. Dosimetry for the bb region generally showed a higher dose of gases in adults than in 3-month-old infants. It was also noted that, based on the K_g value, dosimetry for adults versus 3-month-old infants in the PU region could be slightly different, either higher or lower but not greater than 2-fold different. There were no cases in which gas dose was substantially greater in the respiratory regions of 3-month-old children compared to adults. Estimates of systemic doses of nonreactive gases were greater in 3-month-old children than in adults, especially for liver doses (up to 2-fold) of metabolites for rapidly metabolized gases. Overall, these results suggest the potential for a 2-fold greater inhalation dose in 3-month-old infants (based on data from 3-month-old children) than in adults, although there are cases in which this differential could be greater or less.

As PBPK models configured for elucidating dose to children and infants were recommended in the NAS report and are prominent in the current literature, they will be featured in this section. Studies that provided insight and data for parameters needed for these models and/or for general knowledge about development in early lifestages related to aspects of dosimetry are also presented. These include studies on air flow and CFD modeling as well as respiratory tract growth. Information on inhalation rates in children have been presented earlier (see Section 3.4.1). In addition to the TB and PU regions, information on the ET regions is also included in this section.

3.6.2 Results and Analysis of Inhalation Dosimetry Modeling Considering Children

Firestone et al. (2008) reported results based on analyses conducted by the California EPA's Office of Environmental Health Hazard Assessment (OEHHA) that investigated the potential differences between adult and child (0-18 yr) internal doses resulting from

inhalation exposure to a toxicant. Modified PBPK models for 24 compounds were used to assess child/adult ratios for at least three dose metrics. Detailed methods, equations, and model parameters were not included in the manuscript; however, the chemicals were classified into one of three categories pertaining to the intrahuman uncertainty factor for toxicokinetic variability (UF_{H-TK} , default value = 3.16): $UF_{H-TK} \leq 3.16$; $UF_{H-TK} > 3.16$ to 9.9; and $UF_{H-TK} \geq 10.0$. Twelve of the compounds examined had child/adult ratios ≤ 3.16 , eight had ratios between 3.16 and 9.9, while four had ratios greater than 10. The authors found that majority of the higher ratios were in infants (< 1 yr) and child vs. adult metabolic differences likely account for this observation.

In addition, as reported in Firestone et al. (2008), OEHHA applied modeling to evaluate alternative methods for interspecies extrapolation of gas dosimetry in a limited number of test chemicals. Limited information on the model structures and parameters employed were provided; however, detailed methods, equations, and model parameters were not described. Blood Cmax and AUC for parent and metabolite and amount metabolized were the dose metrics modeled for a 24 hr simulation. Chemical-specific principal effects (i.e. POE vs. systemic) and thus potential target-tissue doses were not modeled. In general, the DAFs calculated using model output for this set of chemicals were lower in adults (Gmean = 1.85) and higher in children (Gmean = 1.94) compared to the current default methods. With the exception of one case (amount of ethylbenzene metabolized), the child/adult DAF ratios were within a 2-fold range. Without more detailed information regarding the methods and parameters used in either analysis, however, broader conclusions cannot be drawn.

Ginsberg et al. (2008) analyzed ozone gas dosimetry in the TB region using a mathematical model for uptake. The TB model consisted of 15 generations of symmetrically-branched airway bifurcations. Air was modeled starting at the entrance of the trachea and thus did not simulate reactions possible in the ET region. The numerical simulations of reactive gas uptake utilized airway and ventilatory parameters specific to children of different ages (0, 4, 8, 12, 16, and 18 yr). The model was exercised to examine the uptake distribution of ozone along the gas-mucus and mucus tissue interfaces of these children at a constant inhalation concentration of 0.1 ppm. The results demonstrated that for all ages and all airway generations, the controlling resistance to uptake was the mucus layer and the overall K_g was not significantly different across ages. In addition, there were no significant differences in the predicted flux of ozone to the mucus and tissue for children of different ages (0-18 yr) modeled in this study. These results are similar to those obtained by Overton and Graham (1989). In their study, an ozone dosimetry model was used to estimate regional and total uptake of ozone in adults (20 yr) and children (0-14 yr), and no appreciable differences in regional or total uptake were predicted.

More recently, Valcke and Krishnan (2011a) examined the impact of exposure route on the kinetic portion of the intrahuman uncertainty factor, UF_{H-TK} . A multiroute,

steady-state, PBPK model was modified from the literature and used to compute the internal dose metrics of the area under the parent compound's arterial blood concentration vs. time curve (AUC_{pc}) and amount metabolized per 24 hours (AMET). Dose metrics were computed for adults (18-64 yr), neonates (10-30 d), children (1-3 yr), elderly (65-90 yr) and pregnant women (15-44 yr) for a 24 hour inhalation exposure scenario to chloroform, bromoform, tri- or per-chloroethylene (TCE or PERC). The inhalation exposure scenarios were performed at a concentration of $5 \mu\text{g}/\text{m}^3$ representative of a low, environmental level. Monte Carlo simulations were performed and the UF_{H-TK} was calculated as the ratio of the 95th percentile value of internal dose metrics in the various population groups to 50th percentile value in adults. On the basis of AUC_{pc} , the highest UF_{H-TK} values were demonstrated in neonates for each scenario compound. The highest UF_{H-TK} computed was 3.6 for bromoform, but in all other cases the UF_{H-TK} values ranged from 1.2 to 2.2. A synthesis of the results from this study are presented in Table 3-13. These results are in agreement with those presented by Firestone et al. (2008) for PERC and chloroform; however, TCE was categorized as having a $UF_{H-TK} \geq 10$ by Firestone et al. (2008) and ≤ 3.16 by Valcke and Krishnan (2011a). The reason for this difference cannot be determined from the limited information provided in the Firestone et al. (2008) report.

Table 3-13 Human kinetic adjustment factors (UF_{H-TK}) obtained for inhalation exposure in each population group using a dose surrogate of 24 hour AUC_{pc}

Substance:	Chloroform	Bromoform	Trichloroethylene	Perchloroethylene
Adults (41, 18-64 yr)^b				
median	15.8	25.7	21.8	37.3
95th percentile	20.2	37.5	28.8	47.2
UF_{H-TK}	1.3	1.5	1.3	1.3
Neonates (14, 0-30 days)				
95th percentile	33.4	93.1	48.4	66.6
UF_{H-TK}	2.1	3.6	2.2	1.8
Children (2, 1-3 yr)				
95th percentile	25.2	51.7	35.1	58.8
UF_{H-TK}	1.6	2.1	1.6	1.6
Elderly (78, 65-90 yr)				
95th percentile	20.4	37.6	28.8	45.8
UF_{H-TK}	1.3	1.5	1.3	1.2
Pregnant women (29, 15-44 yr)				
95th percentile	22.9	44.4	30.6	46.4
UF_{H-TK}	1.5	1.7	1.4	1.3

Note: AUC_{pc} , area under the arterial blood concentration vs. time curve ($\mu\text{g 24 hr/L}$)

^bShown in parentheses are the median age, range for each population group.

^cBolded values indicate the population group with the greater UF_{H-TK} for corresponding internal dose surrogate for each compound.

Source: Reprinted with permission of Elsevier; Valcke and Krishnan (2011a)

In a related study, Valcke and Krishnan (2011b) assessed the impact of exposure duration and concentration on the human kinetic adjustment factor (UF_{H-TK}). A minimally validated, generic inhalation PBPK model was used to compare the dose metrics (blood concentration and hepatic metabolism) in adults, neonates (0-30 days), toddlers (1-3 yrs) and pregnant women following inhalation to benzene, styrene, 1,1,1-TCA, and 1,4-dioxane. The parameters varied across the life stages were BW, height, and hepatic CYP2E1 and the UF_{H-TK} was calculated based on these Monte Carlo simulations. In the low exposure concentration (associated with steady-state chronic inhalation) scenario ranges of blood concentration-based UF_{H-TK} were 1-6.8 depending on the chemical and lifestage, while it ranged from 0.8-2.0 for rate of hepatic metabolism. Neonates were always the most sensitive based on blood concentration, and pregnant women were generally most sensitive based on metabolism (Valcke and Krishnan, 2011b). The greatest difference in internal dose metrics was observed in neonate vs. adult for 1,4-dioxane (628/199=3.2) blood concentration.

Additional research was done to compare the variability in the whole-population vs. distinct sub-population when determining the UF_{H-TK} (Valcke et al., 2012). In the whole population approach the entire population's upper percentile value (99th) was compared to the median value in the entire population. For the distinct sub-population approach, the 99th percentile values in each sub-population was compared with the median adult value or the median individual in the whole population as a referent. For UF_{H-TK} values, associated with the steady-state blood concentration dose metric, for the whole population approach varied between 1.2 and 2.8, while the distinct sub-population values ranged from 1.6 to 8.5. Similar to what was found in Valcke and Krishnan (2011b), the neonate appeared most susceptible based on blood concentration, while the pregnant woman was more susceptible based on rate of metabolism.

Another study by Valcke and Krishnan (2011a) evaluated the impact of physico- and biochemical characteristics on UF_{H-TK} as they impacted systemic clearance of hypothetical chemicals. Here they utilized a physiologically based steady-state algorithm (not a PBPK model) to look at concentration in the blood (C_{blood}) and rate of hepatic metabolism (RAM_L) for some hypothetical chemicals ($H_{b/g}$ between 1-10,000 and hepatic extraction [E_{HR}] ratios between 0.01-0.99) in neonates (0-30d), adult, elderly (65-90yr), and pregnant women (29yr, GW0-40). UF_{H-TK} in neonates was the only one exceeded the typically applied factor of 3.16 for intrahuman variability, when $E_{HR} = 0.3-0.7$ and $H_{b/g} \geq 100$ for inhalation exposures to CYP2E1, CYP3A4, and ADH substrates, while it was higher for CYP1A2 metabolized compounds. This study showed the impact of chemical characteristics, metabolic pathways, and lifestages on intrahuman variability.

Liao et al. (2007) developed a hybrid PBPK/pharmacodynamic (PD) model to investigate chloroform toxicity and carcinogenicity. The PBPK model was configured for rats, mice, and humans with the human configuration expanded to consider different age groups (1 month, 3 month, 6 month, 1 year, 5 year, and 25 year old) with the age-specific physiological values being obtained from documented literature sources (see the *Status II Report* for details). The PD model was used to quantitatively estimate rates for mode-of-action processes known to be prominently involved in the toxicity of chloroform (metabolism, reparable cell damage, cell death, and regenerative cellular proliferation). The human model was used to estimate internal doses at steady state over a range of inhalation exposures (and oral, drinking water) concentrations for different age groups to identify the threshold for labeling indices (LI) below which no cytolethality would be expected in each age group. The simulations presented in Table 3-14 indicated that for liver effects, a young child (≤ 5 years) was more sensitive than adults by a factor of about 2. For renal effects, however, the results indicated age-related increases in sensitivity to the toxicity of chloroform with 1-month-old infants nearly 7- to 8-fold less sensitive than adults, 1-year-olds about 3-fold less sensitive than adults, and no difference in concentration corresponding to kidney effects between adults and 5-year-old children.

Table 3-14 Air concentration of chloroform at various ages and genders corresponding to threshold of damage in human liver and kidney

Age	Gender	Air Concentration (ppm)	
		Liver	Kidney
1 Month	Male	5.16 ^a	7.56
	Female	4.86	8.08
3 Month	Male	4.80	2.60
	Female	4.79	2.85
6 Month	Male	5.13	2.19
	Female	4.90	2.29
1 Year	Male	6.07	3.17
	Female	5.66	3.00
5 Year	Male	6.61	1.18
	Female	6.81	1.35
Adult	Male	9.24	0.887
	Female	12.7	1.06

Note: Values generated from model simulations of a PBPK-PD model.

^aResults given as point values only, as estimates of variability were problematic in the absence of data on cell proliferation in human liver and kidneys.

Source: Reprinted with permission of John Wiley and Sons; Liao et al. (2007).

Nong et al. (2006) used a PBPK model to explore the interindividual variability in the internal dose of toluene in various age groups of children (<1month, 1mo-1yr, 1-11yrs, and 12-17yrs) compared to adults (18+yrs), based on variation in hepatic CYP2E1 content and physiology. Variability factors within each age group were calculated as the ratio of the 95th percentile toluene venous blood AUC over the 50th percentile value for that age group, while variability factors for adult-child variability used the child 95th percentile toluene venous blood AUC over the 50th percentile value for the adult. Within each age group, the variability factor was less than 1.5 and the adult-child variability was less than a factor of 2 in most cases, with the exception of adult to neonate (<1month) comparison. For the neonate, the adult-child variability was 2.5 for neonates with high metabolic capacity and 3.9 for neonates with lower metabolic capacity. In neonates, low CYP2E1 concentration was defined as <3.69 pmol/mg microsomal protein while higher CYP2E1 concentration in neonates, older children, and adults was found to be in the range of 4.33 to 55.93 pmol/mg microsomal protein.

Sarangapani et al. (2003) used a PBPK model to evaluate the effect of age- and gender-specific lung morphology and ventilation rate on the inhalation dosimetry of several gases. The gases were selected on the basis of their potential range of reactivity within the respiratory tract, from reactive and soluble (ozone and isopropanol) to relatively insoluble and nonreactive (styrene, vinyl chloride, and perchloroethylene). Ten age-specific PBPK models were run for males and females from 1 month of age to 75 years. Model structure was typical of PBPK models but simplified to three main axial compartments of the respiratory tract: the ET, TB, and PU, with the ET and TB each divided into three lateral subcompartments from airway lumen to circulating blood (for modeling details see the *Status II Report*). Dose metrics evaluated included parent and

metabolite concentrations in blood, liver, and lung. Results for the dose metrics were expressed relative to the young adult (25-year-old) model which were all set at unity. The results from the model indicated that tissue dose metrics at any age generally fell within a factor of 2 of the young adult values for parent ozone, vinyl chloride, styrene, isopropanol, and perchloroethylene. Little variability due to gender was apparent at any age for any of the gases or metrics examined. The only exceptions were those observed in early childhood (either gender), where dose metrics (especially for metabolites) were as much as 12 times higher for a 1-month-old child than young adult values, declining to 2 times by age 5-10 years, for these same compounds. This is shown for the parent isopropanol and its water soluble metabolites (Table 3-15).

Table 3-15 Age-dependent and gender-specific dose metric comparison of inhaled isopropanol

Age	Parent Chemical Concentration		Metabolite Concentration	
	Male	Female	Male	Female
1 Month	1.75	1.74	8.02	11.44
3 Month	1.77	1.78	6.68	9.14
6 Month	1.77	1.75	5.70	8.01
1 Year	1.54	1.54	4.12	5.96
5 Year	1.25	1.18	1.98	2.55
10 Year	1.05	1.03	1.53	2.04
15 Year	1.09	1.14	1.46	1.70
25 Year	1	1	1	1
50 Year	0.94	1.00	0.80	0.82
75 Year	1.04	1.03	0.89	0.93

Note: Comparisons presented as % ratio of metric at a specific age to the 25-yr-old adult set at 100%.

Source: Reprinted with permission of Informa Healthcare; Sarangapani et al. (2003)

An inhalation PBPK model for furan predicted steady-state blood concentrations in children, modeled ages of 6, 10, and 14 years old, to be 1.5 times greater than the blood concentration of adults exposed under the same conditions (1 ppb for 30 hrs), while the difference in liver concentration of furan metabolite was less (a factor of about 1.25) (Price et al., 2003). This PBPK prediction could be similar for other highly metabolized inhaled chemicals when comparing adults and children 6-14 yrs of age. Other age groups were not considered in this analysis due primarily to lack of data on liver blood flow information, which was found to be a critical model parameter for these differences.

Pelekis et al. (2001) developed a PBPK model for adults of low (50 kg) and high (90 kg) body weights and for a 10 kg child (1 to 2 years old). The model was applied to inhalation exposures of dichloromethane, tetrachloroethylene, toluene, m-xylene, styrene,

carbon tetrachloride, chloroform, and trichloroethylene. The parent compound concentrations in arterial blood (CA) and venous blood (CV), and tissues (C_{tissue}) (but no metabolites) were evaluated. The ratios of the metrics from these different runs characterize the pharmacokinetic behavior of the child relative to the adult (e.g., $\text{adult}_{\text{high}}/\text{child}_{\text{average}}$). The exposure scenario simulated was 1 ppm continuous for 720 hrs (30 days). These ratios indicated that the estimation of concentrations in children's blood were about the same as for the adult. With other tissues metrics, however, values were considerably higher in a few instances. For example, the $\text{adult}_{\text{high}}/\text{child}_{\text{average}}$ ratio for the concentration in the liver (which was dependent on metabolism) was predicted as 0.033 for styrene, 0.037 for m-xylene, 0.061 for trichloroethylene, 0.092 for dichloromethane, and 0.11 for chloroform. These predictions indicate concentrations of the VOC chemicals in livers of 1-2 year-old children that ranged from similar to the adult liver concentrations up to 10- to 30-fold higher for three of the eight chemicals. The average $\text{adult}_{\text{high}}/\text{child}_{\text{average}}$ ratios for the various dose metrics estimated for the composite runs by Pelekis et al. (2001) are shown in Table 3-16.

These adult/child ratios calculated by Pelekis et al. (2001) differ from other laboratories (Valcke and Krishnan, (2011a), in that the 95th percentile child values are more often compared to median or average adult values. The approach used by Pelekis et al. (2001) is more likely to underestimate the potential differences between children and adults.

Table 3-16 Tissue concentrations in various compartments expressed as adult/child (1 to 2 years old) ratios for 8 different gases

Gas	Adult _{high} /Child _{average} Ratios of Concentrations ^a			
	Venous Blood	Arterial Blood	Fat	Liver
Dichloromethane	0.70	0.91	0.25	0.092
Tetrachloroethylene	1.61	1.74	0.47	0.75
Toluene	0.86	0.98	0.27	0.34
<i>m</i> -Xylene	0.50	0.63	0.17	0.037
Styrene	0.34	0.45	0.12	0.033
Carbon tetrachloride	1.81	2.20	0.60	0.57
Chloroform	0.78	1.02	0.28	0.11
Trichloroethylene	0.77	0.97	0.27	0.061
Average ± SD	0.92 ± 0.52	1.11 ± 0.58	0.30 ± 0.16	0.25 ± 0.28

^aSteady-state concentration ratios for 1 ppm continuous exposures.

Note: Initial values are all from PBPK simulations.

Source: Reprinted with permission of Elsevier; Pelekis et al. (2001).

In an effort to evaluate the potential effects in the nasal cavity of inhaled methyl iodide (MeI) exposure, a PBPK model was developed by Mileson et al. (2009) and Sweeney et

al. (2009), complete with parameters for sensitive populations and lifestyles including children (for model details see the *Status II Report*). These models relied on recent data gathered using a novel method to provide measures of MeI nasal absorption and clearance in intact animals (Thrall et al., 2009). The modeled point-of-departure for the effect of MeI in the nasal tract was a decrease (either 25% or 50% decrement from untreated levels) in glutathione (GSH) concentrations in the olfactory epithelium. The adult human model indicated that depletion of GSH in the dorsal olfactory epithelium to 50% of control would be achieved after 24 hours of exposure to 72 ppm MeI. For workers exposed for 8 hrs, 50% GSH depletion would be achieved by the end of the shift at an exposure concentration of 110 ppm. At a target POD of 25% GSH depletion at 24 hrs, the 24-hr adult value was 36 ppm and the 8-hr (worker) value was 50 ppm. When configured for the 3-month-old child the corresponding 24-hr concentration for 25% depletion of olfactory GSH was 8.2 ppm under these conditions. No other age-related results were given in the study. This concentration differential for the POD, 36 ppm for the adult and 8.2 ppm for the 3-month-old child, indicates differential sensitivity of 3-4 fold resulting from a combination of biochemical (e.g., GSH turnover) and physiological (e.g., respiration rate) factors. The equivalent rat exposure concentration (associated with a 50% depletion of GSH) upon which the adult and child modeled HECs were based was 3.8 ppm (21 ppm for 6 hr/day, 5 d/wk for 4 or 13 wks).

Clewell et al. (2004) constructed a PBPK lifestage model specifically to evaluate age- and gender-specific differences in tissue dosimetry for oral, dermal, and inhalation exposures to a range of chemicals with various physical and toxic properties. The model was mostly parameterized using equations that described various age-dependent alterations derived from U.S. EPA (1997), which was also the source for ventilation rates (m^3/day); pulmonary ventilation for various ages were converted to alveolar ventilation based on the assumption that alveolar ventilation is approximately two-thirds of pulmonary ventilation. The results for the isopropanol inhalation model are the only ones discussed here; however, the predictions of this age-dependent model were only able to be validated against human kinetic data for the adult. The arterial blood concentrations of isopropanol and acetone (the principal metabolite of isopropanol), were estimated for a 1 ppb continuous inhalation exposure and summarized in age-group ranges of birth to 6 months, 6 months to 5 years, 5 to 25 years, and 25 to 75 years. In general, the model estimations for the average internal concentration of inhaled isopropanol and its metabolite acetone varied 2 to 4-fold across the range of lifestages. The highest dose ratio (constructed from the lifestage/average daily inhalation dose for a 25-year-old adult) among the lifestages was 2.0 for isopropanol (birth–6 months) and 3.9 (birth–6 months) for acetone.

Ginsberg et al. (2002) investigated child/adult pharmacokinetic differences through analysis of pharmacokinetic (PK) data from 45 different chemicals, nearly all therapeutic drugs and all administered by routes other than inhalation. In an initial metabolic

evaluation, the drugs were classified as to their excretion: unchanged in urine, CYP (various) metabolism, glucuronidation, sulfation, GSH conjugation or unclassified. The infants/children were classified in age as premature neonates (≤ 1 week), full-term neonates (≤ 1 week), newborns (1 week-2 months), early infants (2-6 months), toddlers (6 months-2 years), preadolescents (2-12 years), adolescents (12-18 years) and adults. There were data from 118 adults and 248 infants/children. The kinetic parameters evaluated included AUC, clearance, C_{max} , half-life ($t_{1/2}$), and volume of distribution (Vd). Relationships between age groups and the kinetic parameters were evaluated by regression analysis.

The combined results showed that, for those chemicals with clearance data (27 substrates), premature to 2-6 months of age infants showed significantly lower clearance ($P < 0.01$) whereas 6-month-old to 12-year-old children had significantly higher clearance ($P < 0.0001$) than adults. The combined results (40 substrates) indicated also that the drug half lives in the youngest age groups (premature neonates, full-term neonates, and newborn infants up to 2 months) tended to be longer (average 2-to-4-fold) than adults, although the infant half lives then declined such that half lives for infants 2-6 months of age reflected those of adults. Other results included those for the chemicals identified as CYP1A2 substrates (caffeine and theophylline) for which neonates to infants 2 months of age showed about 4 to 9-fold longer half-lives than adults while older age groups (6-months to 12 years) had significantly shorter half-lives than adults. A similar pattern was observed with those chemicals thought to be metabolized primarily through CYP3A.

These data are for drugs orally administered, rather than from toxics being inhaled, but nonetheless are relevant to situations involving dosimetry at systemic sites of children versus adults, and thus indicate a potential for internal dose of some chemicals to be greater during the short period of early infancy (prior to 2 months of age) than later lifestages. These data also demonstrate empirically the prominent feature and likely mechanism for susceptibility during early infancy, decreased clearance functions.

3.6.3 Respiratory Tract Air Flow Models Considering Children

Garcia et al. (2009) obtained the MRI or CT head scans of seven individuals including those of two children, a male (7 years) and a female (8 years) and five adults in a vanguard study to examine inter-individual variability of nasal air flows in human subjects using CFD. Several prior studies had shown actual airflow patterns in the nasal tract of both animals and (adult) humans are highly non-uniform with highly localized areas of flow that have been correlated with (at least in laboratory animals) areas of focal pathology in air exposures to reactive gases. Breathing rates for the flow simulations were set at 5.5 L/min for the 7-year-old boy and 5.8 L/min for the 8-year-old girl with flows for the adults each allometrically adjusted with a final range of between 6.8 and 9.0

L/min. Simulations of nasal uptake of inhaled gas (concentration in ambient air defined to be 1 ppm by volume) were conducted under one of two boundary conditions - one to simulate a maximum gas uptake and a second boundary condition to simulate moderate uptake (approximately 80% of maximum) at the nasal tract walls. The simulations predicted that, under both boundary conditions, gas was rapidly absorbed by the nasal mucosa once it entered the nostrils. At the end of the nasal septum, gas concentration in the inspired air had dropped to ~13% and ~29% of the inlet concentration for the maximum and moderate uptake scenarios, respectively. The spatial distribution of wall fluxes, especially under the maximum uptake boundary condition, were shown to be highly non-uniform for all scans including those of the two children. Further analysis of the subjects showed that the extent of the non-uniform flows (where areas of non-uniformity were divided into categories of increasing mass flux) were not appreciably different among the subjects, including between adults and the two children (the minimal number of subjects precluded any statistical analysis). Additional analysis also showed that the overall rate of uptake in the nasal region, although highly non-uniform under localized internal conditions as shown by this study, was very similar from one individual to the next with no apparent differences between adults and the two children. Importantly, delivered dose estimated in terms of maximum (99th percentile) or average flux was not different between adults and children. These principal results from the maximum uptake condition, including some of the first available ET surface areas for children, are shown in Table 3-17.

Table 3-17 Summary listing of findings on morphometry and gas flow/uptake simulations for human nasal cavities

Parameter (units)	Subjects						
	Adults					Children	
Gender	Male ^a	Male	Female	Female	Female ^a	Male	Female
Age (years)	53	NA	NA	NA	37	7	8
ET area (cm ²)	20,085	23,219	16,683	20,688	17,752	12,093	13,027
ET volume (mL)	18.0	26.5	15.4	23.8	18.7	10.7	13.7
Total gas uptake, maximum conditions (%)	93.5	93.1	92.4	89.2	91.5	92.0	88.2
Average flux, left cavity (10 ⁻⁸ kg /sm ²) ^b	1.8	1.6	1.5	1.2	1.4	1.9	1.6
Maximum flux ^c , left cavity (10 ⁻⁸ kg/sm ²) ^b	10.8	11.0	10.8	10.6	10.8	11.8	12.3

^aData obtained from repaired casts.

^bGas absorption rate

^cThe 99th percentile flux (i.e., the flux value below which 99% of flux values fall)

NA = data not available

Source: Reprinted with permission of Informa Healthcare; Garcia et al. (2009).

In a follow-on study to Garcia et al. (2009), Schroeter et al. (2010) utilized the reactive gas hydrogen sulfide (H₂S) to characterize the interhuman variability of H₂S dosimetry to the olfactory region arising from inter-individual differences in nasal anatomy, airflow, and inspiratory uptake patterns using CFD. This study used essentially the same conditions of CFD modeling as employed by Garcia et al. (2009). Olfactory regions were mapped into the nasal models of all subjects as consistently as possible based on the prior descriptions of the extent of olfactory epithelial in humans. The H₂S specific kinetic parameters used were previously estimated by the authors by fitting in vivo uptake data in rats, then allometrically scaled to humans based on nasal surface areas. Flows were simulated at three different concentrations, 1, 5 and 10 ppm. Comparisons among individuals were made for the 99th percentile flux (i.e., the flux value below which 99% of flux values fall) and average flux in the olfactory regions at an exposure concentration of 1 ppm.

Results included morphological measurements in human adults and children of nasal cavity surface areas and estimates of olfactory epithelia and airflow apportionment. The modeling results in terms of average flux, maximum flux, and distribution of flux ranges within the target area of olfactory epithelium showed uniform responses despite the morphological ranges characterized. Differences in nasal anatomy and ventilation among adults and children were not predicted to have a significant effect on H₂S dosimetry in the olfactory region (Table 3-18). The 99th percentile flux ranged from 153.1 to 170.1 in

adults compared to 149.2 and 159 in children, while the average flux ranged from 12.2 to 13.6 in adults compared to 11.8 and 12.1 in children.

Table 3-18 Selected morphologic and simulated modeling results of hydrogen sulfide dosimetry in casts of human nasal cavities

Parameter (units)	Subject						
	Adults					Children	
Gender	Male ^a	Male	Female	Female	Female ^a	Male	Female
Age (years)	53	NA	NA	NA	37	7	8
Surface area of main nasal cavity (cm ²)	198.7	231.5	167.3	207.9	177.0	118.9	135.1
Surface area of olfactory region (cm ²)	14.4	11.5	10.5	9.9	11.2	9.1	9.6
Olfactory airflow allocation (%)	4.8	5.5	7.9	2.6	4.9	16.2	1.6
99th percentile flux (pg/cm ² -s) @ 1ppm	167.7	170.1	158.9	161.3	153.1	149.2	159.0
Average flux (pg/cm ² -s) @ 1ppm H ₂ S	13.6	13.5	12.7	12.8	12.2	12.1	11.8

^aData obtained from repaired casts.

NA = data not available

Source: Reprinted with permission of Informa Healthcare; Schroeter et al. (2010)

3.6.4 Respiratory Tract Growth

It has been well established that the human respiratory system passes through several distinct stages of maturation and growth that involve branching morphogenesis and cellular differentiation during the first several years of life and into adolescence (Pinkerton and Joad, 2000). The proportion of surface area to ventilation volume may be markedly different during these developmental stages. The significance of these disproportions with regard to toxicant exposure overall or to the sites of active cellular differentiation have yet to be elucidated. The major proposed processes in human lung growth and development are:

- an increase in numbers of alveoli via septation of elementary saccules, followed by
- increases in dimensions of all of the lung structures including alveolar size and, most prominently, the diameter of airways, followed by
- distension of lung due to changes in the mechanical properties of the chest wall.

These changes are postulated to result in a relative under-distension of the lung followed by a relative over-distension (Zeltner et al., 1987). De Jong et al. (2003) postulated that indications of these processes could be determined through in situ scanning and

visualization techniques. Therefore an institutionally sanctioned study was conducted where the CT scans of 35 children (age range from 15 days to 17.6 years of age; 17 males, 18 females) were obtained and examined for these indications of growth and development. The data on lung expansion expressed as gas volume per g of tissue (mL/g) showed a decline from birth to 2 years of age and an increase thereafter. This finding would be anticipated as alveolar tissue is rapidly added, the alveoli are of uniform size and divisions of existing airspace into smaller units via septation would cause the gas volume to fall. The subsequent increase in gas volume of tissue from age 2–8 years would be consistent with expansion in the size of alveoli in combination with a gradual increase in functional residual capacity (FRC) due to changes in the mechanical properties of the lung and chest wall.

In a companion study de Jong et al. (2006) used CT scans from a group of 50 young individuals (age range 0 – 17.2 years) to obtain estimates of various lung dimensions also through the period of growth. Clinical CT scans were performed and analyzed as above for lung weight, gas volume, lung expansion, lung surface/volume ratio, airway wall area, airway lumen area, airway lumen perimeter, arterial area and airway surface length/area ratio. The authors discussed the nature of these ratios in relation to length and growth of the individual but did not give specifically determined estimates of measures such as surface areas. For example, lung alveolar surface area to total lung volume ratio (S/V) was calculated using the lung expansion values at total lung capacity (TLC) per the following equation:

$$S/V \text{ lung} = e^{6.84(0.32 \times \text{lung expansion at TLC})}$$

Equation 3-3

The regression of these ratios against other growth parameters, such as body length, suggest that the relationship between these various measures is closely linked.

Collectively these results provide functional indications of lung growth processes using noninvasive methods and demonstrate that CT scans can be used to provide valuable information about normal lung growth in addition to the more typical application of diagnosis of lung disease.

Rao and coworkers (2010) evaluated lung growth and development in vivo in infants and toddlers using multi-slice CT. The developmental process is thought to be sequential in terms of the alveoli, with new alveoli being added until about 24 months of age followed by alveolar expansion with no new alveoli added after 24 months. The high resolution capability of CT was applied to a group of 38 subjects (14 male, 24 female) of ages in this range (17 to 142 weeks; 4 to ~ 36 months). This in vivo assessment suggests that the growth of the lung parenchyma in infants and toddlers occurs with a constant relationship between air volume and lung tissue, which is consistent with lung growth occurring

primarily by the addition of alveoli rather than the expansion of alveoli. In addition, the central conducting airways grow proportionately in infants and toddlers.

The pulmonary growth sequence in early life of alveolar septation followed by alveolar expansion was examined by Balinotti et al. (2009) with pulmonary function testing. The basis of the hypothesis relates to the ratio between pulmonary diffusion capacity of carbon monoxide (DLCO) and alveolar volume (VA). During the process of alveolarization, usually considered to be in the first two years of life, this ratio would remain constant whereas during alveolar expansion, i.e., in children older than 2 years, it would decrease. The authors measured DLCO and VA using single breath-hold maneuvers at elevated lung volumes in 50 sleeping infants and toddlers between the ages of 3 and 23 months. Both alveolar volume and pulmonary diffusing capacity increased with increasing age in both male and female children. Significantly, ratio of pulmonary diffusing capacity to alveolar volume remained constant in this age group. The constant ratio for DLCO/VA in infants and toddlers is consistent with lung growth in this age occurring primarily by the addition of alveoli rather than the expansion of volume.

Zeman and Bennett (2006) employed in vivo methodology, aerosol-derived airway morphometry (ADAM), to measure the age-related changes in air space caliber of the small airways and alveolar dimensions. The subjects recruited from the general local population included 53 children (6–22 years) and 59 adults (23–80 years). The principal of ADAM related to predictable gravitational settling of small inhaled particles to infer the vertical distance or effective air space dimension, (EAD), that the particles must have settled to become lost to the airway wall. ADAM involves individuals inhaling to TLC a particle aerosol of known size characteristics followed by breath-holds for 0-10 seconds and (non-deposited) particle recovery upon exhalation. Data were collected, then regressed according to age. Alveolar diameters were found to increase with age, from 184 μm at age 6 to 231 μm at age 22 based on the regression equations derived. This observation would account for the increase in TLC observed over this age range. The caliber of transitional bronchioles (average 572 μm) did not increase with TLC, but did increase with subject age and height when the entire age range of 6–80 years was included (Zeman and Bennett, 2006). The anatomical dead space scaled linearly with lung volume, but relative to TLC did not change with age, averaging $7.04 \pm 1.55\%$ of TLC. The authors concluded that from childhood (6 years) to adulthood a constant number of respiratory units is maintained; however, both the smallest bronchioles and alveoli expand in size to produce the increased lung volume with increased age and height.

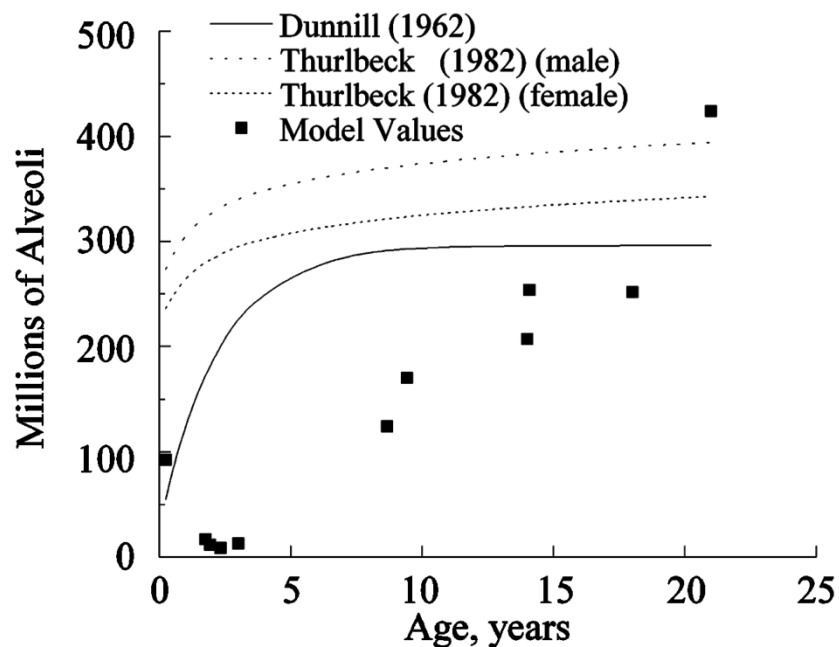
It has been hypothesized by Thurlbeck (1982) that humans grow new alveoli from a few weeks before term birth until approximately 8 years of age, after which the alveoli are thought to enlarge as the lungs increase in volume or size with no new alveoli formed. To this end, Altes and coworkers (2004b) examined the apparent diffusion coefficient (ADC) with a gaseous contrast agent for MRI, hyperpolarized helium-3 (^3He), in a cohort of

twelve individuals. An increase in ADC is a measure of volume maturation. It was expected that in the pediatric age group, the increase in alveolar size with increasing age will be reflected in an increase in ^3He ADC with age. The age range of the 12-member cohort was 7 to 29 years (mean 15.6, standard deviation 6.9 years). All 12 of the subjects had homogenous appearing ADC maps. Comparing the mean ADC with other measures of maturation or lung volume gave correlation coefficients of 0.74 with height, 0.64 with weight, 0.76 with forced vital capacity (FVC) in liters, 0.81 with the predicted FVC based on the subject's age and height, and 0.34 with the percent predicted FVC. In summary, it was found that the mean ADC increased with age in the pediatric population and that the mean ADC was lower in the pediatric age group than in young adults. These observations suggest that the pediatric subjects had smaller airspaces than the young adults. Further, the variability of the airspace structure, as measured by the standard deviation of the ADC values, did not change with age, as expected. Thus ^3He diffusion MRI of lung appears to be able to detect this normal maturation process of increased lung volume via increases in the size of the functioning alveoli.

Altes et al. (2004a) used advanced imaging techniques to detect age-related development in lung microstructure that relate to both lung volume and surface area. ^3He diffusion magnetic resonance scanning produces in vivo images of tissues weighted as to water diffusion through local microstructure. MRIs were acquired for each of 29 individuals (2 separate trials for each), aged four to 30 years, and used to determine the mean ADC and lung volume for each subject. The mean ADC was reported to increase with increasing subject age ($r = 0.8$; $P < 0.001$), with a 55% increase in mean ADC from the youngest (4 years) to oldest (30 years) subject. The lung volumes measured on MRI were highly repeatable for the two acquisitions ($r = 0.980$) and also reflected increased volumes concordant with the ADC. These advanced imaging results gave functional indications that alveoli increase in size rather than number during childhood.

Ménache et al. (2008) generated quantitative whole-lung models from silica casts of the lungs from 11 subjects between 3 months and 21 years of age. The models were based on a combination of cast data and published information on distal airway dimensions and were inclusive of the conducting airways (trachea through terminal bronchioles), the respiratory bronchioles, and the alveolar airways, which include alveolar ducts and sacs. Parameters evaluated from the data included airway generation number count, length and diameter of terminal bronchioles and alveolar ducts, acinar length and alveolar dimensions (assumed spherical), and total alveolar number. Further estimates from these parameters and reasonable assumptions were made for alveolar volumes and the physiological volumes of TLC and FRC. Model dimensions for the conducting airways, as well as the estimated dead space, for all children fell within the range of the limited published information. The assumptions and estimates used produced results that were reasonably consistent with available physiological data for children 8 years and older. The predicted TLC for the older individuals (aged 8 to 21 yr) fell within or near the range

arising from published scaling equations. However, the models for children 3 years of age and younger resulted in predicted TLCs well below those predicted using these same equations by as much as an order of magnitude (data not shown). Another unexpected result was the total number of model calculated alveoli compared to the published number of alveoli as a function of age. As shown in Figure 3-10, the calculated number of alveoli increased linearly as a function of age in contrast to the data of Dunnill (1962) and Thurlbeck (Thurlbeck, 1982). This suggested that the fixed relationship between respiratory airway volumes and alveolar volumes assumed for all ages was incorrect and that the relationship must be different in the younger children. These differences might be explained by growth in early childhood when the alveolar region is growing more than the airways. The airways show symmetric growth since they are complete, while the alveoli are increasing in both number and size. These results suggest that the geometry model airway dimensions for all ages are appropriate for use with dosimetry models; however, they also point out a need for a greater understanding of lung development for children 3 years of age and under.



Source: Reprinted with permission of Informa Healthcare; Ménache et al. (2008); using data from Dunnill (1962) and Thurlbeck (Thurlbeck, 1982)

Figure 3-10 Alveoli count per lung as a function of age.

Ogiu et al. (1997) presented detailed physical mass measurements of various organs in 4,667 Japanese subjects, aged 0-95 years, including 3,023 males and 1,644 females. Analyses of age-dependent changes in weights of the brain, heart, lung, kidney, spleen, pancreas, thymus, thyroid gland, and adrenal gland and also of correlations between

organ weights and body height, weight, or surface area were carried out. It was concluded that organ weights, including lung, in the growing generation (under 19 years) generally increased with a coefficient expressed as (body height) \times body weight^{0.5}. Specific coefficients were derived for both right and left lungs and for both males and females. It was also noted that adult males had heavier lungs than adult females, and that the male:female lung weight ratios were nearly the same, 1.27 for the right lung and 1.28 for the left lung. The age-specific weights presented in this study for lungs only, 0-15 years of age, are shown in Table 3-19.

In a translated Japanese study, Inagi (1992) described the collection and measurement of the heights of the mucous membrane in the human nasal septum from 74 cadavers, including 5 males and 4 females classified as “fetal/infant,” and 5 males and 3 females aged 1 to 19 years referred to as the “infant/adolescent” group, as well as older aged groups. The purpose of the study was to examine histological changes in mucosal tissues although measurements were made in relation to age including heights of the mucous membrane, including both the epithelium and the underlying lamina propria. The average height for the epithelium of the “fetal/infant” group was estimated to be $\sim 0.4 \mu\text{m}$ with a range of $\sim 0.35 - 0.5 \mu\text{m}$. For the remainder of the groups, the average and range of height was estimated to be $\sim 0.7 \mu\text{m}$ with a range of $\sim 0.4 - 0.9 \mu\text{m}$. Estimation of the lamina propria heights (described and given as being from the convex and concave sides of the nasal septum) yielded: average height for fetal/infant group $\sim 500 \mu\text{m}$ with a range of $\sim 300 - 700 \mu\text{m}$; for the remainder of the groups the average and range of height was estimated to be $\sim 900 \mu\text{m}$ with a range of $\sim 400 - 1500 \mu\text{m}$. Such data and results may have utility in gas dosimetry as they give a basis for diffusion distance in mass transport processes, in this case across age groups including the very young.

Table 3-19 Lung weights (right and left) of males and females from birth to adulthood

Age	Males				Females			
	Left Lung		Right Lung		Left Lung		Right Lung	
	N	Average wt (g ± SD)	N	Average wt (g ± SD)	N	Average wt (g ± SD)	N	Average wt (g ± SD)
0	39	22.3 ± 5.7	40	28.4 ± 8.0	54	23.1 ± 7.1	52	29.1 ± 8.3
1 mo	5	42.1 ± 12.7	6	49.3 ± 16.1	4	38.7 ± 7.7	4	43.8 ± 8.1
2	11	48.4 ± 6.6	12	56.6 ± 11.0	7	45.7 ± 9.9	7	52.2 ± 8.7
3	3	46.3 ± 6.4	3	62.7 ± 11.7	6	50.2 ± 8.1	6	66.3 ± 15.6
4	11	51.1 ± 9.7	11	62.7 ± 11.5	5	51.5 ± 12.8	4	61.6 ± 14.5
5	4	51.8 ± 16.1	4	58.0 ± 18.6	7	48.3 ± 10.1	8	58.9 ± 9.6
6	8	55.5 ± 12.1	8	68.3 ± 12.4	6	62.1 ± 6.9	6	70.2 ± 6.8
7	6	72.2 ± 8.5	6	86.7 ± 12.1	1	55.0	1	68.0
8	7	66.5 ± 8.9	8	82.2 ± 19.0	5	62.0 ± 10.2	5	74.8 ± 16.8
9	1	66.0	2	108.0 ± 31.1	8	67.6 ± 12.9	8	81.3 ± 16.1
10	4	71.9 ± 24.9	4	77.7 ± 27.6	3	53.3 ± 10.4	3	67.3 ± 9.3
11	1	50.0	1	62.0	-	-	-	-
1 yr	15	83.9 ± 20.2	15	93.9 ± 21.9	22	76.8 ± 23.7	23	87.4 ± 30.4
2	7	100.5 ± 28.4	7	101.4 ± 21.2	14	94.8 ± 26.7	13	107.7 ± 32.0
3	17	108.4 ± 28.3	16	129.4 ± 36.0	11	112.5 ± 21.0	11	117.9 ± 25.8
4	11	118.5 ± 38.5	10	122.8 ± 32.2	4	117.3 ± 23.6	5	158.4 ± 43.2
5	8	138.1 ± 38.2	9	159.7 ± 34.3	4	113.0 ± 50.6	5	128.6 ± 43.2
6	4	194.8 ± 16.0	4	230.3 ± 18.4	3	143.3 ± 12.6	4	197.5 ± 62.9
7	13	170.8 ± 61.6	14	186.9 ± 63.7	8	163.8 ± 44.2	8	200.0 ± 47.8
8	10	169.8 ± 54.7	10	204.4 ± 63.7	8	215.0 ± 50.1	8	242.5 ± 70.3
9	10	232.5 ± 75.5	9	243.3 ± 60.0	9	208.3 ± 62.8	9	247.9 ± 81.2
10	12	245.6 ± 71.9	13	255.2 ± 96.9	5	314.2 ± 42.0	4	368.0 ± 85.4
11	10	254.8 ± 77.1	10	298.5 ± 78.1	10	287.5 ± 77.4	9	300.6 ± 90.1
12	12	370.8 ± 130.1	12	398.8 ± 129.6	6	289.2 ± 89.4	6	280.0 ± 107.9
13	8	248.5 ± 131.9	8	383.4 ± 131.8	4	269.5 ± 93.2	4	303.5 ± 62.9
14	10	402.5 ± 146.1	10	467.0 ± 203.0	6	339.3 ± 54.4	6	389.2 ± 72.3
15	14	442.0 ± 155.6	13	500.3 ± 127.7	8	297.6 ± 191.9	7	344.0 ± 224.8
20-24	68	363.8 ± 129.1	61	444.9 ± 164.6	37	343.9 ± 118.1	41	363.6 ± 122.8

Source: Reprinted with permission of Lippincott Williams & Wilkins; Ogiu et al. (1997)

4 FINDINGS AND CONCLUSIONS

1 The overall goal of this report is to summarize and put into context the scientific
2 developments that have occurred in the fundamental areas of target tissue dosimetry of
3 gases both between species and between children and adults related to the *RfC Methods*.
4 An alternative method to the use of the strict gas categorization is also presented. Much
5 of the information discussed in this report was presented in more detail in the prior
6 reports ([U.S. EPA, 2011b](#), [2009b](#)). This report examines the state of the science in
7 specific areas of research related to inhalation gas dosimetry and the *RfC Methods*.
8 Consequently it has limitations in its scope. Other active and future areas of research not
9 addressed in this report include: (1) the effects of common diseases on gas distribution
10 within the respiratory tract and on mucus composition and thickness; (2) the effects of
11 exercise on ventilation, oral breathing, and gas dosimetry; (3) the potential effects of race
12 and other genetic factors on upper airway anatomy, and on metabolism; (4) the effects of
13 defensive or toxic responses, e.g., changes in ventilation that exposure to some gases can
14 produce; and (5) the potential effects of particles on gas dosimetry. Each of these
15 components should be carefully considered in inhalation risk assessment as the science
16 becomes available.

17 One of the most basic aspects in describing target tissue dosimetry presented in these
18 reports is a scheme for characterizing gases that differs fundamentally from the *RfC*
19 *Methods*. The *RfC Methods* gas scheme related physicochemical properties of gases to a
20 numerical category; this category was then related to the observed toxicity, including that
21 of the target tissue. **The alternative scheme proposed by Medinsky and Bond (2001),
22 and featured in these reports, provides a direct and simplified descriptor approach
23 for characterizing gases that relates the properties of the gas to the site of the
24 observed toxicity without the need for categorization.** Rather than assigning specific
25 numerical categories to gases, these descriptors are placed on a chart that represents
26 reactivity and water solubility as continuous variables (see Figure 3-1). It is important to
27 note that this scheme provides examples of gases that fit these discrete descriptors, but
28 that the majority of gases may not fit one particular descriptor. In addition, the potential
29 role of metabolism and its influence on uptake and toxicity is not directly accounted for
30 in this scheme. Thus, this approach also has limitations.

31 The scientific developments presented in these reports should inform users of the utility
32 and inherent limitations in the existing default *RfC Methods* which employ dose estimates
33 from V_E and SA, especially in the ET region. The general aspects to consider are air
34 phase transport (related to V_E in the default approach) and disposition of gases into the
35 liquid/tissue phase (related to SA).

36 The capacity of CFD techniques to solve and describe air phase behavior in complex
37 geometries represented by different species has been clearly demonstrated. For the ET

1 region, this technique has been repeatedly shown to estimate potential exposure (through
2 flux) of target tissues with greater accuracy than the use of V_E and SA ratios as a basic
3 default procedure.

4 The development of PBPK models to describe the toxicokinetic behavior of gas flow and
5 disposition into the tissue phase relating to SA_{ET} has been illustrated and demonstrated to
6 be a valid approach. Models comprised of tissue stacks with underlying blood flow that
7 simulate gas flow into and through the tissues have demonstrated a correlation of CFD-
8 estimated flux and target tissue dose with observed effects.

9 The capabilities of CFD and PBPK models to describe these individual phases have been
10 integrated in a quantitative manner with CFD- PBPK hybrid modeling approaches. The
11 development of this approach through use of a “permeability” coefficient (i.e. overall
12 mass transport coefficient, K_g) to combine elements of flux from CFD modeling and of
13 permeability from PBPK modeling in defining the diffusion of the gas through the air and
14 tissue phases has been demonstrated. For target tissue dose, CFD- PBPK hybrid models
15 represent a best available model for air and tissue phase elements of target tissue
16 dosimetry that the V_E/SA_{ET} surrogate attempts to approximate. Finally, this section
17 demonstrates the application of the best available model of tissue dosimetry, the CFD-
18 PBPK hybrid models. **These published applications consistently demonstrate that**
19 **interspecies target tissue doses (human:animal) in the ET region relative to external**
20 **exposure are close to or greater than 1:1.**

21 The results of the analysis for the ET region are graphically summarized in Figure 4-1.
22 This figure may be viewed as an update to Figures 2-3 and 3-6 reflecting the state of the
23 science presented in these reports related to the underlying assumptions and outcome of
24 applying the current default method. Studies have shown that air flow and gas deposition
25 to surface areas in the ET region are nonuniform. Also, the results from modeling
26 approaches such as CFD-PBPK hybrid models which have the capability to integrate and
27 apply conditions of nonuniform gas behavior in predicted target-tissue dose have been
28 entered into this schematic as well. As shown in Table 3-7, the interspecies dosimetry
29 modeling results indicate that for the ET region, the dose (i.e., HEC) to animals is either
30 greater (up to sevenfold) compared to humans or close to unity. Comparison of these
31 approaches demonstrates this point whether the dosimeter is quantitative (e.g., based on
32 target tissue flux, target tissue concentration of parent or metabolite) or qualitative (e.g.
33 based on overall or regional mass transfer coefficients – K_g and k_g) over a range of gases
34 having differing solubility, reactivity, uptake, and partition coefficients.

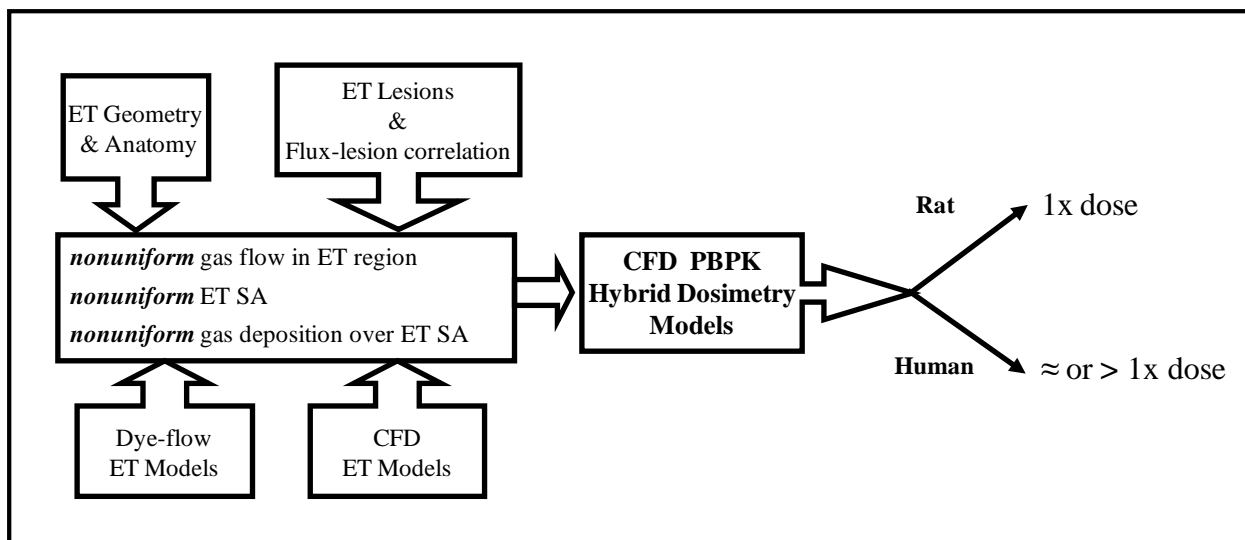


Figure 4-1 A revised schematic representation of the outcomes for interspecies inhalation dosimetry of gases for the ET region following from the advances presented.

1 The new studies dealing with overall gas dosimetry in the TB and PU airways support
 2 many of the principles and approaches of dosimetry in *RfC Methods*. Although the use of
 3 a simplified geometric model of the airways limited the breadth of their conclusions, the
 4 tissue metric for the alveolar area ($\text{g}/\text{cm}^2/\text{min}$) arrived at by Tsujino et al. (2005) is
 5 similar to that used in the *RfC Methods*. Morris and Hubbs (2009) showed a similar result
 6 in TB region for diacetyl using CFD-PBPK hybrid modeling. However, in the PU region
 7 Gloede et al (2011) observed target tissue concentrations to be 3-7 times greater in the
 8 human than the rat for diacetyl. The methods for extension of CFD evaluation to the
 9 lower airways of Zhang et al.(2011; 2006), Madasu (2007), and Harding and Robinsion
 10 (2010) should provide refinement and further resolution to flow and dose in the lower
 11 airways as has been done extensively for the upper airways. Additional studies , such as
 12 the novel work by Corley et al. (2012), need to encompass CFD simulations in the rat and
 13 human lower respiratory tracts to be able to compare gas uptake rates between species,
 14 similar to what has been done for the URT.

15 **The studies and information relating directly to dosimetry of the tracheobronchial**
 16 **(TB) and pulmonary (PU) regions generally support the dosimetric approaches and**
 17 **assumptions of *RfC Methods*.** Methodological advances and increased resolution of
 18 several in vivo imaging techniques indicate highly homogenous and uniform flows in the
 19 alveolar regions. On the other hand, examination of the tracheobronchial (TB) region
 20 with human models and advanced dynamic fluid flow programs reveal a degree of
 21 non-uniformity of flow for this region although apparently not to the extent that has been
 22 documented for the upper airway. As discussed in the *Status I Report* (U.S. EPA, 2009b),
 23 these assumptions and thus, the default dosimetric procedure for the ET region were not

1 supported as studies consistently demonstrated highly non-uniform airflow and
2 deposition to airway surfaces, and advance kinetic models clearly demonstrated the
3 animal/human dose to be ≥ 1 .

4 Marked advances in morphometry of these regions are being achieved with the
5 development and application of stereology. These techniques, described as the estimation
6 of higher dimensional information from lower dimensional samples, have and continue to
7 provide more accurate estimates of measures and vital parameters such as alveoli number
8 and size characteristics, volumes and surface areas in both humans (e.g., [Ochs et al.,
9 2004](#)) and laboratory animals ([Knust et al., 2009](#)), all of which may influence and refine
10 inhalation dosimetry of gases.

11 The significance of the blood:gas (air) partition coefficient ($H_{b/g}$) to the advanced PBPK
12 models have apparently been responsible for the generation of a number of direct and
13 surrogate approaches for providing these values, both animal and human. The critical and
14 comprehensive analyses of Payne and Kenny ([2002](#)) and Abraham et al. ([2005](#)) of human
15 and animal (rat) $H_{b/g}$ for a large number of volatile organics from several sources and
16 approaches made several conclusions. A major indirect conclusion affecting interspecies
17 dosimetry is that there is no significant difference for VOCs between rat and human $H_{b/g}$.
18 The other strategy to evaluate the $H_{b/g}$ for purposes of interspecies dosimetry involved
19 inspection of published inhalation PBPK models that were configured for interspecies
20 extrapolation, and therefore had $H_{b/g}$ s that were validated with simulations compared to
21 relevant human empirical data. **The modeling results indicate the current dosimetry
22 approach in the *RfC Methods* that uses ratios of animal to human $H_{b/g}$ as a basis of
23 dosimetry for systemic (SYS) sites may result in human equivalent concentrations
24 that are less than those estimated by PBPK models.**

25 An overview of the literature available on children's dosimetry closely follows the
26 recommendations and guidance of the NAS on children's risk ([NRC, 1993](#)). These
27 recommendations include the proposal to use PBPK models to explore and evaluate
28 potential child susceptibility. A recommendation linked to the development and
29 utilization of models is the need to generate accurate measurements and parameters to be
30 used in these models. Accordingly there exist a number of studies examining various
31 parameters essential to inhalation modeling including physiological daily inhalation rates,
32 lung tissue and lower airway measures and function. A compelling dataset (orally
33 administered therapeutics) documents the generally slower clearance rate in children
34 ([Ginsberg et al., 2002](#)). Flow models are available that examine uptake differences of
35 gases in the upper airways of both adults and children. Also, several PBPK models that
36 are configured to specifically consider child versus adult dosimetry have been developed.
37 Although the actual number of datasets and models relating to gas dosimetry in children
38 is not yet plentiful, a number of methods and approaches are available. **The available
39 methods and modeling approaches are fairly uniform in their indications of
40 potential higher inhaled doses in young children (3 mo), which may be 2- to 3-fold**

1 **more than in adults, but can be more or less.** The *RfC Methods* uses the human
2 interindividual uncertainty factor (UF_H) of 10 to accommodate pharmacokinetic and
3 pharmacodynamic variability and for consideration of potential sensitive population and
4 lifestages including children. **In some cases, chemical-specific information may**
5 **warrant consideration of alternative modeling approaches or adjustments to**
6 **account for this lifestage.** For example, in the development of shorter-term reference
7 values specific to a very early lifestage (e.g., infancy), when available chemical-specific
8 information – such as demonstrated differences in metabolism - may indicate
9 consideration of a data-informed approach differing from the default dosimetric
10 adjustments established for the RfC. It is anticipated that information will continue to
11 become available to further inform this issue.

12 An overview of the major findings related to the current default procedure for
13 interspecies dosimetric extrapolation of gases and for children's inhalation dosimetry is
14 presented below in Table 4-1 and Table 4-2.

Table 4-1 Overview of major findings related to the state of the science for inhalation dosimetry of gases

	Extrathoracic (ET)	Tracheobronchial (TB)	Pulmonary (PU)	Systemic (SYS)
Basis for Default DAF (addresses PK only)	V_E / SA ratio in animals and humans	V_E / SA ratio in animals and humans	V_E / SA ratio in animals and humans	$H_{b/g}$ (blood:gas (air) partition coefficient) animal to human ratio
Assumptions for default	Uniform flow to SA, uniform deposition to SA	Uniform flow to SA, uniform deposition to SA	Uniform flow to SA, uniform deposition to SA	Human and animal exposure scenarios are equivalent. Human blood concentration integrated over time is \leq animal, animal blood concentration = human equilibrium blood concentration
Default DAF	0.2 – 0.3	> 2	> 2	1
Models vs. DAF	Robust PK and CFD modeling database for a variety of chemicals shows dose metric in animals \geq humans (i.e. DAF is ≥ 1 not 0.2)	Limited to 2. Shows equivalent animal and human dose. Other modeling information is descriptive and does not provide information for extrapolation purposes.	Limited to 1. Shows potential for greater dose in humans for specific chemical.	Fairly robust PK database shows modeled derived DAFs to be ≥ 1 .
Current Evidence and Conclusions	Strong evidence indicating that in the absence of modeling the default DAF = 1. Uniformity of flow and deposition to SA assumptions not supported in studies examining airflow patterns, airflow and lesion correlation, nor by CFD modeling.	Limited evidence. The available information from airflow modeling suggests assumptions may hold or that there is not any compelling evidence that they do not.	Limited evidence. The available information from airflow modeling suggests assumptions may hold or that there is not any compelling evidence that they do not.	Modeling and partition coefficient information suggests that the default DAF may be conservative. However, there is no apparent pattern of the relationship between modeled derived DAFs/HECs, and PCs.
Source	<i>Status I Report</i> (2009b)	<i>Status II Report</i> (2011b)	<i>Status II Report</i> (2011b)	<i>Status II Report</i> (2011b)

Table 4-2 Summary of major finding related to state of the science of children’s inhalation dosimetry

	Extrathoracic (ET)	Tracheobronchial (TB)	Pulmonary (PU)	Systemic (SYS)
Children’s Dosimetry	Current information based on CFD model simulations and other analyses suggest no significant differences between children (e.g., 3 mo, and 7-8 year old) and adults are apparent.	Current but limited evidence suggests no significant differences between children and adults are apparent.	Evidence suggests the potential for a 2 to 3-fold greater inhalation dose in children (3 mo) vs. adults. Select cases may be more or less. Limited modeling information. No models are available that extrapolate from laboratory animals or adult humans to human models for specific early lifestages.	A few well parameterized PK models available. Evidence suggests the potential for a 2-fold greater systemic dose in children vs. adults from inhalation exposure. Select cases may be more or less depending upon the chemical and/or parent vs. metabolite.
Source	<i>Status II Report (U.S. EPA, 2011b)</i>			

5 REFERENCES

- Abraham, M.; Kamlet, M.; Taft, R.; Doherty, R.; Weathersby, P. (1985) Solubility properties in polymers and biological media. 2. The correlation and prediction of the solubilities of nonelectrolytes in biological tissues and fluids. *J Med Chem* 28: 865-870. <http://dx.doi.org/10.1021/jm00145a004>.
- Abraham, M. and Weathersby, P. (1994) Hydrogen bonding. 30. Solubility of gases and vapors in biological liquids and tissues. *J Pharm Sci* 83: 1450-1456. <http://dx.doi.org/10.1002/jps.2600831017>.
- Abraham, M. H.; Ibrahim, A.; Acree, W. E., Jr. (2005) Air to blood distribution of volatile organic compounds: A linear free energy analysis. *Chem Res Toxicol* 18: 904-911. <http://dx.doi.org/10.1021/tx050066d>.
- Altes, T.; Rehm, P.; Harrell, F.; Salerno, M.; Daniel, T.; De Lange, E. (2004a) Ventilation imaging of the lung: Comparison of hyperpolarized helium-3 MR imaging with Xe-133 scintigraphy. *Acad Radiol* 11: 729-734. <http://dx.doi.org/10.1016/j.acra.2004.04.001>.
- Altes, T. A.; Mata, J.; de Lange, E. E.; Brookeman, J. R.; Mugler JP, I. I. I. (2004b) Assessment of lung development using hyperpolarized helium-3 diffusion MR imaging. *J Magn Reson Imaging* 24: 1277-1283. <http://dx.doi.org/10.1002/jmri.20723>.
- Andersen, M.; Sarangapani, R.; Gentry, R.; Clewell, H.; Covington, T.; Frederick, C. B. (2000) Application of a hybrid CFD-PBPK nasal dosimetry model in an inhalation risk assessment: An example with acrylic acid. *Toxicol Sci* 57: 312-325.
- Asgharian, B.; Price, O. T.; Schroeter, J. D.; Kimbell, J. S.; Singal, M. (2012) A lung dosimetry model of vapor uptake and tissue disposition. *Inhal Toxicol* 24: 182-193. <http://dx.doi.org/10.3109/08958378.2012.654857>.
- Aylward, L. L.; Becker, R. A.; Kirman, C. R.; Hays, S. M. (2011) Assessment of margin of exposure based on biomarkers in blood: an exploratory analysis. *Regul Toxicol Pharmacol* 61: 44-52. <http://dx.doi.org/10.1016/j.yrtph.2011.06.001>.
- Balinotti, J. E.; Tiller, C. J.; Llapur, C. J.; Jones, M. H.; Kimmel, R. N.; Coates, C. E., . . . Tepper, R. S. (2009) Growth of the lung parenchyma early in life. *Am J Respir Crit Care Med* 179: 134-137. <http://dx.doi.org/10.1164/rccm.200808-1224OC>.
- Benignus, V.; Boyes, W.; Bushnell, P. (1998) A dosimetric analysis of behavioral effects of acute toluene exposure in rats and humans. *Toxicol Sci* 43: 186-195. <http://dx.doi.org/10.1006/toxs.1998.2458>.
- Bogdanffy, M. S.; Sarangapani, R.; Plowchalk, D. R.; Jarabek, A. M.; Andersen, M. E. (1999) A biologically based risk assessment for vinyl acetate-induced cancer and noncancer inhalation toxicity. *Toxicol Sci* 51: 19-35.
- Bolle, I.; Eder, G.; Takenaka, S.; Ganguly, K.; Karrasch, S.; Zeller, C., . . . Schulz, H. (2008) Postnatal lung function in the developing rat. *J Appl Physiol* 104: 1167-1176. <http://dx.doi.org/10.1152/japplphysiol.00587.2007>.
- Brochu, P.; Ducre-Robitaille, J. F.; Brodeur, J. (2006a) Physiological daily inhalation rates for free-living pregnant and lactating adolescents and women aged 11 to 55 years, using data from doubly labeled water measurements for use in health risk assessment. *Hum Ecol Risk Assess* 12: 702-735. <http://dx.doi.org/10.1080/10807030600801592>.
- Brochu, P.; Ducre-Robitaille, J. F.; Brodeur, J. (2006b) Physiological daily inhalation rates for free-living individuals aged 2.6 months to 96 years based on doubly labeled water measurements:

- Comparison with time-activity-ventilation and metabolic energy conversion estimates. *Hum Ecol Risk Assess* 12: 736-761. <http://dx.doi.org/10.1080/10807030600801626>.
- [Brochu, P.; Ducré-Robitaille, J. F.; Brodeur, J.](#) (2006c) Physiological daily inhalation rates for free-living individuals aged 1 month to 96 years, using data from doubly labeled water measurements: A proposal for air quality criteria, standard calculations and health risk assessment. *Hum Ecol Risk Assess* 12: 675-701. <http://dx.doi.org/10.1080/10807030600801550>.
- [Brochu, P.; Brodeur, J.; Krishnan, K.](#) (2011) Derivation of physiological inhalation rates in children, adults, and elderly based on nighttime and daytime respiratory parameters. *Inhal Toxicol* 23: 74-94. <http://dx.doi.org/10.3109/08958378.2010.543439>.
- [Bush, M. L.; Frederick, C. B.; Kimbell, J. S.; Ultman, J. S.](#) (1998) A CFD-PBPK hybrid model for simulating gas and vapor uptake in the rat nose. *Toxicol Appl Pharmacol* 150: 133-145. <http://dx.doi.org/10.1006/taap.1998.8407>.
- [Chang, J. C. F.; Gross, E. A.; Swenberg, J. A.; Barrow, C. S.](#) (1983) Nasal cavity deposition, histopathology, and cell proliferation after single or repeated formaldehyde exposures in B6C3F1 mice and F-344 rats. *Toxicol Appl Pharmacol* 68: 161-176.
- [Clewell, H. J.; Gentry, P. R.; Covington, T. R.; Sarangapani, R.; Teeguarden, J. G.](#) (2004) Evaluation of the potential impact of age- and gender-specific pharmacokinetic differences on tissue dosimetry. *Toxicol Sci* 79: 381-393. <http://dx.doi.org/10.1093/toxsci/kfh109>.
- [Corley, R., A.; Kabilan, S., .; Kuprat, A., .P.; Carson, J., .P.; Minard, K., .R.; Jacob, R., .E., . . . Einstein, D., .R.](#) (2012) Comparative computational modeling of airflows and vapor dosimetry in the respiratory tracts of a rat, monkey, and human. *Toxicol Sci* 128: 500-516. <http://dx.doi.org/10.1093/toxsci/kfs168>.
- [Corley, R. A.; Bartels, M. J.; Carney, E. W.; Weitz, K. K.; Soelberg, J. J.; Gies, R. A.; Thrall, K. D.](#) (2005) Development of a physiologically based pharmacokinetic model for ethylene glycol and its metabolite, glycolic acid, in rats and humans. *Toxicol Sci* 85: 476-490. <http://dx.doi.org/10.1093/toxsci/kfi119>.
- [Cronin, W.; Oswald, E.; Shelley, M.; Fisher, J.; Flemming, C.](#) (1995) A trichloroethylene risk assessment using a Monte Carlo analysis of parameter uncertainty in conjunction with physiologically-based pharmacokinetic modeling. *Risk Anal* 15: 555-565.
- [Csanády, G. A. and Filser, J. G.](#) (2007) A physiological toxicokinetic model for inhaled propylene oxide in rat and human with special emphasis on the nose. *Toxicol Sci* 95: 37-62. <http://dx.doi.org/10.1093/toxsci/kfl140>.
- [Dallas, C. E.; Chen, X. M.; Muralidhara, S.; Varkonyi, P.; Tackett, R. L.; Bruckner, J. V.](#) (1995) Physiologically based pharmacokinetic model useful in prediction of the influence of species, dose, and exposure route on perchloroethylene pharmacokinetics. *J Toxicol Environ Health* 44: 301-317. <http://dx.doi.org/10.1006/taap.1994.1179>.
- [de Jong, P. A.; Nakano, Y.; Lequin, M. H.; Merkus, P. J.; Tiddens, H. A.; Hogg, J. C.; Coxson, H. O.](#) (2003) Estimation of lung growth using computed tomography. *Eur Respir J* 22: 235-238. <http://dx.doi.org/10.1183/09031936.03.00089702>.
- [de Jong, P. A.; Long, F. R.; Wong, J. C.; Merkus, P. J.; Tiddens, H. A.; Hogg, J. C.; Coxson, H. O.](#) (2006) Computed tomographic estimation of lung dimensions throughout the growth period. *Eur Respir J* 27: 261-267. <http://dx.doi.org/10.1183/09031936.06.00070805>.

- DeJongh, J.; Verhaar, H.; Hermens, J. (1997) A quantitative property-property relationship (QPPR) approach to estimate in vitro tissue-blood partition coefficients of organic chemicals in rats and humans. *Arch Toxicol* 72: 17-25.
- Dorman, D. C.; Struve, M. F.; Wong, B. A.; Gross, E. A.; Parkinson, C.; Willson, G. A., . . . Andersen, M. E. (2008) Derivation of an inhalation reference concentration based upon olfactory neuronal loss in male rats following subchronic acetaldehyde inhalation. *Inhal Toxicol* 20: 245-256. <http://dx.doi.org/10.1080/08958370701864250>.
- Dunnill, M. S. (1962) Postnatal growth of the lung. *Thorax* 17: 329-333.
- Finck, M.; Hänel, D.; Wlokas, I. (2007) Simulation of nasal flow by lattice Boltzmann methods. *Comput Biol Med* 37: 739-749. <http://dx.doi.org/10.1016/j.compbiomed.2006.06.013>.
- Firestone, M.; Sonawane, B.; Barone, S.; Salmon, A. G.; Brown, J. P.; Hattis, D.; Woodruff, T. (2008) Potential new approaches for children's inhalation risk assessment. *J Toxicol Environ Health A* 71: 208-217. <http://dx.doi.org/10.1080/15287390701597905>.
- Fiserova-Bergerova, V. and Diaz, M. L. (1986) Determination and prediction of tissue-gas partition coefficients. *Int Arch Occup Environ Health* 58: 75-87. <http://dx.doi.org/10.1007/BF00378543>.
- Fisher, J. W. and Allen, B. C. (1993) Evaluating the risk of liver cancer in humans exposed to trichloroethylene using physiological models. *Risk Anal* 13: 87-95.
- Frederick, C. B.; Bush, M. L.; Lomax, L. G.; Black, K. A.; Finch, L.; Kimbell, J. S., . . . Ultman, J. S. (1998) Application of a hybrid computational fluid dynamics and physiologically based inhalation model for interspecies dosimetry extrapolation of acid vapors in the upper airways. *Toxicol Appl Pharmacol* 152: 211-231.
- Frederick, C. B.; Lomax, L. G.; Black, K. A.; Finch, L.; Scribner, H. E.; Kimbell, J. S., . . . Morris, J. B. (2002) Use of a hybrid computational fluid dynamics and physiologically based inhalation model for interspecies dosimetry comparisons of ester vapors. *Toxicol Appl Pharmacol* 183: 23-40.
- Garcia, G. J.; Schroeter, J. D.; Segal, R. A.; Stanek, J.; Foureman, G. L.; Kimbell, J. S. (2009) Dosimetry of nasal uptake of water-soluble and reactive gases: A first study of interhuman variability. *Inhal Toxicol* 21: 607-618. <http://dx.doi.org/10.1080/08958370802320186>.
- Gargas, M. L.; Burgess, R. J.; Voisard, D. E.; Cason, G. H.; Andersen, M. E. (1989) Partition coefficients of low-molecular-weight volatile chemicals in various liquids and tissues. *Toxicol Appl Pharmacol* 98: 87-99.
- Gargas, M. L.; Tyler, T. R.; Sweeney, L. M.; Corley, R. A.; Weitz, K. K.; Mast, T. J., . . . Hays, S. M. (2000) A toxicokinetic study of inhaled ethylene glycol monomethyl ether (2-ME) and validation of a physiologically based pharmacokinetic model for the pregnant rat and human. *Toxicol Appl Pharmacol* 165: 53-62. <http://dx.doi.org/10.1006/taap.2000.8928>.
- Geelhaar, A. and Weibel, E. R. (1971) Morphometric estimation of pulmonary diffusion capacity III The effect of increased oxygen consumption in Japanese Waltzing mice. *Respir Physiol Neurobiol* 11: 354-366. [http://dx.doi.org/10.1016/0034-5687\(71\)90009-0](http://dx.doi.org/10.1016/0034-5687(71)90009-0).
- Gehr, P.; Mwangi, D. K.; Ammann, A.; Maloiy, G. M.; Taylor, C. R.; Weibel, E. R. (1981) Design of the mammalian respiratory system. V. Scaling morphometric pulmonary diffusing capacity to body mass: wild and domestic mammals. *Respir Physiol* 44: 61-86.
- Gentry, P. R.; Covington, T. R.; Andersen, M. E.; Clewell, H. J., III. (2002) Application of a physiologically based pharmacokinetic model for isopropanol in the derivation of a reference dose and reference concentration. *Regul Toxicol Pharmacol* 36: 51-68.

- [Ginsberg, G.; Hattis, D.; Sonawane, B.; Russ, A.; Banati, P.; Kozlak, M., . . . Goble, R.](#) (2002) Evaluation of child/adult pharmacokinetic differences from a database derived from the therapeutic drug literature. *Toxicol Sci* 66: 185-200.
- [Ginsberg, G. L.; Foos, B. P.; Firestone, M. P.](#) (2005) Review and analysis of inhalation dosimetry methods for application to children's risk assessment. *J Toxicol Environ Health A* 68: 573-615. <http://dx.doi.org/10.1080/15287390590921793>.
- [Ginsberg, G. L.; Asgharian, B.; Kimbell, J. S.; Ultman, J. S.; Jarabek, A. M.](#) (2008) Modeling approaches for estimating the dosimetry of inhaled toxicants in children. *J Toxicol Environ Health A* 71: 166-195. <http://dx.doi.org/10.1080/15287390701597889>.
- [Gloede, E.; Cichocki, J. A.; Baldino, J. B.; Morris, J. B.](#) (2011) A validated hybrid computational fluid dynamics-physiologically based pharmacokinetic model for respiratory tract vapor absorption in the human and rat and its application to inhalation dosimetry of diacetyl. *Toxicol Sci* 123: 231-246. <http://dx.doi.org/10.1093/toxsci/kfr165>.
- [Gross, E. A.; Swenberg, J. A.; Fields, S.; Popp, J. A.](#) (1982) Comparative morphometry of the nasal cavity in rats and mice. *J Anat* 135: 83-88.
- [Guilmette, R. A.; Wicks, J. D.; Wolff, R. K.](#) (1989) Morphometry of human nasal airways in vivo using magnetic resonance imaging. *J Aerosol Med Pulm Drug Deliv* 2: 365-377.
- [Harding, E. M. and Robinson, R. J.](#) (2010) Flow in a terminal alveolar sac model with expanding walls using computational fluid dynamics. *Inhal Toxicol* 22: 669-678. <http://dx.doi.org/10.3109/08958371003749939>.
- [Hissink, A. M.; Krüse, J.; Kulig, B. M.; Verwei, M.; Muijser, H.; Salmon, F., . . . McKee, R. H.](#) (2007) Model studies for evaluating the neurobehavioral effects of complex hydrocarbon solvents III. PBPK modeling of white spirit constituents as a tool for integrating animal and human test data. *Neurotoxicology* 28: 751-760. <http://dx.doi.org/10.1016/j.neuro.2007.03.005>.
- [Hyde, D.; Tyler, N.; Putney, L.; Singh, P.; Gundersen, H.](#) (2004) Total number and mean size of alveoli in mammalian lung estimated using fractionator sampling and unbiased estimates of the Euler characteristic of alveolar openings. *Anat Rec* 277: 216-226. <http://dx.doi.org/10.1002/ar.a.20012>.
- [ICRP.](#) (International Commission on Radiological Protection). (1993) *Gases and vapours*. Ottawa, Canada.
- [Inagi, K.](#) (1992) [Histological study of mucous membranes in the human nasal septum]. *Nippon Jibiinkoka Gakkai Kaiho* 95: 1174-1189.
- [Kaneko, T.; Wang, P. Y.; Sato, A.](#) (1994) Partition coefficients of some acetate esters and alcohols in water, blood, olive oil, and rat tissues. *Occup Environ Med* 51: 68-72.
- [Kauczor, H. U.; Hanke, A.; Van Beek, E. J.](#) (2002) Assessment of lung ventilation by MR imaging: Current status and future perspectives. *Eur Radiol* 12: 1962-1970. <http://dx.doi.org/10.1007/s00330-002-1379-1>.
- [Kawahara, J.; Tanaka, S.; Tanaka, C.; Aoki, Y.; Yonemoto, J.](#) (2011) Estimation of daily inhalation rate in preschool children using a tri-axial accelerometer: a pilot study. *Sci Total Environ* 409: 3073-3077. <http://dx.doi.org/10.1016/j.scitotenv.2011.04.006>.
- [Kawahara, J.; Tanaka, S.; Tanaka, C.; Aoki, Y.; Yonemoto, J.](#) (In Press) (In Press) Daily Inhalation Rate and Time-Activity/Location Pattern in Japanese Preschool Children. <http://dx.doi.org/10.1111/j.1539-6924.2011.01776.x>.

- [Keyhani, K.; Scherer, P. W.; Mozell, M. M.](#) (1995) Numerical simulation of airflow in the human nasal cavity. *J Biomech Eng* 117: 429-441.
- [Kimbell, J. S.; Gross, E. A.; Joyner, D. R.; Godo, M. N.; Morgan, K. T.](#) (1993) Application of computational fluid dynamics to regional dosimetry of inhaled chemicals in the upper respiratory tract of the rat. *Toxicol Appl Pharmacol* 121: 253-263. <http://dx.doi.org/10.1006/taap.1993.1152>.
- [Kimbell, J. S.; Godo, M. N.; Gross, E. A.; Joyner, D. R.; Richardson, R. B.; Morgan, K. T.](#) (1997a) Computer simulation of inspiratory airflow in all regions of the F344 rat nasal passages. *Toxicol Appl Pharmacol* 145: 388-398. <http://dx.doi.org/10.1006/taap.1993.1152>.
- [Kimbell, J. S.; Gross, E. A.; Richardson, R. B.; Conolly, R. B.; Morgan, K. T.](#) (1997b) Correlation of regional formaldehyde flux predictions with the distribution of formaldehyde-induced squamous metaplasia in F344 rat nasal passages. *Mutat Res* 380: 143-154. [http://dx.doi.org/10.1016/S0027-5107\(97\)00132-2](http://dx.doi.org/10.1016/S0027-5107(97)00132-2).
- [Kimbell, J. S.; Overton, J. H.; Subramaniam, R. P.; Schlosser, P. M.; Morgan, K. T.; Conolly, R. B.; Miller, F. J.](#) (2001a) Dosimetry modeling of inhaled formaldehyde: Binning nasal flux predictions for quantitative risk assessment. *Toxicol Sci* 64: 111-121.
- [Kimbell, J. S.; Subramaniam, R. P.; Gross, E. A.; Schlosser, P. M.; Morgan, K. T.](#) (2001b) Dosimetry modeling of inhaled formaldehyde: comparisons of local flux predictions in the rat, monkey, and human nasal passages. *Toxicol Sci* 64: 100-110.
- [Kimbell, J. S. and Subramaniam, R. P.](#) (2001) Use of computational fluid dynamics models for dosimetry of inhaled gases in the nasal passages. *Inhal Toxicol* 13: 325-334. <http://dx.doi.org/10.1080/08958370120442>.
- [Kirman, C. R.; Gargas, M. L.; Marsh, G. M.; Strother, D. E.; Klaunig, J. E.; Collins, J. J.; Deskin, R.](#) (2005a) Cancer dose--response assessment for acrylonitrile based upon rodent brain tumor incidence: use of epidemiologic, mechanistic, and pharmacokinetic support for nonlinearity. *Regul Toxicol Pharmacol* 43: 85-103. <http://dx.doi.org/10.1016/j.yrtph.2005.06.007>.
- [Kirman, C. R.; Sweeney LM; Corley, R.; Gargas, M. L.](#) (2005b) Using physiologically-based pharmacokinetic modeling to address nonlinear kinetics and changes in rodent physiology and metabolism due to aging and adaptation in deriving reference values for propylene glycol methyl ether and propylene glycol methyl ether acetate. *Risk Anal* 25: 271 - 284. <http://dx.doi.org/10.1111/j.1539-6924.2005.00588.x>.
- [Kliment, V.](#) (1973) Similarity and dimensional analysis, evaluation of aerosol deposition in the lungs of laboratory animals and man. *Folia Morphol (Warsz)* 21: 59-64.
- [Knust, J.; Ochs, M.; Gundersen, H.; Nyengaard, J.](#) (2009) Stereological estimates of alveolar number and size and capillary length and surface area in mice lungs. *Anat Rec* 292: 113-122. <http://dx.doi.org/10.1002/ar.20747>.
- [Lechner, A. J.](#) (1978) The scaling of maximal oxygen consumption and pulmonary dimensions in small mammals. *Respir Physiol Neurobiol* 34: 29-44. [http://dx.doi.org/10.1016/0034-5687\(78\)90047-6](http://dx.doi.org/10.1016/0034-5687(78)90047-6).
- [Lee, K. M.; Dill, J. A.; Chou, B. J.; Roycroft, J. H.](#) (1998) Physiologically based pharmacokinetic model for chronic inhalation of 2-butoxyethanol. *Toxicol Appl Pharmacol* 153: 211-226. <http://dx.doi.org/10.1006/taap.1998.8518>.
- [Liao, K. H.; Tan, Y. M.; Conolly, R. B.; Borghoff, S. J.; Gargas, M. L.; Andersen, M. E.; III, C. H.](#) (2007) Bayesian estimation of pharmacokinetic and pharmacodynamic parameters in a mode-of-action-based cancer risk assessment for chloroform. *Risk Anal* 27: 1535-1551. <http://dx.doi.org/10.1111/j.1539-6924.2007.00987.x>.

- [Lu, Y.; Rieth, S.; Lohitnavy, M.; Dennison, J.; El-Masri, H.; Barton, H. A., . . . Yang, R. S.](#) (2008) Application of PBPK modeling in support of the derivation of toxicity reference values for 1,1,1-trichloroethane. *Regul Toxicol Pharmacol* 50: 249-260. <http://dx.doi.org/10.1016/j.yrtph.2007.12.001>.
- [Madasu, S.](#) (2007) Gas uptake in a three-generation model geometry during steady expiration: Comparison of axisymmetric and three-dimensional models. *Inhal Toxicol* 19: 199-210. <http://dx.doi.org/10.1080/08958370601067855>.
- [Madasu, S.; Ultman, J. S.; Borhan, A.](#) (2008) Comparison of axisymmetric and three-dimensional models for gas uptake in a single bifurcation during steady expiration. *J Biomech Eng* 130: 011013. <http://dx.doi.org/10.1115/1.2838041>.
- [Medinsky, M. A. and Bond, J. A.](#) (2001) Sites and mechanisms for uptake of gases and vapors in the respiratory tract. *Toxicology* 160: 165-172.
- [Ménache, M. G.; Hofmann, W.; Ashgarian, B.; Miller, F. J.](#) (2008) Airway geometry models of children's lungs for use in dosimetry modeling. *Inhal Toxicol* 20: 101-126. <http://dx.doi.org/10.1080/08958370701821433>.
- [Mercer, R. R.; Russell, M. L.; Crapo, J. D.](#) (1994a) Alveolar septal structure in different species. *J Appl Physiol* 77: 1060-1066.
- [Mercer, R. R.; Russell, M. L.; Roggli, V. L.; Crapo, J. D.](#) (1994b) Cell number and distribution in human and rat airways. *Am J Respir Cell Mol Biol* 10: 613-624.
- [Meulenberg, C. and Vijverberg, H.](#) (2000) Empirical relations predicting human and rat tissue: Air partition coefficients of volatile organic compounds. *Toxicol Appl Pharmacol* 165: 206-216. <http://dx.doi.org/10.1006/taap.2000.8929>.
- [Mileson, B. E.; Sweeney, L. M.; Gargas, M. L.; Kinzell, J.](#) (2009) Iodomethane human health risk characterization. *Inhal Toxicol* 21: 583-605. <http://dx.doi.org/10.1080/08958370802601627>.
- [Minard, K. R.; Einstein, D. R.; Jacob, R. E.; Kabilan, S.; Kuprat, A. P.; Timchalk, C. A., . . . Corley, R. A.](#) (2006) Application of magnetic resonance (MR) imaging for the development and validation of computational fluid dynamic (CFD) models of the rat respiratory system. *Inhal Toxicol* 18: 787-794. <http://dx.doi.org/10.1080/08958370600748729>.
- [Morgan, K. T.; Kimbell, J. S.; Monticello, T. M.; Patra, A. L.; Fleishman, A.](#) (1991) Studies of inspiratory airflow patterns in the nasal passages of the F344 rat and rhesus monkey using nasal molds: Relevance to formaldehyde toxicity. *Toxicol Appl Pharmacol* 110: 223-240. [http://dx.doi.org/10.1016/S0041-008X\(05\)80005-5](http://dx.doi.org/10.1016/S0041-008X(05)80005-5).
- [Morris, J. B.](#) (1997) Uptake of acetaldehyde vapor and aldehyde dehydrogenase levels in the upper respiratory tracts of the mouse, rat, hamster, and guinea pig. *Toxicol Sci* 35: 91-100.
- [Morris, J. B.](#) (1998) Effect of acrolein vapor on upper respiratory tract uptake of acetaldehyde. *Inhal Toxicol* 10: 843-856. <http://dx.doi.org/10.1080/089583798197411>.
- [Morris, J. B.; Banton, M. I.; Pottenger, L. H.](#) (2004) Uptake of inspired propylene oxide in the upper respiratory tract of the f344 rat. *Toxicol Sci* 81: 216-224. <http://dx.doi.org/10.1093/toxsci/kfh198>.
- [Morris, J. B. and Hubbs, A. F.](#) (2009) Inhalation dosimetry of diacetyl and butyric acid, two components of butter flavoring vapors. *Toxicol Sci* 108: 173-183. <http://dx.doi.org/10.1093/toxsci/kfn222>.
- [Mosges, R.; Buchner, B.; Kleiner, M.; Freitas, R.; Horschler, I.; Schroder, W.](#) (2010) Computational fluid dynamics analysis of nasal flow. *B-ENT* 6: 161-165.

- Moulin, F. J.; Breneman, K. A.; Kimbell, J. S.; James, R. A.; Dorman, D. C. (2002) Predicted regional flux of hydrogen sulfide correlates with distribution of nasal olfactory lesions in rats. *Toxicol Sci* 66: 7-15.
- Nong, A.; McCarver, D. G.; Hines, R. N.; Krishnan, K. (2006) Modeling interchild differences in pharmacokinetics on the basis of subject-specific data on physiology and hepatic CYP2E1 levels: a case study with toluene. *Toxicol Appl Pharmacol* 214: 78-87.
<http://dx.doi.org/10.1016/j.taap.2005.12.001>.
- NRC. (National Research Council). (1993) Pesticides in the diets of infants and children. Washington, DC: National Academy Press.
- Ochs, M.; Nyengaard, J. R.; Jung, A.; Knudsen, L.; Voigt, M.; Wahlers, T., . . . Gundersen, H. J. (2004) The number of alveoli in the human lung. *Am J Respir Crit Care Med* 169: 1-10.
- OECD. (Organisation for Economic Co-operation and Development). (2011) Guidance document for the derivation of an acute reference concentration (ARFC). (ENV/JM/MONO(2011)33). Paris, France. <http://www.oecd.org/dataoecd/41/60/48542016.pdf>.
- OEHHA. (California Office of Environmental Health Hazard Assessment). (2008) Air toxics hot spots program technical support document for the derivation of noncancer reference exposure levels. Oakland, CA: Office of Environmental Health Hazard Assessment; California Environmental Protection Agency.
- Ogiu, N.; Nakamura, Y.; Ijiri, I.; Hiraiwa, K.; Ogiu, T. (1997) A statistical analysis of the internal organ weights of normal Japanese people. *Health Phys* 72: 368-383.
- Osterman-Golkar, S.; Czene, K.; Lee, M. S.; Faller, T. H.; Csanády, G. A.; Kessler, W., . . . Segerbäck, D. (2003) Dosimetry by means of DNA and hemoglobin adducts in propylene oxide-exposed rats. *Toxicol Appl Pharmacol* 191: 245-254.
- Overton, J. H. and Graham, R. C. (1989) Predictions of ozone absorption in human lungs from newborn to adult. *Health Phys* 1: 29-36.
- Overton, J. H.; Kimbell, J. S.; Miller, F. J. (2001) Dosimetry modeling of inhaled formaldehyde: The human respiratory tract. *Toxicol Sci* 64: 122-134.
- Padaki, A., ; Ultman, J., . S.; Borhan, A., . (2009) Ozone uptake during inspiratory flow in a model of the larynx, trachea and primary bronchial bifurcation. *Chem Eng Sci* 64: 4640-4648.
<http://dx.doi.org/10.1016/j.ces.2009.05.017>.
- Pastino, G. M.; Sultatos, L. G.; Flynn, E. J. (1996) Development and application of a physiologically based pharmacokinetic model for ethanol in the mouse. *Alcohol Alcohol* 31: 365-374.
- Pastino, G. M.; Asgharian, B.; Roberts, K.; Medinsky, M. A.; Bond, J. A. (1997) A comparison of physiologically based pharmacokinetic model predictions and experimental data for inhaled ethanol in male and female B6C3F1 mice, F344 rats, and humans. *Toxicol Appl Pharmacol* 145: 147-157. <http://dx.doi.org/10.1006/taap.1997.8161>.
- Payne, M. P. and Kenny, L. C. (2002) Comparison of models for the estimation of biological partition coefficients. *J Toxicol Environ Health A* 65: 897-931.
<http://dx.doi.org/10.1080/00984100290071171>.
- Pelekis, M.; Gephart, L. A.; Lerman, S. E. (2001) Physiological-model-based derivation of the adult and child pharmacokinetic intraspecies uncertainty factors for volatile organic compounds. *Regul Toxicol Pharmacol* 33: 12-20. <http://dx.doi.org/10.1006/rtph.2000.1436>.

- Phalen, R. F.; Stuart, B. O.; Lioy, P. J. (1988) Rationale for and implications of particle size-selective sampling (Industrial hygiene science series ed.). Chelsea, MI: Lewis Publishers, Inc.
- Pinkerton, K. E. and Joad, J. P. (2000) The mammalian respiratory system and critical windows of exposure for children's health. *Environ Health Perspect* 108: 457-462.
- Poulin, P. and Krishnan, K. (1995) A biologically-based algorithm for predicting human tissue: Blood partition coefficients of organic chemicals. *Hum Exp Toxicol* 14: 273-280.
<http://dx.doi.org/10.1177/096032719501400307>.
- Price, K.; Haddad, S.; Krishnan, K. (2003) Physiological modeling of age-specific changes in the pharmacokinetics of organic chemicals in children. *J Toxicol Environ Health A* 66: 417-433.
<http://dx.doi.org/10.1080/15287390306450>.
- Rao, L.; Tiller, C.; Coates, C.; Kimmel, R.; Applegate, K. E.; Granroth-Cook, J., . . . Tepper, R. S. (2010) Lung growth in infants and toddlers assessed by multi-slice computed tomography. *Acad Radiol* 17: 1128-1135. <http://dx.doi.org/10.1016/j.acra.2010.04.012>.
- Reitz, R. H.; McDougal, J. N.; Himmelstein, M. W.; Nolan, R. J.; Schumann, A. M. (1988) Physiologically based pharmacokinetic modeling with methylchloroform: Implications for interspecies, high dose/low dose, and dose route extrapolations. *Toxicol Appl Pharmacol* 95: 185-199. [http://dx.doi.org/10.1016/0041-008X\(88\)90155-X](http://dx.doi.org/10.1016/0041-008X(88)90155-X).
- Ríos-Blanco, M. N.; Ranasinghe, A.; Lee, M. S.; Faller, T.; Filser, J. G.; Swenberg, J. A. (2003) Molecular dosimetry of N7-(2-hydroxypropyl)guanine in tissues of F344 rats after inhalation exposure to propylene oxide. *Carcinogenesis* 24: 1233-1238.
<http://dx.doi.org/10.1093/carcin/bgg087>.
- Sarangapani, R.; Gentry, P. R.; Covington, T. R.; Teeguarden, J. G.; Clewell HJ, I. I. I. (2003) Evaluation of the potential impact of age- and gender-specific lung morphology and ventilation rate on the dosimetry of vapors. *Inhal Toxicol* 15: 987-1016. <http://dx.doi.org/10.1080/08958370390226350>.
- Sarangapani, R.; Teeguarden, J. G.; Gentry, P. R.; Clewell, H. J.; Barton, H. A.; Bogdanffy, M. S. (2004) Interspecies dose extrapolation for inhaled dimethyl sulfate: A PBPK model-based analysis using nasal cavity N7-methylguanine adducts. *Inhal Toxicol* 16: 593-605.
<http://dx.doi.org/10.1080/08958370490464562>.
- Schreck, S.; Sullivan, K. J.; Ho, C. M.; Chang, H. K. (1993) Correlations between flow resistance and geometry in a model of the human nose. *J Appl Physiol* 75: 1767-1775.
- Schreider, J. P. and Hutchens, J. O. (1980) Morphology of the guinea pig respiratory tract. *Anat Rec* 196: 313-321. <http://dx.doi.org/10.1002/ar.1091960307>.
- Schroeter, J. D.; Kimbell, J. S.; Andersen, M. E.; Dorman, D. C. (2006) Use of a pharmacokinetic-driven computational fluid dynamics model to predict nasal extraction of hydrogen sulfide in rats and humans. *Toxicol Sci* 94: 359-367. <http://dx.doi.org/10.1093/toxsci/kfl112>.
- Schroeter, J. D.; Kimbell, J. S.; Gross, E. A.; Willson, G. A.; Dorman, D. C.; Tan, Y. M.; III, C. H. (2008) Application of physiological computational fluid dynamics models to predict interspecies nasal dosimetry of inhaled acrolein. *Inhal Toxicol* 20: 227-243.
<http://dx.doi.org/10.1080/08958370701864235>.
- Schroeter, J. D.; Garcia, G. J.; Kimbell, J. S. (2010) A computational fluid dynamics approach to assess interhuman variability in hydrogen sulfide nasal dosimetry. *Inhal Toxicol* 22: 277-286.
<http://dx.doi.org/10.3109/08958370903278077>.

- Steward, A.; Allott, P. R.; Cowles, A. L.; Mapleson, W. W. (1973) Solubility coefficients for inhaled anaesthetics for water, oil and biological media. *Br J Anaesth* 45: 282-293. <http://dx.doi.org/10.1093/bja/45.3.282>.
- Subramaniam, R. P.; Richardson, R. B.; Morgan, K. T.; Kimbell, J. S.; Guilmette, R. A. (1998) Computational fluid dynamics simulations of inspiratory airflow in the human nose and nasopharynx. *Inhal Toxicol* 10: 91-120. <http://dx.doi.org/10.1080/089583798197772>.
- Sweeney, L. M.; Andersen, M. E.; Gargas, M. L. (2004) Ethyl acrylate risk assessment with a hybrid computational fluid dynamics and physiologically based nasal dosimetry model. *Toxicol Sci* 79: 394-403. <http://dx.doi.org/10.1093/toxsci/kfh116>.
- Sweeney, L. M.; Kirman, C. R.; Gannon, S. A.; Thrall, K. D.; Gargas, M. L.; Kinzell, J. H. (2009) Development of a physiologically based pharmacokinetic (PBPK) model for methyl iodide in rats, rabbits, and humans. *Inhal Toxicol* 21: 552-582. <http://dx.doi.org/10.1080/08958370802601569>.
- Tardif, R.; Charest-Tardif, G.; Brodeur, J.; Krishnan, K. (1997) Physiologically based pharmacokinetic modeling of a ternary mixture of alkyl benzenes in rats and humans. *Toxicol Appl Pharmacol* 144: 120-134. <http://dx.doi.org/10.1006/taap.1996.8096>.
- Taylor, A. B.; Borhan, A.; Ultman, J. S. (2007) Three-dimensional simulations of reactive gas uptake in single airway bifurcations. *Ann Biomed Eng* 35: 235-249. <http://dx.doi.org/10.1007/s10439-006-9195-4>.
- Teeguarden, J. G.; Deisinger, P. J.; Poet, T. S.; English, J. C.; Faber, W. D.; Barton, H. A., . . . Clewell, H. J., III. (2005) Derivation of a human equivalent concentration for n-butanol using a physiologically based pharmacokinetic model for n-butyl acetate and metabolites n-butanol and n-butyric acid. *Toxicol Sci* 85: 429-446. <http://dx.doi.org/10.1093/toxsci/kfi103>.
- Teeguarden, J. G.; Bogdanffy, M. S.; Covington, T. R.; Tan, C.; Jarabek, A. M. (2008) A PBPK model for evaluating the impact of aldehyde dehydrogenase polymorphisms on comparative rat and human nasal tissue acetaldehyde dosimetry. *Inhal Toxicol* 20: 375-390. <http://dx.doi.org/10.1080/08958370801903750>.
- Tenney, S. M. and Remmers, J. E. (1963) Comparative quantitative morphology of the mammalian lung: diffusing area. *Nature* 197: 54-56.
- Thrall, K. D.; Woodstock, A. D.; Soelberg, J. J.; Gargas, M. L.; Kinzell, J. H.; Corley, R. A. (2009) A real-time methodology to evaluate the nasal absorption of volatile compounds in anesthetized animals. *Inhal Toxicol* 21: 531-536. <http://dx.doi.org/10.1080/08958370802601452>.
- Thurlbeck, W. M. (1967) The internal surface area of nonemphysematous lungs. *Am Rev Respir Dis* 95: 765-773.
- Thurlbeck, W. M. (1982) Postnatal human lung growth. *Thorax* 37: 564-571.
- Tsuda, A.; Rogers, R. A.; Hydron, P. E.; Butler, J. P. (2002) Chaotic mixing deep in the lung. *PNAS* 99: 10173-10178. <http://dx.doi.org/10.1073/pnas.102318299>.
- Tsujino, I.; Kawakami, Y.; Kaneko, A. (2005) Comparative simulation of gas transport in airway models of rat, dog, and human. *Inhal Toxicol* 17: 475-485. <http://dx.doi.org/10.1080/08958370590964476>.
- U.S. EPA. (U.S. Environmental Protection Agency). (1994) Methods for derivation of inhalation reference concentrations and application of inhalation dosimetry. (EPA/600/8-90/066F). Research Triangle Park, NC. <http://cfpub.epa.gov/ncea/cfm/recordisplay.cfm?deid=71993>.

- U.S. EPA. (U.S. Environmental Protection Agency). (1997) Exposure factors handbook (final report). (EPA/600/P-95/002Fa-c). Washington, DC.
<http://cfpub.epa.gov/ncea/cfm/recordisplay.cfm?deid=12464>.
- U.S. EPA. (U.S. Environmental Protection Agency). (2002) A review of the reference dose and reference concentration processes. (EPA/630/P-02/002F). Washington, DC.
<http://cfpub.epa.gov/ncea/cfm/recordisplay.cfm?deid=51717>.
- U.S. EPA. (U.S. Environmental Protection Agency). (2004) Air quality criteria for particulate matter. (EPA/600/P-99/002aF-bF). Research Triangle Park, NC.
<http://cfpub.epa.gov/ncea/cfm/recordisplay.cfm?deid=87903>.
- U.S. EPA. (U.S. Environmental Protection Agency). (2006a) A framework for assessing health risk of environmental exposures to children. (EPA/600/R-05/093F). Washington, DC.
<http://cfpub.epa.gov/ncea/cfm/recordisplay.cfm?deid=158363>.
- U.S. EPA. (U.S. Environmental Protection Agency). (2006b) Peer review handbook (3rd edition). (EPA/100/B-06/002). Washington, DC. <http://www.epa.gov/peerreview/>.
- U.S. EPA. (U.S. Environmental Protection Agency). (2008) Child-specific exposure factors handbook. (EPA/600/R-06/096F). Washington, DC.
<http://cfpub.epa.gov/ncea/cfm/recordisplay.cfm?deid=199243>.
- U.S. EPA. (U.S. Environmental Protection Agency). (2009a) Integrated science assessment for particulate matter - Annexes with errata. (EPA/600/R-08/139). Washington, DC.
<http://cfpub.epa.gov/ncea/cfm/recordisplay.cfm?deid=216546>.
- U.S. EPA. (U.S. Environmental Protection Agency). (2009b) Status report: Advances in inhalation dosimetry of gases and vapors with portal of entry effects in the upper respiratory tract. (EPA/600/R-09/072). Research Triangle Park, NC.
<http://cfpub.epa.gov/ncea/cfm/recordisplay.cfm?deid=212131>.
- U.S. EPA. (U.S. Environmental Protection Agency). (2009c) Integrated science assessment for particulate matter. (EPA/600/R-08/139F). Research Triangle Park, NC.
<http://cfpub.epa.gov/ncea/cfm/recordisplay.cfm?deid=216546>.
- U.S. EPA. (U.S. Environmental Protection Agency). (2011a) Exposure factors handbook 2011 edition (final). (EPA/600/R-09/052F). <http://cfpub.epa.gov/ncea/cfm/recordisplay.cfm?deid=236252>.
- U.S. EPA. (U.S. Environmental Protection Agency). (2011b) Status report: Advances in inhalation dosimetry for gases with lower respiratory tract and systemic effects. (EPA/600/R-11/067). Washington, DC.
- Valcke, M. and Krishnan, K. (2011a) Evaluation of the impact of the exposure route on the human kinetic adjustment factor. *Regul Toxicol Pharmacol* 59: 258-269.
<http://dx.doi.org/10.1016/j.yrtph.2010.10.008>.
- Valcke, M. and Krishnan, K. (2011b) Assessing the impact of the duration and intensity of inhalation exposure on the magnitude of the variability of internal dose metrics in children and adults. *Inhal Toxicol* 23: 863-877. <http://dx.doi.org/10.3109/08958378.2011.609918>.
- Valcke, M.; Nong, A.; Krishnan, K. (2012) Modeling the Human Kinetic Adjustment Factor for Inhaled Volatile Organic Chemicals: Whole Population Approach versus Distinct Subpopulation Approach. *Journal of Toxicology* 2012: 404329. <http://dx.doi.org/10.1155/2012/404329>.
- Wen, J.; Inthavong, K.; Tu, J.; Wang, S. (2008) Numerical simulations for detailed airflow dynamics in a human nasal cavity. *Respir Physiol Neurobiol* 161: 125-135.
<http://dx.doi.org/10.1016/j.resp.2008.01.012>.

- Wiebe, B. M. and Laursen, H. (1995) Human lung volume, alveolar surface area, and capillary length. *Microsc Res Tech* 32: 255-262. <http://dx.doi.org/10.1002/jemt.1070320308>.
- Willems, B.; Melnick, R.; Kohn, M.; Portier, C. (2001) A physiologically based pharmacokinetic model for inhalation and intravenous administration of naphthalene in rats and mice. *Toxicol Appl Pharmacol* 176: 81-91. <http://dx.doi.org/10.1006/taap.2001.9269>.
- Yu, C. P. and Xu, G. B. (1987) Predictive models for deposition of inhaled diesel exhaust particles in humans and laboratory species. (Research Report No. 10). Cambridge, MA: Health Effects Institute. <http://pubs.healtheffects.org/view.php?id=138>.
- Zeltner, T. B.; Caduff, J. H.; Gehr, P.; Pfenninger, J.; Burri, P. H. (1987) The postnatal development and growth of the human lung. I. Morphometry. *Respir Physiol* 67: 247-267. [http://dx.doi.org/10.1016/0034-5687\(87\)90057-0](http://dx.doi.org/10.1016/0034-5687(87)90057-0).
- Zeman, K. L. and Bennett, W. D. (2006) Growth of the small airways and alveoli from childhood to the adult lung measured by aerosol-derived airway morphometry. *J Appl Physiol* 100: 965-971. <http://dx.doi.org/10.1152/jappphysiol.00409.2005>.
- Zhang, Z.; Kleinstreuer, C.; Kim, C. S. (2006) Transport and uptake of MTBE and ethanol vapors in a human upper airway model. *Inhal Toxicol* 18: 169-184. <http://dx.doi.org/10.1080/08958370500434172>.
- Zhang, Z. and Kleinstreuer, C. (2011) Deposition of naphthalene and tetradecane vapors in models of the human respiratory system. *Inhal Toxicol* 23: 44-57. <http://dx.doi.org/10.3109/08958378.2010.540261>.

APPENDIX A. SUMMARY AND DISPOSITION OF INDEPENDENT EXTERNAL PEER REVIEW COMMENTS

1 The report “*Advances in Inhalation Gas Dosimetry for Derivation of a Reference*
2 *Concentration (RfC) and Use in Risk Assessment*” has undergone a formal external peer
3 letter review performed by scientists in accordance with EPA guidance on peer review
4 ([U.S. EPA, 2006b](#)). The reviewers were tasked with providing written answers to charge
5 questions on both general and specific scientific aspects of the report. A summary of
6 significant comments made by the external reviewers to these charge questions and
7 EPA’s responses to these comments arranged by charge question follow. Several
8 reviewers suggested additional references for consideration and incorporation into the
9 document. Those references incorporated into the document are indicated in the
10 responses to specific charge questions where appropriate. Editorial comments were
11 considered and incorporated directly into the document as appropriate.

A.1 External Peer Reviewer Comments - Comments and Response to Charge:

A.1.1 Charge Question 1

12 This report provides new information on the pharmacokinetic component of interspecies
13 gas dosimetry for effects in the ET, TB, PU regions, and SYS sites as it relates to the
14 current default procedures. Issues related to pharmacodynamics, including variability in
15 response, are specifically excluded from this report. Is the scope and primary focus of this
16 report clear?

Comments:

17 All of the reviewers were in agreement that the scope and primary focus of the report is
18 clear. One suggested breaking up Chapter 3 into two new chapters (adults and children).
19 A second reviewer understood the scope of the document, but asked why a detailed
20 discussion of pharmacodynamics was excluded from the report. A third reviewer thought
21 that the title is more general than the actual scope and focus of the document and
22 suggested the addition of a subtitle to clarify that this report focuses on interspecies
23 extrapolation. This reviewer also provided several suggestions for consideration for the
24 future evolution of this work. Another reviewer commented that it is stated several times
25 that the report does not include new data on pharmacodynamics or on variability of
26 response. This reviewer thought that the scope and primary focus of this report are clear
27 and includes an extensive summary of the recent (since 1994) advances in the
28

1 pharmacokinetic component of interspecies dosimetry. The fifth reviewer noted that the
2 scope and focus are very clear and the report is both educational and valuable.

3 Response:

4 Consideration was given to dividing Chapter 3 into separate chapters for children and
5 adults; however, the subsections for these chapters would not be compatible for children
6 and adults since there is a paucity of data for children compared to the available data for
7 adults.

8 The scope of this report was limited to evaluating the scientific advances related to the
9 default procedure for interspecies extrapolation as presented in the *1994 RfC Methods*.
10 As described in this document the focus of this current work was to evaluate the new
11 science as it relates to the kinetic portion of this extrapolation. To further clarify the
12 scope of this report, additional text was added to the Executive Summary. Subtitles were
13 considered, but a subtitle was not added to this report. The method to derive an RfC relies
14 on interspecies extrapolation, thus the current title does implicitly pertain to interspecies
15 extrapolation.

A.1.2 Charge Question 2

16 Have the principal studies examining interspecies gas dosimetry for effects in the ET,
17 TB, PU regions, and SYS sites that have been reported since the issuance of the *1994 RfC*
18 *Methods* been identified in this report? Please identify and provide a rationale for any
19 other key studies that could contribute to support or refinement of the current default
20 procedures for derivation of an RfC.

21 Comments:

22 Four reviewers commented that it is clear a comprehensive and focused review of the
23 literature pertaining to the focus of this report. These reviewers also thought that the
24 major developments in this area were presented in a clear and concise manner, providing
25 sufficient information to support understanding of these developments. Three of these
26 four reviewers suggested additional references for consideration in this work. One
27 reviewer suggested including research conducted by the radiological community on
28 development of dosimetry lung models, the emerging field of molecular dosimetry, while
29 another reviewer suggested including references that are not directly related to
30 interspecies gas dosimetry but may provide insight into respiratory uptake. A reviewer
31 suggested the effects of particles on gas dosimetry should be covered.

32 Lastly, one reviewer commented that there was an incomplete analysis of uptake
33 modeling in the lower respiratory tract, as several studies dealing with whole-lung
34 dosimetry modeling are missing. This reviewer suggested a few relevant references for

1 consideration that predict the uptake of various gases in specific locations and the entire
2 lung, thus allowing interspecies extrapolation based on gas flux to the lung surfaces or
3 lung tissue concentration.

4 Response:

5 All references suggested by the reviewers were evaluated for consideration in this report
6 and many of them are included in this final report. The references pertaining to
7 dosimetry of radioactive gases were reviewed in depth, but were found not to include
8 novel information related to interspecies inhalation gas dosimetry. The effect of particles
9 on gas dosimetry was not within the scope of this report; however, additional text was
10 added in Section 4 stating that the effect of particles should be considered in inhalation
11 risk assessment.

12 Molecular markers are emerging as useful dosimeters. The references suggested by a
13 reviewer were included in Section 3.2.5.3; however, a detailed discussion of molecular
14 dosimetry was not provided.

15 Osterman-Golkar, S.; Czene, K.; Lee, M. S.; Faller, T. H.; Csanády, G. A.; Kessler,
16 W., . . . Segerbäck, D. (2003) Dosimetry by means of DNA and hemoglobin adducts
17 in propylene oxide-exposed rats. *Toxicol Appl Pharmacol* 191: 245-254.

18 Ríos-Blanco, M. N.; Ranasinghe, A.; Lee, M. S.; Faller, T.; Filser, J. G.; Swenberg, J.
19 A. (2003) Molecular dosimetry of N7-(2-hydroxypropyl)guanine in tissues of F344
20 rats after inhalation exposure to propylene oxide. *Carcinogenesis* 24: 1233-1238.

21 The references provided by a reviewer regarding whole-lung dosimetry modeling were
22 useful and added to this report in Section 3.3.4 and 3.6.2, respectively.

23 Asgharian, B.; Price, O. T.; Schroeter, J. D.; Kimbell, J. S.; Singal, M. (2012) A lung
24 dosimetry model of vapor uptake and tissue disposition. *Inhal Toxicol* 24: 182-193.

25 Overton, J. H. and Graham, R. C. (1989) Predictions of ozone absorption in human
26 lungs from newborn to adult. *Health Phys* 1: 29-36.

27 One reviewer suggested other studies that are related to the interspecies extrapolation for
28 gas dosimetry. These additional studies were included in Section 3.2.2.2, 3.2.2.2, 3.6.2,
29 and 3.3.1, respectively.

30 Finck, M.; Hänel, D.; Wlokas, I. (2007) Simulation of nasal flow by lattice
31 Boltzmann methods. *Comput Biol Med* 37: 739-749.

32 Mosges, R.; Buchner, B.; Kleiner, M.; Freitas, R.; Horschler, I.; Schroder, W. (2010)
33 Computational fluid dynamics analysis of nasal flow. *B-ENT* 6: 161-165.

1 Thrall, K. D.; Woodstock, A. D.; Soelberg, J. J.; Gargas, M. L.; Kinzell, J. H.;
2 Corley, R. A. (2009) A real-time methodology to evaluate the nasal absorption of
3 volatile compounds in anesthetized animals. *Inhal Toxicol* 21: 531-536.

4 Zhang, Z. and Kleinstreuer, C. (2011) Deposition of naphthalene and tetradecane
5 vapors in models of the human respiratory system. *Inhal Toxicol* 23: 44-57.

A.1.3 Charge Question 3

6 The state of the science that serves as the basis for this report is presented in detail in the
7 *Status I and II Reports*. Are the summaries and critical information included in this report
8 related to gas dosimetry clearly and accurately presented? Are the analyses and evaluations of
9 the scientific evidence supported by the studies cited?

10 Comments:

11 Four reviewers indicated that the document clearly and accurately presented an overview
12 of the science pertaining to inhalation gas dosimetry and that it adequately covers the
13 available material. Two of these reviewers each suggested a few places in the document
14 that could be improved: Section 2.4.3 regarding V_E/SA substance and clarity; while an
15 improvement upon the numerical scheme, the descriptor scheme limitations should be
16 expanded upon; and lack of gender specific information.

17 A fifth reviewer commented on a few issues with the description and interpretation of
18 some studies on gas dosimetry procedures related to the 1994 *RfC Methods*. This
19 reviewer thought that there appears to be a misunderstanding regarding the basis of
20 V_E/SA as DAF for category I gases, its interpretation from a dose-metric perspective, and
21 that the description in the report is a bit confusing. This reviewer commented that a 5-
22 fold higher V_E/SA in humans than in animals means a 5 fold lower HEC than C_A and not
23 a 5 fold higher dose. This reviewer also suggested more thought be placed into clarifying
24 the descriptor scheme, noting limitations of the CFD modeling, and made several
25 comments to verify Equation 3-1 and a related equation.

26 Response:

27 The assumptions regarding the application of V_E/SA in Section 2.4.3 were modified by
28 removing confusing text and clarifying language on the assumptions. Clarification that
29 the Medinsky and Bond scheme is not a perfect scheme either, was added to the report in
30 Section 3.1 and the lack of consideration of metabolism in these categorization schemes
31 was acknowledged. Figure 3-1 was also updated to include a systemic acting gas. There
32 is a lack of gender specific data available for the majority of the models, and the values
33 presented are typically considered to be population averages.

1 The description of V_E/SA in Section 2 of this report is depictly correctly based upon the
2 1994 *RfC Methods*. The reviewer is correct that, for the ET region, a 5-fold higher
3 V_E/SA in humans means a 5-fold lower HEC. Therefore, for a given animal POD (C_A)
4 the corresponding human dose per unit surface area is up to 5-fold greater.

5 The limitations of CFD modeling and other models are described throughout the report,
6 specifically for CFD modeling in Sections 3.2 and 3.3, and additional text was also added
7 at the beginning of Section 3.3. However, these models represent a vast improvement
8 over the default *RfC Methods*.

9 Equations 3-1 and 3-2 were verified with the source material ([Frederick et al., 1998](#)) as
10 being correctly depicted in this report.

A.1.4 Charge Question 4

11 Please comment on the effectiveness of the report in describing advances in the state of the
12 science since publication of the 1994 *RfC Methods* document. Please identify any additions,
13 deletions or changes that would improve the effectiveness of this document in presenting the
14 state of the science as it relates to the default procedures for interspecies gas dosimetry in *RfC*
15 *Methods*.

Comments:

16
17 One reviewer commented that the report is effective, but mentioned additional limitations
18 that should be listed to benefit readers and future users. A second reviewer offered that
19 the effectiveness of the report would be enhanced if there was a discussion of future
20 research needs, including the potential for increased use of molecular dosimetry
21 measurements.

22 Another reviewer stated that this document identifies a number of existing issues
23 surrounding the 1994 *RfC Methods*; however, many of the difficulties have been resolved
24 for the purpose of describing interspecies inhalation dosimetry while certain assumptions
25 and uncertainties are likely to always be present in human health risk assessments. The
26 reviewer also thought that this document adequately summarized the new information
27 and appropriately weighted the strengths and limitations of the literature when drawing
28 the conclusions.

29 A fourth reviewer commented that report is very effective in describing advances in the
30 state of the science specifically related to procedures for interspecies gas dosimetry in
31 *RfC Methods*. This reviewer also commended the selection of the collection of figures
32 cited in the document that help to communicate the insights offered by the more
33 advanced modeling methods. This reviewer suggested improvements to several figures
34 and the accompanying text to improve clarity and effectiveness.

1 Lastly, one reviewer commented that for the upper airways (oral and nasal passages), the
2 report nicely presents recent advances and highlights the short comings of *RfC Methods*.
3 In regards to the gas categorization scheme, this reviewer said the report correctly
4 concludes that dose extrapolation should be based on the effect in the target tissue (i.e.,
5 dose metric) and not the physico-chemical properties of gases. In addition, the reviewer
6 said the report provides adequate information on the dose-based extrapolation approach.
7 Importantly, this reviewer provided information and references describing the the state of
8 the science regarding whole-lung uptake modeling and suggested more clarity be given
9 on how various lower airway modeling approaches should be considered.

10 Response:

11 Text was added to the end of Section 3.2.5.3 regarding the use of molecular markers as
12 dose metrics. In response to reviewer comments, Figure 3-1 was improved with the
13 addition of a systemic acting gas, and the accompanying text was updated and clarified.
14 In addition, Figure 3-6 was corrected such the graphic better reflected the science
15 indicating nonuniform flow, surface area, and deposition. Whole-lung uptake modeling
16 papers suggested in response to this charge question were also suggested under Charge
17 Question 2. These references were evaluated and were included as appropriate (see
18 Response to Charge Question 2). Additional text was added to the beginning of Section
19 3.3 that provides more information regarding the consideration of the use of various
20 lower airway modeling approaches.

A.1.5 Charge Question 5

21 Section 3 of this report summarizes the advanced state of the science dosimetry models
22 including CFD and the CFD-PBPK hybrid models. The capabilities of these models to
23 estimate target-tissue dose are highlighted in Section 3. However, as with any state of the
24 science approach, limitations exist with respect to application and outcome of these models -
25 some of which have been recognized and discussed (see in particular Section 3.2.5.3). Have
26 the limitations of these advanced models been sufficiently characterized? Similarly, how well
27 does this report differentiate the relative scope of the limitations that exist with these models
28 compared with the existing *RfC Methods* default approach in estimating actual target-tissue
29 dose? Is there any information that would further support as well as limit the overall
30 conclusions drawn from the results of these models?

31 Comments:

32 One reviewer commented that the pharmacokinetic literature appears to be reviewed
33 thoroughly and the limitations and applicability discussed when appropriate, but
34 limitations regarding CFD models should be clarified.

1 Another reviewer commented that a number of advances have become available for
2 improving dosimetry models, including CFD and CFD-PBPK hybrid models, these
3 models do reflect the state-of-the-art of the science, and certain uncertainties and
4 limitations do exist. This reviewer notes that the report discusses the value and limitations
5 of these models and how they could aid in advancing interspecies dosimetry as well as
6 that the report has weighted the strengths and limitations of these modeling approaches,
7 and these factors have been sufficiently characterized. This reviewer also referred to
8 additional references that should be considered in response to Charge Question 2.

9 A third reviewer commented that the report in general succeeds to differentiate clearly
10 the relative scope of the limitations that exist within the state-of-the-science (CFD, hybrid
11 CFD-PBPK) models *vis a vis* those incorporated in the default approach described in the
12 1994 *RfC Methods* for estimating target-tissue dose. This reviewer noted, however, this
13 differentiation takes place very specifically in the (rather limited) context of direct
14 dosimetric interspecies extrapolation for the different regions of the respiratory tract.
15 Thus, the reviewer suggested that for current or future work it would be very useful to - at
16 least briefly - discuss both the default and the more advanced approaches for RfC
17 derivation in a wider but highly relevant context such as their implications in the use for
18 public health problems. This reviewer provided some references related to these broader
19 issues.

20 A fourth reviewer thought that the CFD-PBPK hybrid models were well-presented in
21 Section 3 and the discussion on page 3-20 was especially helpful. However, this reviewer
22 commented that the metabolic capacity of the target tissue will affect the uptake of the
23 gas into the tissue. This reviewer further stated that although metabolism may not fit
24 neatly into a classification system based on the physicochemical properties of the
25 compound, metabolism in the target tissue will definitely affect uptake of the compound
26 into the target tissue. This reviewer suggested that modifying the classification system to
27 include another property: "Potential for metabolism at target site." This reviewer was also
28 pleased to see that molecular dosimetry data are being considered in the CFD-PBPK
29 model shown in Table 3-4.

30 A final reviewer referred to their commentary provided in response to Question 4.

31 Response:

32 Limitations and challenges related to the use of CFD modeling were expanded upon in
33 Section 3.3, as noted in response to Charge Questions 3 and 4. Also, the gas descriptor
34 scheme was updated to reflect systemic acting gases and the accompanying text was
35 modified to include the importance of metabolism. These changes were also described
36 earlier in response to Charge Question 3.

A.1.6 Charge Question 6

1 The state of the science pertaining to children’s inhalation dosimetry is presented in Section
2 3.6. Is the description of the studies in this report, as they pertain to inhalation gas dosimetry,
3 clearly and accurately presented? Are the analyses and evaluations of the scientific evidence
4 supported by the studies cited? Are there additional evidence-based studies and information
5 specific to children’s inhalation dosimetry that should be considered for inclusion that
6 contribute to the science and understanding of inhalation gas dosimetry in children?

7 Comments:

8 Three reviewers commented that the report does a good job describing studies pertaining
9 to children’s inhalation gas dosimetry, the analyses and evaluations of the scientific
10 evidence are supported by the studies cited, and the report covers the theoretical (i.e.,
11 breathing pure gases) children’s gas dosimetry adequately for normal healthy children.
12 Two of these reviewers provided examples of additional recent studies that may have
13 potential value to characterizing children’s inhalation dosimetry for consideration.

14 One reviewer was not clear how the recent findings on lung growth and breathing
15 parameters helps with the improvement of the *RfC Methods*, and how geometry and
16 airflow information can help with improved assessment of DAF for children to replace
17 the uncertainty factor of 10 in the *RfC Methods*.

18 Another reviewer commented that the document is a very useful and comprehensive
19 review of the methodologies presently available for evaluating reduced-risk models
20 appropriate for understanding inhalation gas dosimetry in children. This reviewer stated
21 that while this report meets the challenge of summarizing this rapidly advancing field, it
22 also clearly identifies that much research still remains to be done. As such, in the
23 reviewers opinion this report is a welcome contribution and should be of benefit to chart
24 the activity in this field so that better scientific evidence and interpretation may be made
25 available to assess whether and to what extent age may influence risk assessment. This
26 reviewer suggested an additional reference for consideration.

27 Response:

28 Information presented relating lung growth and breathing parameters might be useful in
29 informing model parameter selection and future model development. None of this
30 information or the children’s inhalation dosimetry data were presented as a means to
31 replace the UF.

32 Additional references added to the document related to estimates of daily inhalation rates
33 for children were included in Section 3.4:

34

1 Brochu, P.; Brodeur, J.; Krishnan, K. (2011) Derivation of physiological inhalation
2 rates in children, adults, and elderly based on nighttime and daytime respiratory
3 parameters. *Inhal Toxicol* 23: 74-94.

4 Kawahara, J.; Tanaka, S.; Tanaka, C.; Aoki, Y.; Yonemoto, J. (In Press) Daily
5 Inhalation Rate and Time-Activity/Location Pattern in Japanese Preschool Children.

6 Kawahara, J.; Tanaka, S.; Tanaka, C.; Aoki, Y.; Yonemoto, J. (2011) Estimation of
7 daily inhalation rate in preschool children using a tri-axial accelerometer: a pilot
8 study. *Sci Total Environ* 409: 3073-3077.

9 The new Valcke et al. (2011) reference pertaining to intrahuman variability as suggested
10 by a reviewer was added to Section 3.6.2:

11 Valcke, M. and Krishnan, K. (2011) Assessing the impact of the duration and
12 intensity of inhalation exposure on the magnitude of the variability of internal dose
13 metrics in children and adults. *Inhal Toxicol* 23: 863-877.

A.2 Other Comments

14 One reviewer commented that, in general, this document meets the challenge of
15 insightfully summarizing and critically reviewing a wide range of evidence and
16 interpretation of the pertinent scientific developments and advancements in inhalation gas
17 dosimetry. The reviewer commented that the authors have successfully interpreted a wide
18 range of evidence focusing on risk assessment and this report is a contribution to the on-
19 going search for proper traditional methodologies focusing on improving our
20 understanding of the problems in today's attempts to assess human health risk using
21 available toxicological data from a number of animal species.

22 A second reviewer commented that the report is well-written, logical, accurate, and
23 thorough within the intended scope. The reviewer stated that risk assessment related
24 applications for extrapolations and for children are clearly described and the report has an
25 scope and level detail that supports its validity and its superiority over previous gas
26 dosimetry modeling approaches. However, this reviewer also suggested that although the
27 assumptions are clearly stated throughout the report where they are relevant, more could
28 be done to discuss the limitations. This reviewer provided some additional important
29 limitations to add to Section 4 to guide further research and educate users of the report on
30 the use of this approach in risk assessments. The reviewer commented that these
31 limitations do not detract from the value of the science in the report, but they are worth
32 listing for educational and cautionary purposes. In addition, this reviewer suggested a few
33 formatting changes to Table 4-1.

34

1 Response:

2 Additional text regarding the limitations of the scope of this report are provided in
3 Section 4.